Cascading Failures in Power Systems: Modeling, Characterization, and Mitigation

Thesis by
Chen Liang

In Partial Fulfillment of the Requirements for the
Degree of
Doctor of Philosophy

CALIFORNIA INSTITUTE OF TECHNOLOGY
Pasadena, California

2022
Defended June 1st, 2022

Chen Liang
ORCID: 0000-0002-0015-7206

ACKNOWLEDGEMENTS

I am so fortunate to pursue my Ph.D. at Caltech.

First and foremost, I would like to express my deepest gratitude to my advisors, Professor Steven Low and Professor Adam Wierman, for their continuous support and guidance throughout my Ph.D. studies. They are always available for help despite their busy schedules, and they have been so patient and encouraging through my challenging moments. Moreover, their guidance extends beyond just research. I have learned so much from their enthusiasm and personality. In my opinion, they are the best academic advisors and perfect role models. Steven and Adam, thank you for your trust, help, and invaluable advice.

Next, I would like to extend my sincere thanks to Professor Yisong Yue and Professor Venkat Chandrasekaran, for serving on my candidacy and final exam committee. I am so grateful for their support and valuable feedback on this thesis. I also learned a lot from their courses at Caltech, providing me with rigorous mathematical theories and practical machine learning techniques.

Many thanks to my wonderful collaborators, Daniel Guo, Alessandro Zocca, Fengyu Zhou, Shuyue Yu, and Janusz Bialek, for their input and contributions to this thesis. Besides, I would like to express my appreciation to my friends and colleagues in Netlab and RSRG: Daniel Guo, Zachary Lee, Tongxin Li, Yiheng Lin, John Pang, Yu Su, Yujie Tang, Zhaojian Wang, Lucien Werner, Pengcheng You, and Fengyu Zhou. It has truly been a pleasure to study and work with these brilliant researchers during my Ph.D. years.

I would like to thank everyone I met at Caltech and all my friends, including my CMS cohort: Sara Beery, Natalie Bernat, Riley Murray, and Eric Zhan; my first-year roommates: Honglie Ning, Ye Qiu, Jin Sima, and Hongnian Yu; and so many more than I can list here. Special thanks go to the CMS staff, especially Christine Ortega and Maria Lopez, for taking care of all the administrative issues.

To my parents and grandparents for their constant love, support, and never-ending faith in me. To my wife, Qianru, whom I met in high school and who has always stood by my side ever since. This thesis would not have been possible without you. I owe you everything.

ABSTRACT

Reliability is a critical goal for power systems. Due to the connectivity of power grids, an initial failure may trigger a cascade of failures and eventually lead to a large-scale blackout, causing significant economic and social impacts. Cascading failure analysis thus draws wide attention from power system practitioners and researchers. A well-known observation is that cascading failures in power systems propagate non-locally because of the complex mechanism of power grids. Such non-local propagation makes it particularly challenging to model, analyze and control the failure process. In this thesis, we tackle these challenges by establishing a mathematical theory to model and characterize failure patterns, discover structural properties of failure propagation, and design novel techniques for failure mitigation.

First, we propose a failure propagation model considering both fast-timescale system frequency dynamics and the slow-timescale line tripping process. This model provides mathematical justifications to the widely used static DC model and can be generalized to capture a variety of failure propagation patterns induced by different control mechanisms of the power grid. More importantly, this model provides flexibility to design real-time control algorithms for failure mitigation and localization.

Second, we provide a complete characterization of line failures under the static DC model. Our results unveil a deep connection between the power redistribution patterns and the network block decomposition. More specifically, we show that a non-cut line failure in a block will only impact the branch power flows on the transmission lines within the block. In contrast, a cut set line failure will propagate globally depending on both the power balancing rules and the network topological structure. Further, we discuss three types of interface networks to connect the sub-grids, all achieving better failure localization performance.

Third, we study corrective control algorithms for failure mitigation. We integrate a distributed frequency control strategy with the network block decomposition to provide provable failure mitigation and localization guarantees on line failures. This strategy operates on the frequency control timescale and supplements existing corrective mechanisms, improving grid reliability and operational efficiency. We further explore the failure mitigation approach with direct post-contingency injection adjustments. Specifically, we propose an optimization-based control method with strong structural properties, which is highly desirable in large-scale power networks.

PUBLISHED CONTENT AND CONTRIBUTIONS

Guo, Linqi, Chen Liang, Alessandro Zocca, Steven H. Low, and Adam Wierman. (2021). "Line Failure Localization of Power Networks Part I: Non-cut Outages." In: *IEEE Transactions on Power Systems* 36.5, pp. 4140–4151. DOI: 10.1109/TPWRS.2021.3066336.

Adapted into Chapter 3 of this thesis.

Guo, Linqi, Chen Liang, Alessandro Zocca, Steven H. Low, and Adam Wierman (2021). "Line Failure Localization of Power Networks Part II: Cut Set Outages." In: *IEEE Transactions on Power Systems* 36.5, pp. 4152–4160. DOI: 10.1109/TPWRS.2021.3068048.

Adapted into Chapter 4 of this thesis.

Liang, Chen, Alessandro Zocca, Steven H. Low, and Adam Wierman (2022). "Interface Networks for Failure Localization in Power Systems." In: *2022 American Control Conference (ACC)*. URL: arxiv.org/abs/2205.06315.

Adapted into Chapter 5 of this thesis.

Liang, Chen, Linqi Guo, Alessandro Zocca, Steven H. Low, and Adam Wierman (2022). "Adaptive Network Response to Line Failures in Power Systems." Accepted: *IEEE Transactions on Control of Network Systems*. URL: arxiv.org/abs/2005.11319.

Adapted into Chapters 2 and 6 of this thesis.

Liang, Chen, Fengyu Zhou, Alessandro Zocca, Steven H. Low, and Adam Wierman (2020). "Mitigating Cascading Failures via Local Responses." In: *2020 IEEE International Conference on Communications, Control, and Computing Technologies for Smart Grids (SmartGridComm)*. DOI: 10.1109/SmartGridComm47815.2020.9302934.

Adapted into Chapter 7 of this thesis.

Liang, Chen, Linqi Guo, et al. (2021). "An Integrated Approach for Failure Mitigation & Localization in Power Systems." In: *Electric Power Systems Research* 190, pp. 106613. DOI: 10.1016/j.epsr.2020.106613

Zocca, Alessandro, Chen Liang, Linqi Guo, Steven H. Low, and Adam Wierman (2021). "A Spectral Representation of Power Systems with Applications to Adaptive Grid Partitioning and Cascading Failure Localization." In: *arXiv preprint arXiv:2105.05234*. URL: arxiv.org/abs/2105.05234

Guo, Linqi, Chen Liang, and Steven H. Low (2017). "Monotonicity Properties and Spectral Characterization of Power Redistribution in Cascading Failures." In: *2017 55th Annual Allerton Conference on Communication, Control, and Computing (Allerton)*. IEEE, pp. 918–925. DOI: 10.1109/ALLERTON.2017.8262836

Chen Liang participated in the conception of the projects, proposing the models and analyzing their performance, and writing the manuscripts.

TABLE OF CONTENTS

LIST OF ILLUSTRATIONS

LIST OF TABLES

Chapter 1

INTRODUCTION

Reliability is a critical goal for power systems. Large-scale blackouts, although rare, cause significant economic and social impacts. For example, the 2003 Northeast blackout is estimated to have caused an economic impact of $7-10 billion [4], and the 2012 India blackout affected more than 620 million people [5]. Typically, the start of a large-scale blackout is an individual failure that triggers a cascade of failures. For instance, when a generator fails and disconnects from the grid, the power becomes imbalanced, and frequency starts to drop. If the generation reserve capacity is not sufficient to support the demand, the frequency will continue to drop, which may cause the disconnection of other generators due to protection mechanisms. This may eventually lead to a system-wide collapse. On the other hand, when a transmission line fails, the power will redistribute over the remaining network and potentially cause other lines to overload. This may cause a cascade of line failures and lead to network islanding.

There have been extensive efforts to prevent cascading failures. For example, the North American Electric Reliability Corporation (NERC) requires the power grids to operate under the $N-1$ security criterion: the system remains safe after any single failure. This preventive security criterion improves grid reliability against failures; however, multiple failures may happen simultaneously. To make things worse, hidden failures, such as human operating errors, may enlarge the impact of failures. Improving grid reliability becomes crucial as the power grid becomes increasingly stressed by more volatile supply and demand fluctuations.

A well-known observation is that the cascading failures in power systems propagate non-locally. This fact is illustrated by the sequence of events leading to the 1996 Western US blackout (as summarized in Fig. 1.1 from [1, 2]), in which successive failures happened hundreds of kilometers away from each other (e.g., from stage ③ to stage ④ and from stage ⑦ to stage ⑧). Such non-local propagation makes it particularly challenging to model the cascading failure process, characterize the failure propagation patterns, and design algorithms to prevent and mitigate failures.

Due to the complex mechanism of the power grid, current industry practice on cascading failure analysis relies on simulation-based approaches. These approaches

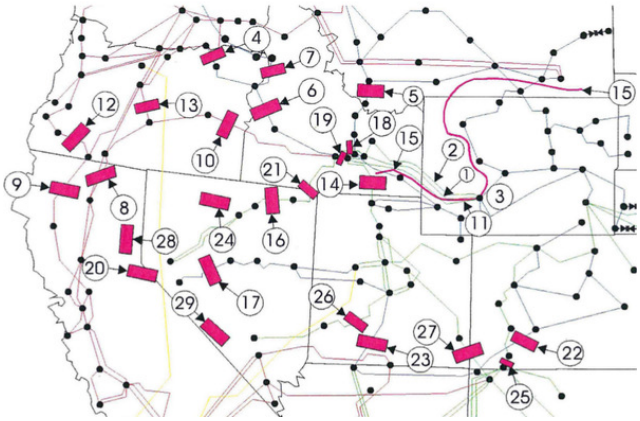

Figure 1.1: The sequence of events, indexed by the circled numbers, that lead to the Western US blackout in 1996 from [1, 2].

are usually constrained by computational power, undermining their effectiveness given the enormous number of components in power networks. The limitations of the current practice have motivated a large body of research on cascading failures. In particular, the literature on analytical properties of cascading failures can be roughly categorized as follows: (a) applying Monte-Carlo methods to analytical models that account for the steady-state power redistribution using DC [6–9] or AC [10–12] power flow models; (b) studying pure topological cascade models built upon simplifying assumptions on the propagation dynamics (e.g., failures propagate to adjacent lines with high probability) and inferring component failure propagation patterns from graph-theoretic properties [13–15]; (c) investigating simplified or statistical cascading failure dynamics [2, 16–18]. In all these approaches, it is often difficult to make general inferences about failure patterns. This lack of structural properties is a critical challenge in modeling, controlling, and mitigating cascading failures in power systems.

The above discussion motivates this thesis. The central theme of this thesis is to *develop a mathematical theory to model and characterize failure patterns, discover structural properties of failure propagation, and design novel techniques for failure mitigation*.

1.1 Modeling of Cascading Failures

A variety of models have been developed to understand, predict, and analyze cascading failures in power systems; see [19] for a recent review. However, due to the complexity of the power system, there is no existing approach that fully captures the cascading failure process. Each model has its own advantages and limitations, as

we now summarize.

The current industry practice for mitigating cascading failures relies on the simulation-based analysis of creditable contingencies [20]. The size of the contingency set, and thus the level of security guarantee, however, is often constrained by computational power, undermining its effectiveness in view of the enormous number of components in power networks. Moreover, after a blackout event, a detailed study typically leads to a redesign of such contingency sets, potentially together with physical network upgrades and system management policies and regulations revision [21]. Simulation-based approaches, constrained by the lack of analytical clarity and methodological rigor, are thus difficult to make general inferences about the failure propagation pattern in large-scale power grids.

High-level probabilistic models are developed to describe the cascading process statistically. The CASCADE model, introduced in [16], uses a simple load distribution and component failure mechanism to show how the system load impacts the system risk. In [22], a branching process is used to approximate the CASCADE model to quantify the failure propagation. The application of the branching process to cascading failures is advanced and validated in various simulations and test systems [23–25]. More recently, a Markovian influence graph model has been proposed to identify critical components [2] and estimate the cascade size [26]. In additon, a Bayesian learning framework is developed to approximate the line outage rate to improve the accuracy of failure propagations [27]. However, these statistical models require large amounts of failure data, which are usually limited in practice and thus generated by simulation-based models.

There have been efforts to understand cascades' structural properties by modeling the power grid as a complex network [13–15]. However, these purely topological models can be misleading since they do not consider electrical features [28]. Improved topological models have incorporated power-related metrics like electrical betweenness, net-ability, and entropic degree [29, 30]. Yet, jury is still out on whether such approaches will provide valuable insights on cascading failures [31].

Models with detailed power grid physics and failure mechanisms are developed to capture the complex propagation pattern, for instance, static models based on DC/AC power flows such as OPA [6, 32, 33] and Manchester model [10], as well as dynamic models based on differential-algebraic equations such as PRA [34, 35] and COSMIC model [12]. The static model with DC power flows, which initiated the field [6, 36, 37], is widely adopted and used to describe the failure pattern [8, 9, 38]

and develop control actions for failure mitigation [39, 40] due to its simplicity and tractability. In practice, however, following a line failure, the power grid will respond with various real-time control and protection mechanisms, resulting in power injection adjustment and a different steady state. The static DC model cannot model such fast-timescale dynamics. The DC model thus relies on specific power balancing rules to adjust post-contingency injections [8, 9, 38], which are not well-justified mathematically. On the other hand, although fast-timescale dynamics are modeled in [12], it is challenging to perform tractable analysis without simulating the whole cascading process at high computational complexity.

Integrated Failure Model

The above review highlights the importance of developing well-grounded deterministic models of cascading failures that are amenable to analysis. Chapter 2 proposes an integrated failure propagation model considering both the fast-timescale dynamics and the slow-timescale line tripping process. Specifically, we explicitly model fast-timescale frequency control dynamics as part of the cascading process. In contrast to a purely dynamic model [12], our approach captures a simplified line tripping dynamic where, after an initiating transmission failure, the next set of line trips does not occur until the frequency dynamics have converged. In particular, our model does not capture the more delicate thermal dynamics that determine the timing of line trips based on line currents and ambient temperatures. The advantage of our line tripping rule is that the equilibrium point of the frequency dynamics can usually be derived as the optimal solution to an optimization problem [3, 41–43]. This assumption makes it possible to theoretically understand the cascading failure process and provide tractable analysis.

Our model not only provides mathematical justifications to the widely used static DC model [9, 40, 44] from the transient frequency control perspective, but can be generalized to capture a variety of failure propagation patterns induced by different control mechanisms of the power grid. More importantly, this model provides flexibility to design real-time control algorithms for failure mitigation and localization, as we will show in Chapter 6.

1.2 Characterization of Cascading Failures

Failures in power systems may cascade and propagate in a very complicated manner, and typically exhibit different patterns for different networks [38]. When a failure happens, power will redistribute over the surviving network. The power flow over

a specific transmission line can increase, decrease or even reverse its direction as cascading failure unfolds [45]. Such complexity, originated from the interplay between network topology and physical mechanisms, is aggravated by hidden failures and human errors.

Even though it might be straightforward to simulate the cascading failure process, mathematical characterization and analysis turn out to be highly nontrivial. Most work adopts the DC power flow model and studies the flow redistribution after line failures through sensitivity factors: power transfer (PTDF) and line outage (LODF) distribution factors [46–49]. These distribution factors have been derived and studied through multiple papers with different approaches, as we now summarize.

The reference [46] seems to be the first to introduce the use of matrix inversion lemma to power systems to study the impact of network changes on line currents. It adopts the Ohm's law $\boldsymbol{I} = \boldsymbol{Y}\boldsymbol{V}$ where $\boldsymbol{Y}$ is a network Laplacian matrix, e.g., nodal admittance or Jacobian matrix from the linearization of AC power flow equations. The changes can be changes in the line parameters Y_{ij} or outages of an arbitrary set of lines, or changes in the nodal injections $\boldsymbol{I}$ or outages of an arbitrary set of generators. This linear system is mathematically equivalent to the DC power flow model. In [47], the method of [46] is applied to the DC power flow model to characterize the flow change for an arbitrary set of line outages. The paper [47] also allows generator outages and uses these formulae to rank contingencies in security analysis quickly. LODF for multi-line failures, which we refer to as the generalized LODF (GLODF), is also developed in [50], but without the simplification of the matrix inversion lemma. The formula of GLODF is re-discovered in [48, 49] using a different method, likely unaware of the results of [46, 47]. The underlying idea of the letter [48] is to emulate line outages through changes in injections on the pre-contingency network by judiciously choosing injection at the tail of each disconnected line and withdrawal at its head using PTDF. They start from the expression for a single-line outage and prove the general non-cut set case by induction. The paper [49] uses the PTDFs to detect whether line failures will lead to islanding. See also [51] for another derivation of GLODF in terms of PTDF. While PTDF and LODF determine the sensitivity of power flow solutions to parameter changes, one can also study the sensitivity of optimal power flow solutions to parameter changes; see, e.g., [52, 53]. LODFs are also studied more recently as a tool to quantify network robustness and flow rerouting [54].

These distribution factors are revisited in [38, 55–57]. [38] shows that a failure

can affect remote lines, consistent with the well-known observation that failures in power systems do not necessarily propagate locally. [55–57] aim to accelerate the analysis for multi-line failures since the size of possible multi-line failures grows exponenetially in the number of tripped lines. [55, 56] consider 2-line failures and provide a fast screening algorithm based on iterative bounding and pruning. [57] proposes the disturbance value to quantify the impact of k-line failures, which can be approximately computed in $O(1)$ time complexity.

Besides the computation of distribution factors, there have been efforts to understand the localizability of power system failures with respect to network topological structures. Most papers focus on summarizing empirical results. For example, [38] observes that the LODF decreases as the distance from the tripped line increases, and [54] defines another distance metric that better captures such decay. More recently, a new approach based on the spectral representation of transmission networks to understand the structural propertiess of cascading dynamics has been developed in [58]. This has motivated a series of work on characterizing failure localization for power grids, including the work presented in Chapters 3, 4, and 5 of this thesis. This spectral perspective is powerful as it reveals surprisingly simple characterizations of complex system behaviors, e.g., on system robustness in terms of effective resistance [59], on Kron reduction of the power network [60], on controllability and observability of power system dynamics [61], and on monotonicity properties and power flow redistribution [58].

Failures and Network Block Decomposition

In Chapters 3 and 4, we establish a mathematical theory that characterizes line failure localization properties of power systems. This theory makes crucial use of the weighted Laplacian matrix of a transmission network and its spectral properties. Our results unveil a deep connection between power redistribution patterns and the distribution of different families of (sub)trees of the power network topology. We show how specific topological structures naturally emerge in the analysis of several important and well-studied quantities in power system contingency analysis, such as the generation shift sensitivity factors and the line outage redistribution factors.

In Chapter 3, we restrict our attention to the case where the network remains connected after the line failures and study how such failures impact the branch flows on the surviving network. In this scenario, the power injections remain balanced and are not adjusted after the contingency. Our theory reveals a decoupling structure of

the transmission network that leads to failure localizability in a cascading process. More specifically, we show that when a non-cut set of lines trips, any other line that is not in the same block (see Definition 3.1) of one of the tripped lines is not affected. In other words, non-cut failures cannot cross the boundaries of the block decomposition of the transmission network.

In Chapter 4, we consider the scenario where the set of tripped lines disconnects the network into two or more connected components, called islands, and injections must be adjusted to rebalance the power injections. Our results demonstrate how the impact of cut set outages propagates globally in a way that depends on both the design of power balancing rules and the network topological structure.

Failures and Interface Networks

Our failure localizability analysis in Chapter 3 shows that non-cut failures are localized if sub-grids are connected in a tree structure and that, if multiple lines connect sub-grids, failures cannot be completely localized. This observation suggests switching off certain transmission lines to leave only one line between sub-grids for grid reliability.

However, maintaining a tree structure at the sub-grid level is at odds with the $N-1$ security standard. As shown in Chapter 4, those bridge failures can be critical and will affect the whole power grid. Further, a tree-connected power network significantly reduces the power transmission capacity between the sub-grids, increasing the cost of power dispatch. It is therefore desirable to have multiple lines between sub-grids to ensure there are no single-point vulnerabilities and increase the power transmission capacity.

In Chapter 5, we extend our localizability analysis to the case when the sub-grids are connected by interface networks. Specifically, we study three interface networks that can decrease the LODFs between sub-grids and maintain robust connectivity. We further show that, by carefully designing the line susceptances, the complete bipartite interface network can eliminate failure propagation to other sub-grids while maintaining the same impact on surviving lines in the same sub-grid.

1.3 Mitigation of Cascading Failures

To prevent cascading failures, system operators require the power system to operate under specific security criteria: *preventive* security criteria [62] ensure that the power system remains safe after a contingency without any additional control action, while

corrective security criteria [63] provide post-contingency control actions that ensure the system remains stable.

Improving grid reliability is crucial as the power grid becomes increasingly stressed by more volatile supply and demand fluctuations. Indeed, the increased and strongly correlated uncertainty from renewable energy sources makes preventive security less robust. As a result, power systems that operate under preventive security criteria are forced to have more extensive reserves and thus incur higher costs to account for such uncertainty. technological advances with ubiquitous monitoring and control provide the possibility of implementing corrective actions in response to failures in real-time [64].

Various corrective control policies have been proposed in the literature. One line of research focuses on line switching actions, such as transmission system reconfiguration and controlled system islanding [65–67]. Controlled islanding splits the power grid into several self-supported components to prevent large-scale blackouts; see [68] for a recent review of various controlled islanding strategies. The essence of islanding is to switch off a set of transmission lines to create islands with the objective of minimizing power imbalances [69, 70], minimizing power flow disruptions [71–73], and satisfying generator coherency constraints [74, 75]. More recently, following our analysis in Chapter 3, a novel emergency measure to create tree-partitioned sub-grids is proposed in [67]. The tree-partition-based approach achieves the same failure localization while maintaining the connectivity of the power grid, so that the shock to the system is less compared with controlled islanding.

Another line of research focuses on adjusting the post-contingency operational set-points, such as generation rescheduling and load shedding [76]. While existing corrective strategies exploit the flexibility of controllable devices in response to contingencies, the control actions for set-point adjustments are often designed using heuristics, e.g., uniformly scaling down the injections [9], which may result in a large amount of load loss. A variety of optimization-based corrective control policies have been proposed in [64, 77, 78], where the objective is to minimize the cost of control actions while ensuring that the post-contingency operating condition is safe. In addition, [39, 40] consider the optimal control of injections for multiple stages to minimize the load loss. While [39] restricts itself to affine control actions, [40] adopts a dynamic programming framework and proposes a branch and bound algorithm.

Adaptive Network Response

Although optimization-based load shedding algorithms aim to minimize the loss of power demand (possibly through multiple stages of the cascade), they require a centralized controller to monitor the system states, calculate the control actions for each node, and communicate the derived injection adjustments[1]. Such control actions thus require a longer time to take effect after failures.

Moreover, as we discussed in Section 1.1, fast-timescale control will be involved following a line failure. Our integrated failure model, by explicitly modeling such dynamics, is not only more realistic, but also offers additional means to mitigate cascading failures through better design of the frequency control mechanism. In Chapter 6, we propose a novel and complementary control strategy that builds upon this extra freedom and reacts to line outages on a timescale of minutes. It can be synergistically integrated with existing corrective mechanisms for grid reliability.

Specifically, we integrate a distributed frequency control strategy with a tree-partitioned network to provide provable failure mitigation and localization guarantees on line failures. This strategy operates on a different timescale and supplements current practice, improving both grid reliability and operational efficiency. To the best of our knowledge, this is the first attempt to leverage results from the frequency regulation literature in the context of cascading failures, bringing new perspectives and insights to both communities. Our proposed strategy guarantees that (a) whenever it is feasible to avoid it, line failures do not propagate, and (b) the impact of line failures is localized as much as possible in a manner configurable by the system operator.

Local Injection Response

In Chapter 7, we continue to explore the failure mitigation approach with injection adjustments. In contrast to optimal load shedding proposed in [64, 77, 78], which is usually solved in a centralized manner, we propose a different control method with strong structural properties, named the optimal injection adjustment (OIA).

Our contribution is two-fold. We first prove that OIA's control action exhibits a local injection adjustment pattern. At any given node, an injection adjustment is not required unless at least one of its neighboring nodes closer to the line failure has already reached its adjustment limit. Secondly, we compare OIA with traditional

[1] Distributed control might be achieved if we restrict the set of control actions and consider special cases [39].

optimization-based corrective controls that focus on optimal load shedding (OLS) using numerical experiments. These experiments highlight that OIA achieves near-optimal control costs using localized control actions.

The design of OIA paves the way for further study of local corrective control policies. Our analytic results show that it is possible to provide near-optimal corrective control using local injection adjustments by exposing the topological pattern of optimal corrective actions. Such a structural property is highly desirable in large-scale power networks where distributed fast control policies are preferred. Further, our numerical results highlight the trade-off between locality and control costs, especially when enforcing line capacity limits.

Chapter 2

POWER FLOW AND CASCADING FAILURE MODELS

In this chapter, we present the power grid model as well as some basic definitions and notations that are used throughout this thesis. We further present a novel cascading failure model that considers both the fast-timescale system dynamics and the slow-timescale line tripping process. Our model offers more flexibility in modeling different failure processes that will be discussed in later chapters.

2.1 Summary of Notations

Throughout this thesis, we use bold uppercase characters to denote matrices (e.g., $\boldsymbol{A}$) and bold lowercase characters to denote vectors (e.g., $\boldsymbol{p}$). For a matrix $\boldsymbol{A}$, A_{ij} denotes the element at the i-th row and j-th column. Depending on the context, we use $\boldsymbol{A}_i$ to denote the i-th row vector or the i-th column vector. For a vector $\boldsymbol{p}$, p_i denotes its i-th element.

We describe a transmission power grid using a graph $\mathcal{G} = (\mathcal{N}, \mathcal{E})$, whose node set $\mathcal{N} = \{1, \ldots, n\}$ models the $n = |\mathcal{N}|$ buses and whose edge set $\mathcal{E} \subseteq \mathcal{N} \times \mathcal{N}$ models the $m = |\mathcal{E}|$ transmission lines. We use the terms bus/node and line/edge interchangeably. An edge in $\mathcal{E}$ between node i and j is denoted either as e or (i, j). Without loss of generality, we assume the graph is simple and we assign an arbitrary orientation to the edges in $\mathcal{E}$ so that if $(i, j) \in \mathcal{E}$ then $(j, i) \notin \mathcal{E}$.

2.2 DC Power Flow

The power grids are analyzed under the alternating current (AC) power flow model in electrical engineering. The AC power flow model uses a set of nonlinear equations to describe the power flows over transmission lines from generators to loads. Due to nonlinearity, the analysis of large power networks under the AC power flow model is usually infeasible or intractable.

The DC power flow model characterizes the power flows using a set of linear equations. It provides a linear approximation of the active power flows in the AC model. Due to its linearity, many practitioners and researchers rely on the DC model to provide reliable and fast analysis of the cascading failure. In this thesis, we use the DC model for all our theoretical analysis while the AC model will be used in

some numerical experiments.

We now present the DC power flow model. For each transmission line $e = (i, j)$, we use $B_e = B_{ij}$ to denote its susceptance (weighted by nodal voltage magnitudes). The susceptance matrix is the $m \times m$ diagonal matrix $\boldsymbol{B} := \mathrm{diag}(B_e : e \in \mathcal{E})$. The incidence matrix of graph $\mathcal{G}$ is the $n \times m$ matrix $\boldsymbol{C}$ defined as

$$C_{ie} = \begin{cases} 1 & \text{if node } i \text{ is the source of } e, \\ -1 & \text{if node } i \text{ is the target of } e, \\ 0 & \text{otherwise.} \end{cases}$$

Let $\boldsymbol{f}$ be the m-dimensional vector consisting of all branch flows, with f_e denoting the flow on edge e. We introduce the n-dimensional vectors $\boldsymbol{p}$ and $\boldsymbol{\theta}$, where p_i and θ_i are the power injection and voltage phase angle at node i, respectively. We follow the convention that $p_i > 0$ indicates a generator at node i and $p_i < 0$ indicates a load. With the above notation, the DC power flow model is described by the following equations in matrix form:

$$\boldsymbol{p} = \boldsymbol{C}\boldsymbol{f} \tag{2.1a}$$

$$\boldsymbol{f} = \boldsymbol{B}\boldsymbol{C}^T\boldsymbol{\theta} \tag{2.1b}$$

where (2.1a) is the flow conservation (Kirchhoff's) law and (2.1b) is the Ohm's laws. Given an injection vector $\boldsymbol{p}$ that is *balanced* over the network, i.e., $\sum_{j \in \mathcal{N}} p_j = 0$, the DC model (2.1) has a solution $(\boldsymbol{\theta}, \boldsymbol{f})$ that is unique up to an arbitrary reference angle. Without loss of generality, we choose node n as a reference node and set $\theta_n = 0$. Using this convention, the solution $(\boldsymbol{\theta}, \boldsymbol{f})$ is unique.

2.3 Laplacian Matrix

The DC power flow equations (2.1) imply that

$$\boldsymbol{p} = \boldsymbol{C}\boldsymbol{B}\boldsymbol{C}^T\boldsymbol{\theta} = \boldsymbol{L}\boldsymbol{\theta},$$

where $\boldsymbol{L} := \boldsymbol{C}\boldsymbol{B}\boldsymbol{C}^T \in \mathbb{R}^{n \times n}$ is called the Laplacian matrix of $\mathcal{G}$ [79]. It is well-known that $\boldsymbol{L}$ is a symmetric and positive semi-definite matrix with zero row sums. If $\mathcal{G}$ is connected, then $\boldsymbol{L}$ is of rank $n - 1$, its null space is spanned by the vector $\mathbf{1} = (1, \ldots, 1) \in \mathbb{R}^n$, and the Penrose-Moore pseudo-inverse of $\boldsymbol{L}$ is the $n \times n$ matrix

$$\boldsymbol{L}^\dagger := \left(\boldsymbol{L} + \mathbf{1}\mathbf{1}^T/n\right)^{-1} - \mathbf{1}\mathbf{1}^T/n.$$

Given a balanced injection vector $\boldsymbol{p}$, a power flow solution can also be written in terms of $\boldsymbol{L}^\dagger$ as $\boldsymbol{\theta} = \boldsymbol{L}^\dagger \boldsymbol{p}$ and $\boldsymbol{f} = \boldsymbol{B}\boldsymbol{C}^T\boldsymbol{L}^\dagger \boldsymbol{p}$. This formulation yields unique branch flows $\boldsymbol{f}$ and phase angles $\boldsymbol{\theta}$. However, it may not satisfy the aforementioned convention prescribing the reference phase angle to be zero, as it may be that $\theta_n \neq 0$. Let the reduced Laplacian matrix $\overline{\boldsymbol{L}}$ be the submatrix of $\boldsymbol{L}$ obtained by deleting its n-th row and column (corresponding to the reference node). If the network is connected, then $\overline{\boldsymbol{L}}$ is invertible and we can define an $n \times n$ matrix $\boldsymbol{A}$ by

$$\boldsymbol{A} = \begin{bmatrix} \left(\overline{\boldsymbol{L}}\right)^{-1} & \mathbf{0} \\ \mathbf{0} & 0 \end{bmatrix}. \tag{2.2}$$

We will refer matrix $\boldsymbol{A}$ as the extended inverse (e-inverse) Laplacian matrix throughout the thesis. Given a balanced injection vector $\boldsymbol{p}$, the power flow solution can also be written in terms of $\boldsymbol{A}$ as $\boldsymbol{\theta}' = \boldsymbol{A}\boldsymbol{p}$ and $\boldsymbol{f}' = \boldsymbol{B}\boldsymbol{C}^T\boldsymbol{A}\boldsymbol{p}$. In this representation, the reference phase angle satisfies $\theta'_n = 0$. Moreover, we have $\boldsymbol{\theta}' = \boldsymbol{\theta} - \theta_n \mathbf{1}$, i.e., the two phase angle vectors differ by a constant reference angle. It should be noted that the branch flow vector is always unique, $\boldsymbol{f} = \boldsymbol{f}'$.

Graphical Interpretation

We now introduce some additional notations useful to work with *spanning trees* of the graph $\mathcal{G}$ and present a preliminary graphical interpretation of matrix $\boldsymbol{A}$ in terms of tree structures in $\mathcal{G}$.

A spanning tree of a graph $\mathcal{G}$ is a subgraph that is a tree which includes all the vertices $\mathcal{N}$. Given a subset $H \subseteq \mathcal{E}$ of edges, we denote by $\mathcal{T}_H$ the set of spanning trees of $\mathcal{G}$ with edges from H and by $\mathcal{T}_{-H}$ the set of spanning trees with edges from $-H := \mathcal{E} \setminus H$. In particular, $\mathcal{T}_{\mathcal{E}}$ is the set of all spanning trees on $\mathcal{G}$. For any pair of subsets $\mathcal{N}_1, \mathcal{N}_2 \subset \mathcal{N}$, we define $\mathcal{T}(\mathcal{N}_1, \mathcal{N}_2)$ to be the set of spanning forests of $\mathcal{G}$ consisting of exactly two disjoint trees that contain $\mathcal{N}_1$ and $\mathcal{N}_2$, respectively (see Fig. 2.1). By definition, $\mathcal{T}(\mathcal{N}_1, \mathcal{N}_2) = \emptyset$ if $\mathcal{N}_1 \cap \mathcal{N}_2 \neq \emptyset$. To further simplify notations, we omit the braces when there is no confusion, e.g., we write $\mathcal{T}(ij, \hat{i}\hat{j})$ for $\mathcal{T}(\{i, j\}, \{\hat{i}, \hat{j}\})$ and $\mathcal{T}_{-e}$ for $\mathcal{T}_{-\{e\}}$. Given a subset $H \subseteq \mathcal{E}$ of edges, we define its weight as

$$\beta(H) := \prod_{e \in H} B_e.$$

Note that $\beta(H) > 0$ since the susceptances B_e, $e \in \mathcal{E}$, are all positive.

The Kirchhoff's Matrix Tree Theorem relates the determinant of the reduced Laplacian matrix $\overline{\boldsymbol{L}}$ and its minors to the total weight of (a specific collection of) the

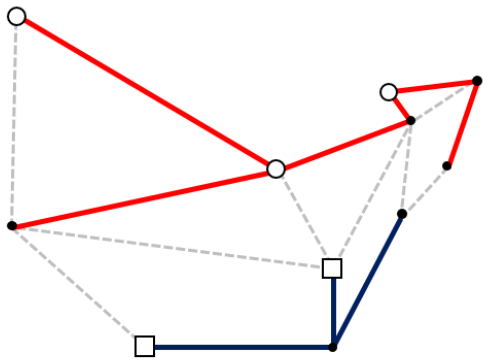

Figure 2.1: An example element in $\mathcal{T}(\mathcal{N}_1, \mathcal{N}_2)$, where circles correspond to elements in $\mathcal{N}_1$ and squares correspond to elements in $\mathcal{N}_2$. The two trees containing $\mathcal{N}_1$ and $\mathcal{N}_2$ are highlighted as solid lines.

spanning trees of $\mathcal{G}$ [80].

Lemma 2.1 (Matrix Tree Theorem [80])**.**

1. *The determinant of* $\overline{\boldsymbol{L}}$ *is given by*

$$\det(\overline{\boldsymbol{L}}) = \sum_{H \in \mathcal{T}_{\mathcal{E}}} \beta(H).$$

2. *The determinant of the matrix* $\overline{\boldsymbol{L}}^{ij}$ *obtained from* $\overline{\boldsymbol{L}}$ *by deleting the* i*-th row and* j*-th column is given by*

$$\det\left(\overline{\boldsymbol{L}}^{ij}\right) = (-1)^{i+j} \sum_{H \in \mathcal{T}(ij,n)} \beta(H).$$

Lemma 2.1 leads to a graphical interpretation of the entries of the matrix $\boldsymbol{A}$ as summarized in the following theorem.

Theorem 2.2 (Spectral Representation)**.** *If* $\mathcal{G}$ *is connected, then for any pair of nodes* $i, j \in \mathcal{N}$*, we have*

$$A_{ij} = \frac{\sum_{H \in \mathcal{T}(ij,n)} \beta(H)}{\sum_{H \in \mathcal{T}_{\mathcal{E}}} \beta(H)}. \tag{2.3}$$

Proof. Recall that, without loss of generality, we choose node n as reference node and define the matrix $\boldsymbol{A}$ accordingly in (2.2). If $i = n$ or $j = n$, it is easy to see that $\mathcal{T}(ij, n) = \emptyset$ so that $A_{ij} = 0$. Now suppose $i, j \neq n$, we can express A_{ij} in terms of the weighted spanning trees through the Cramer's rule. Specifically, let $\boldsymbol{A}_j$ denote

the j-th column of $\boldsymbol{A}$ after removing the reference node. Note from the definition of $\boldsymbol{A}$ that $\overline{\boldsymbol{L}}\boldsymbol{A}_j = \boldsymbol{e}_j$, where $\boldsymbol{e}_j \in \mathbb{R}^{n-1}$ is the vector with 1 as its j-th component and 0 elsewhere. Cramer's rule gives

$$A_{ij} = \frac{\det\left(\overline{\boldsymbol{L}}_j^i\right)}{\det\left(\overline{\boldsymbol{L}}\right)},$$

where $\overline{\boldsymbol{L}}_j^i$ is the matrix obtained by replacing the i-th column of $\overline{\boldsymbol{L}}$ by $\boldsymbol{e}_j$. Now, by Lemma 2.1, we have

$$\det\left(\overline{\boldsymbol{L}}_j^i\right) = (-1)^{i+j} \det\left(\overline{\boldsymbol{L}}^{ij}\right) = \sum_{H \in \mathcal{T}(ij,n)} \beta(H),$$

and using the Kirchhoff's Matrix Tree Theorem we obtain

$$\det\left(\overline{\boldsymbol{L}}\right) = \sum_{H \in \mathcal{T}_{\mathcal{E}}} \beta(H),$$

concluding the proof. □

The denominator in (2.3) is a normalization constant common for all entries of $\boldsymbol{A}$. The sum in the numerator is over all trees in $\mathcal{T}(ij, n)$, which means that A_{ij} is proportional to the (weighted) number of trees that connect i to j without traversing the reference node n, and can be interpreted as the "connection strength" between the nodes i and j in $\mathcal{G}$.

Since $\boldsymbol{A}$ determines the power flow solution $(\boldsymbol{\theta}, \boldsymbol{f})$, Theorem 2.2 allows us to deduce analytical properties of a DC solution using its graph structure. In particular, it provides new graph theoretic expressions for power redistribution after failures, as we derive distribution factors in Chapters 3 and 4.

2.4 Cascading Failure Model

In this section, we propose an integrated failure propagation model considering both the fast-timescale dynamics and slow-timescale line tripping process. In full generality, the failure model applies to both generator failures and line failures, but, to simplify the presentation, in this thesis we focus only on the latter.

We describe the cascading failure process by keeping track of the set of outaged lines $\mathcal{B}(\mathfrak{n}) \subset \mathcal{E}$ over stages $\mathfrak{n} \in \{1, 2, \ldots, N\}$ at a steady state. Following a line outage, we assume that the system evolves on a fast timescale during the transient

phase. When it eventually converges to an equilibrium, we compare the branch flow with the steady-state thermal capacity π_e for the surviving transmission line e. Overloaded lines are then tripped and the cycle repeats.

More specifically, for each stage $\mathfrak{n} \in \{1, 2, \ldots, N\}$, the system evolves according to the dynamics on the topology $\mathcal{G}(\mathfrak{n}) := (\mathcal{N}, \mathcal{E}(\mathfrak{n}))$ where $\mathcal{E}(\mathfrak{n}) := \mathcal{E} \setminus \mathcal{B}(\mathfrak{n})$, and converges to an equilibrium point. At the new equilibrium point, the power injections $\boldsymbol{p}(\mathfrak{n})$ might change due to the control actions of the grid. The flows $\boldsymbol{f}(\mathfrak{n})$ thus redistribute over the surviving network $\mathcal{G}(\mathfrak{n})$ satisfying the DC power flow equations (2.1). If at the equilibrium all branch flows $\boldsymbol{f}(\mathfrak{n})$ are within the corresponding line capacities, then the equilibrium is a secure operating point and the cascade stops. Otherwise, let $\mathcal{F}(\mathfrak{n}) := \{e : |f_e(\mathfrak{n})| > \pi_e,\ e \in \mathcal{E}(\mathfrak{n})\}$ be the subset of lines whose branch flows exceed the corresponding line limits. The lines in $\mathcal{F}(\mathfrak{n})$ operate above their limits at a steady state, so we assume they trip at the end of stage $\mathfrak{n}$ and set $\mathcal{B}(\mathfrak{n}+1) = \mathcal{B}(\mathfrak{n}) \cup \mathcal{F}(\mathfrak{n})$. Line overloads during the transient phase before the system converges to equilibrium are considered tolerable because the transient dynamics does not last long enough to overheat a line (spanning only seconds to a few minutes). This process then repeats for the subsequent stages. We remark that our model captures a simplified line trip dynamic where, after an initiating transmission failure (consisting of one or more line trips), the next set of (one or more) line trips does not occur until the fast-timescale dynamics have converged. In particular our model does not capture the finer thermal dynamics that determines the timing of line trips based on line currents and ambient temperatures.

Fast-timescale Dynamics

We now present the fast-timescale dynamics after a line failure. Using the notation in Table 2.1, the post-contingency linearized frequency dynamics are:

$$\dot{\theta}_j = \omega_j, \quad j \in \mathcal{N} \tag{2.4a}$$

$$M_j \dot{\omega}_j = r_j + d_j - D_j \omega_j - \sum_{e \in \mathcal{E}} C_{je} f_e, \quad j \in \mathcal{N} \tag{2.4b}$$

$$f_{ij} = B_{ij}(\theta_i - \theta_j), \quad (i, j) \in \mathcal{E}. \tag{2.4c}$$

The above differential equations model the fast-timescale frequency response of a power grid to a transmission line failure. Note that we assume generator voltage control is local and converges at a faster timescale than generator-load frequency control. Voltages are therefore assumed to be fixed at their nominal values at the frequency control timescale.

$\boldsymbol{\theta} := (\theta_j, j \in \mathcal{N})$	bus voltage angle *deviations* from pre-contingency values
$\boldsymbol{\omega} := (\omega_j, j \in \mathcal{N})$	bus frequency *deviations* from pre-contingency values
$\boldsymbol{r} := (r_j, j \in \mathcal{N})$	system disturbances
$\boldsymbol{d} := (d_j, j \in \mathcal{N})$	power injection/controllable load *deviations* from pre-contingency values for generator/load buses
$\boldsymbol{p} := (p_j, j \in \mathcal{N})$	aggregate post-contingency injection *deviation*
$\overline{d}_j, \underline{d}_j, j \in \mathcal{N}$	upper and lower limits for the adjustable injection d_j
$D_j\omega_j, j \in \mathcal{N}$	aggregate generator damping for generator buses; aggregate load frequency response for load buses
$M_j, j \in \mathcal{N}$	inertia constants
$\boldsymbol{f} := (f_e, e \in \mathcal{E})$	branch flow *deviations* from pre-contingency values
$\overline{f}_e, \underline{f}_e, e \in \mathcal{E}$	upper and lower limits for branch flow deviations
$n := \lvert\mathcal{N}\rvert$	number of buses
$m := \lvert\mathcal{E}\rvert$	number of transmission lines
$\boldsymbol{C} \in \mathbb{R}^{n\times m}$	*post*-contingency incidence matrix
$\boldsymbol{B} := \mathrm{diag}(B_e, e \in \mathcal{E})$	*post*-contingency branch flow linearization coefficients that depend on line susceptances, nominal voltage magnitudes and reference phase angles

Table 2.1: Variables associated with buses and transmission lines.

The post-contingency injection deviation $p_j(t) := r_j + d_j(t)$ is the sum of the post-contingency disruption r_j and the system response $d_j(t)$. The disruption $\boldsymbol{r} := (r_j, j \in \mathcal{N})$ comes from the effect of transmission line failures. In particular, suppose a failure of line (s, t) with pre-contingency flow f_{st}^{pre} happens, the post-contingency disruption is $r_s = f_{st}^{\mathrm{pre}}$, $r_t = -f_{st}^{\mathrm{pre}}$ and $r_j = 0$ for all other entries. The vector $\boldsymbol{d}(t) := (d_j(t), j \in \mathcal{N})$ models frequency control and their values are determined by a feedback control mechanism (a non-controllable constant-power load is simply a special case where the controls are set as $d_j(t) \equiv d_j$). We assume that the feedback controller is stabilizing and drives the closed-loop system towards an equilibrium as long as the post-contingency disruption $\boldsymbol{r}$ can be feasibly mitigated (see Chapter 6 for more discussion).

Definition 2.3. *A state* $\boldsymbol{x}^* := (\boldsymbol{\theta}^*, \boldsymbol{\omega}^*, \boldsymbol{d}^*, \boldsymbol{f}^*) \in \mathbb{R}^{3n+m}$ *is said to be a* **closed-loop equilibrium** *or simply an* **equilibrium** *of* (2.4) *if the right hand sides of* (2.4a)(2.4b)

are zero and (2.4c) *is satisfied at* $\boldsymbol{x}^*$.

The frequency dynamics (2.4) implies that any equilibrium configuration $\boldsymbol{x}^*$ satisfies

$$\boldsymbol{\omega}^* = \mathbf{0}, \quad \boldsymbol{p}^* = \boldsymbol{r} + \boldsymbol{d}^* = \boldsymbol{C}\boldsymbol{f}^*, \quad \boldsymbol{f}^* = \boldsymbol{B}\boldsymbol{C}^T\boldsymbol{\theta}^*.$$

In other words, $\boldsymbol{x}^*$ satisfies the DC power flow model. [1]

The equilibrium to which the closed-loop system (2.4) converges thus determines the post-contingency DC power flow solution and can in turn impact how failures propagate in the network. A key insight from [3, 41–43, 81] is that the closed-loop equilibrium $\boldsymbol{x}^*$ of (2.4) is also an optimal solution of a certain DC-based optimization problem that can be determined explicitly. Different frequency controllers $d(t)$ induce different dynamics (2.4), whose closed-loop equilibria solve optimization problems with corresponding objective functions and constraints. As such, different frequency controllers can alternatively be modelled by the underlying optimization problems that their equilibria solve.

We remark that the model (2.4) can be extended to include load buses j where $M_j = 0$. This system of differential algebraic equations assumes that the load dynamics evolve at a faster timescale than generator dynamics and are described by power flow equations. Including load buses does not change the stability properties of the closed-loop system, though the argument is slightly more complicated [41, 43].

Recovering DC Cascading Failure Models

The dynamic model (2.4) describes secondary frequency control where the frequency deviations $\boldsymbol{\omega}(t)$ are driven to zero. When we focus on controllers that only achieve primary frequency control, the equilibrium frequency $\boldsymbol{\omega}^*$ may be nonzero. That is, as the system converges in this sense, the phase angles $\boldsymbol{\theta}^*(t)$ do not necessarily stay at a constant value, but may change in constant rate over time. In such context, we can modify (2.4) as follows to describe primary frequency dynamics:

$$M_j\dot{\omega}_j = r_j + d_j - D_j\omega_j - \sum_{e\in\mathcal{E}} C_{je}f_e, \quad j \in \mathcal{N} \tag{2.5a}$$

$$f_{ij} = B_{ij}(\theta_i - \theta_j), \quad (i,j) \in \mathcal{E}. \tag{2.5b}$$

[1] In primary frequency control literature (see [3, 41] for instance), the right hand side of (2.4a) is not required to be zero for an equilibrium point $\boldsymbol{x}^*$. We impose this requirement on (2.4a) here as our discussion focuses on controllers that achieve secondary frequency control and thus $\boldsymbol{\omega}^* = \mathbf{0}$ always holds. Our model and results can be readily extended to the case where $\boldsymbol{\omega}^* \neq \mathbf{0}$ as we show later in this section.

By relaxing the requirement on $\boldsymbol{\omega}^* = 0$ at equilibrium, the above model enables extra freedom in the choice of d_j. We now show that by using the classical droop control [82] as the dynamics for d_j's in (2.5), the static DC cascading failure model used in Chapters 3 and 4 and previous literature such as [9, 38, 40, 44] can be readily recovered. The DC failure model assumes that, following a line failure, the power injections adjust under the power balancing rule $\mathcal{R}_c$. Specifically, *the injections do not change after a non-cut failure, and injections change proportionally to compensate for the power imbalance after a cut set failure*.

As shown in [3], the *closed-loop* equilibrium of (2.5) under droop control is the unique[2] optimal solution to the following optimization on the post-contingency network:

$$\min_{\boldsymbol{\theta},\boldsymbol{\omega},\boldsymbol{d},\boldsymbol{f}} \quad \sum_{j\in\mathcal{N}} \frac{d_j^2}{2Z_j} + \frac{D_j\omega_j^2}{2} \tag{2.6a}$$

$$\text{s.t.} \quad \boldsymbol{r} - \boldsymbol{d} - \boldsymbol{D}\boldsymbol{\omega} = \boldsymbol{C}\boldsymbol{f} \tag{2.6b}$$

$$\boldsymbol{f} - \boldsymbol{B}\boldsymbol{C}^T\boldsymbol{\theta} = \boldsymbol{0} \tag{2.6c}$$

$$\underline{d}_j \le d_j \le \overline{d}_j, \quad j \in \mathcal{N}, \tag{2.6d}$$

where Z_j's are the generators' participation factors [82]. By plugging (2.6c) into (2.6b), it is easy to check that any feasible point $\boldsymbol{x} = (\boldsymbol{\theta}, \boldsymbol{\omega}, \boldsymbol{d}, \boldsymbol{f})$ of (2.6) satisfies $\sum_j r_j = \sum_j (d_j + D_j\omega_j)$. Cauchy-Schwarz inequality then implies that

$$\begin{aligned}\Big(\sum_{j\in\mathcal{N}} r_j\Big)^2 &= \Big[\sum_{j\in\mathcal{N}} \big(d_j + D_j\omega_j\big)\Big]^2 \\ &\le \sum_{j\in\mathcal{N}} \Big(\frac{d_j^2}{2Z_j} + \frac{D_j\omega_j^2}{2}\Big) \sum_{j\in\mathcal{N}} \big(2Z_j + 2D_j\big),\end{aligned}$$

for which equality holds if and only if

$$d_j = \frac{Z_j}{\sum_j \big(Z_j + D_j\big)} \sum_j r_j, \quad \omega_j = \frac{\sum_j r_j}{\sum_j \big(Z_j + D_j\big)}. \tag{2.7}$$

Therefore, if the control limits (2.6d) are not active, (2.7) is always satisfied at the optimal point $\boldsymbol{x}^* = (\boldsymbol{\theta}^*, \boldsymbol{\omega}^*, \boldsymbol{d}^*, \boldsymbol{f}^*)$.

Now, consider a line e being tripped from the transmission network $\mathcal{G}$, and for simplicity assume the control limits (2.6d) are not active. If e is a bridge, the

[2]The equilibrium is unique up to an arbitrary reference phase angle.

tripping of e results in two islands of $\mathcal{G}$, say $\mathcal{D}_1$ and $\mathcal{D}_2$, and two optimization problems (2.6) correspondingly. For $l = 1, 2$, $\sum_{j\in\mathcal{D}_l} r_j$ represents the total net power imbalance in $\mathcal{D}_l$, and therefore (2.7) implies that droop control adjusts the system injections so that the power imbalance is distributed to all generators proportional to their participation factors in both $\mathcal{D}_1$ and $\mathcal{D}_2$. If $e = (i, j)$ is not a bridge, denoting the original flow on e before it is tripped as f_e, then $r_i = f_e$, $r_j = -f_e$ and $r_k = 0$ otherwise. As a result, we have $\sum_{j\in\mathcal{N}} r_j = 0$ in this case, and thus (2.7) implies the system operating point remains unchanged in equilibrium, i.e., $d_j = \omega_j = 0, \forall j \in \mathcal{N}$. Moreover, one can show that this still holds when (2.6d) is active with a more involved analysis on the KKT conditions of (2.6).

Remarks

The crux of our integrated failure propagation model lies in the interplay between the slow-timescale line tripping process and the fast-timescale dynamics. By explicitly modeling fast-timescale dynamics as part of the cascading process, our model offers more flexibility in both modeling the failure process and designing control actions. On the one hand, different choices of $\boldsymbol{d}(t)$ induce different cascading failure process. As we show earlier, if we adopt droop control for $\boldsymbol{d}(t)$, the classical DC failure model can be readily recovered. As another example, if automatic generation control (AGC) is adopted for $\boldsymbol{d}(t)$, the cascading process will unfold in a way where injections and line flows are changed even after a non-cut failure. Since traditional AGC does not enforce congestion management, some lines may carry flows above their thermal limits and are tripped subsequently.

On the other hand, the integrated model offers an additional means to mitigate cascading failures through a better design of the frequency control mechanism on a fast timescale. In Chapter 6, we propose a failure mitigation approach that leverages this extra freedom by adopting the unified controller (UC) for $\boldsymbol{d}(t)$. In contrast to traditional AGC, UC drives the closed-loop system to an equilibrium that respects line limits whenever possible. The proposed adaptive control strategy offers strong guarantees in both the mitigation and localization of line failures.

It should be noted that even though the proposed integrated model considers fast-timescale dynamics after line failures, the equilibrium is described by the optimal solution to an optimization problem. Therefore, the complicated and time-consuming dynamic system simulations can be avoided. This advantage makes theoretical analysis for the failure propagation tractable.

We conclude this section by summarizing the models that will be used in this thesis. In Chapters 3-5, our goal is to characterize the failure propagation pattern in power systems. Therefore, we adopt the commonly used DC failure model which is underlied by the droop control mechanism. Starting from Chapter 6, we explore the active control actions to mitigate the failure. In Chapter 6, we adopt the unified controller and provably show that our strategy greatly improves grid reliability. In Chapter 7, we propose a corrective control method that achieves near-optimal control costs despite using only localized control actions.

Chapter 3

FAILURES IN POWER SYSTEMS: NON-CUT OUTAGES

Cascading failures in power systems propagate non-locally, making their analysis and mitigation difficult. The current industry practice for mitigating cascading failures relies on simulation-based analysis of creditable contingencies [20]. The size of this contingency set, and thus the level of security guarantee, is often constrained by computational power, undermining its effectiveness in view of the enormous number of components in power networks. More importantly, this approach is difficult to make general inferences about failure patterns. This lack of structural properties is a key challenge in the modeling, control, and mitigation of cascading failures in power systems.

In the following two chapters, we focus on transmission line failures and establish a mathematical theory that characterizes line failure localization properties of power systems. This theory makes crucial use of the weighted Laplacian matrix of a transmission network and its spectral properties. Our results unveil a deep connection between power redistribution patterns and the network block decomposition of a grid. We show how specific topological structures naturally emerge in the analysis of several important and well-studied quantities in power system contingency analysis, such as the generation shift sensitivity factors and the line outage redistribution factors. In contrast to pure graphical models such as those in [14, 83, 84], our topological interpretations do not rely on any simplifications on failure propagation, but capture Kirchhoff's and Ohm's Law in a precise way under the widely-used steady-state DC power flow model [9, 38, 40, 44]. In particular, we adopt the classical balancing rule $\mathcal{R}_c$.

In this chapter, we restrict our attention to the case where the network remains connected after line failures and study how such failures impact the branch flows on the surviving network. In this scenario, the power injections remain balanced and do not change after the contingency. Our theory reveals a decoupling structure of the transmission network that leads to failure localizability in a cascading process. More specifically, we show that when a non-cut set of lines trips, any other line that is not in the same block (see Definition 3.1) of one of the tripped lines is not affected. In other words, non-cut failures cannot cross the boundaries of the block

decomposition of the transmission network. In the next chapter, we consider the scenario where the set of tripped lines disconnects the network into two or more connected components, called islands, and injections must be adjusted to rebalance the power injections.

Our theoretical analysis relies on Theorem 2.2 that relates the power redistribution to graphical structures. In particular, Theorem 2.2 states that the distribution of specific collections of subtrees of the transmission network fully determines the system state under a given set of injections. We then establish a new set of graphical representations of power transfer distribution factors and line outage distribution factors in contingency analysis. This novel graph-theoretical viewpoint enables us to derive precise algebraic properties of power redistribution using purely graphical argument, and shows that disturbances propagate through "subtrees" in a power network. Using this framework, we derive the *Simple Cycle Criterion* that precisely determines whether the failure of one line can impact another line in a given network and fully characterizes non-cut failure propagation.

3.1 Block Decomposition

Recall that in Theorem 2.2, we relate the reduced Laplacian matrix $\boldsymbol{L}$ and the extended inverse Laplacian matrix $\boldsymbol{A}$ explicitly to the graph structure. We now define several concepts in graph theory that will be useful in the rest of this chapter.

Consider a connected undirected graph $\mathcal{G} = (\mathcal{N}, \mathcal{E})$. Let $\mathfrak{R}$ be the relation on the edges of $\mathcal{G}$ defined by $e_1 \mathfrak{R} e_2$ if (and only if) $e_1 = e_2$ or they belong to a common simple cycle of $\mathcal{G}$[1]. It can be shown that $\mathfrak{R}$ is an equivalence relation on the set of edges $\mathcal{E}$, inducing network blocks as follows.

Definition 3.1 (Blocks, bridges, cut vertices)**.**

1. *The subgraphs of $\mathcal{G}$ induced by the equivalence classes of $\mathfrak{R}$ are called* **blocks** *of $\mathcal{G}$.*
2. *A node of $\mathcal{G}$ that is part of two or more blocks is called a* **cut vertex** *of $\mathcal{G}$.*
3. *An edge in a singleton equivalent class is called a* **bridge** *of $\mathcal{G}$. A block that is not a bridge is called a* **non-bridge** *block.*

[1] A cycle is simple if the only repeated vertex is the first/last one.

4. *A subset $F \subseteq \mathcal{E}$ of edges is called a* **cut set** *of $\mathcal{G}$ if removing all edges in F disconnects the graph. A set $F \subseteq \mathcal{E}$ is called a* **non-cut set** *if F is not a cut set.*

A block is also called a biconnected (or 2-connected) component of $\mathcal{G}$ because the block will remain connected if any 1 edge is removed from the block. The removal of a cut vertex disconnects $\mathcal{G}$. A bridge is a cut set of size one, since its removal disconnects $\mathcal{G}$. Two non-bridge blocks are connected either by a bridge or by a cut vertex. These definitions are illustrated in Figure 3.1.

The block decomposition of a graph $\mathcal{G}$ is unique and there exist efficient algorithms to find all blocks of a graph $\mathcal{G}$ that run in $O(|\mathcal{N}| + |\mathcal{E}|)$ in time and space on a single processor or run in $O(\log |\mathcal{N}|)$ in time and $O(|\mathcal{N}| + |\mathcal{E}|)$ in space on $O(|\mathcal{N}| + |\mathcal{E}|)$ processors [85].

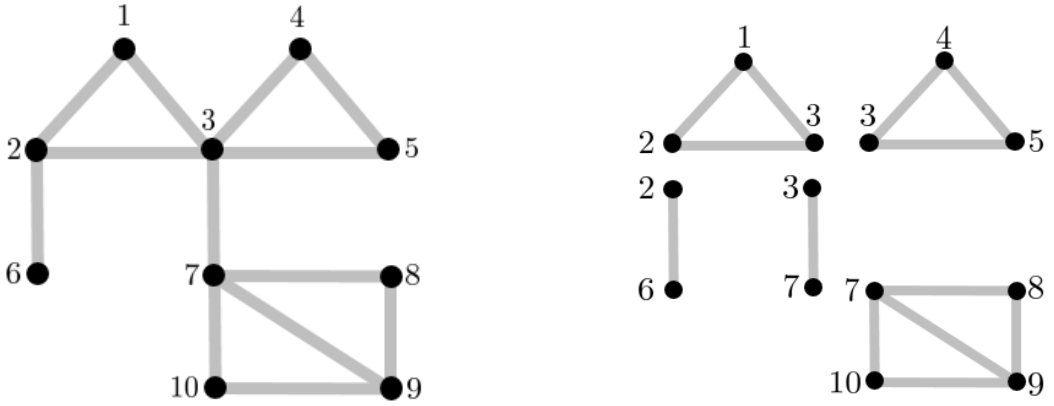

(a) An undirected graph $\mathcal{G}$.

(b) The block decomposition of $\mathcal{G}$.

Figure 3.1: An illustration of the network block decomposition. Vertices $2, 3, 7$ are cut vertices of $\mathcal{G}$. Edges $(2, 6)$ and $(3, 7)$ are bridges.

3.2 Distribution Factors

In this section, we focus on *distribution factors* widely used in contingency analysis, and derive novel expressions for them in terms of network graph structures. We also explain the implication of this spectral representation of network graph on distribution factors. In Section 3.3, we use these results to reveal the decoupling structure of distribution factors and the resulting failure localization property of a power network.

Power Transfer Distribution Factor (PTDF)

Consider a pair of buses $\hat{i}$ and $\hat{j}$, not necessarily adjacent in the graph $\mathcal{G}$. Suppose the injection at bus $\hat{i}$ is increased by $\Delta_{\hat{i}\hat{j}}$, the injection at bus $\hat{j}$ is reduced by $\Delta_{\hat{i}\hat{j}}$, and all other injections remain unchanged so that the new injections remain balanced. Let f_e and $\tilde{f_e}$ denote the branch flow on any line $e \in \mathcal{E}$ before and after the injection change (both uniquely determiend by the DC power flow equations (2.1)) and let $\Delta f_e := \tilde{f_e} - f_e$ be their difference. The *power transfer distribution factor (PTDF)*, also known as *generation shift sensitivity factor*, is defined as [86]:

$$D_{e,\hat{i}\hat{j}} := \frac{\tilde{f_e} - f_e}{\Delta_{\hat{i}\hat{j}}} = \frac{\Delta f_e}{\Delta_{\hat{i}\hat{j}}}.$$

Let $e = (i, j)$, then the factor $D_{e,\hat{i}\hat{j}}$ can be explicitly computed in terms of matrix $\boldsymbol{A}$ (see (2.2) for the definition of $\boldsymbol{A}$) [86]:

$$D_{e,\hat{i}\hat{j}} = B_e(A_{i\hat{i}} + A_{j\hat{j}} - A_{i\hat{j}} - A_{j\hat{i}}).$$

Recall the definitions of spanning trees and spanning forests of a graph in Section 2.3. Applying Theorem 2.2 to this formula yields the following result, proved in Section 3.5.

Theorem 3.2. *If $\mathcal{G}$ is connected, then for any pair of nodes $\hat{i}, \hat{j} \in \mathcal{N}$ and any edge $e = (i, j) \in \mathcal{E}$, we have*

$$D_{e,\hat{i}\hat{j}} = \frac{B_e \left(\sum_{H \in \mathcal{T}(i\hat{i}, j\hat{j})} \beta(H) - \sum_{H \in \mathcal{T}(i\hat{j}, j\hat{i})} \beta(H) \right)}{\sum_{H \in \mathcal{T}_{\mathcal{E}}} \beta(H)}.$$

Despite its apparent complexity, this formula carries an intuitive graphical meaning. The two sums in the numerator are over the spanning forests $\mathcal{T}(i\hat{i}, j\hat{j})$ and $\mathcal{T}(i\hat{j}, j\hat{i})$. Each element in $\mathcal{T}(i\hat{i}, j\hat{j})$, as illustrated in Fig. 3.2, specifies a way to connect $\hat{i}$ to i and $\hat{j}$ to j through disjoint trees and represents a possible path for buses $\hat{i}, \hat{j}$ to "spread" impact to line (i, j). Similarly, elements in $\mathcal{T}(i\hat{j}, j\hat{i})$ represents possible paths for buses $\hat{i}, \hat{j}$ to "spread" impact to (j, i), which counting orientation, contributes negatively to line l. Theorem 3.2 thus implies that the impact of shifting generations from $\hat{j}$ to $\hat{i}$ propagates to the line $e = (i, j)$ through all possible spanning forests that connect the endpoints $\hat{i}, \hat{j}, i, j$ (accounting for orientation). The relative strength of the trees in these two families determines the sign of $D_{e,\hat{i}\hat{j}}$.

If $\hat{e} = (\hat{i}, \hat{j}) \in \mathcal{E}$ is also a transmission line in the grid, we use the more compact notation $D_{e\hat{e}}$ for $D_{e,\hat{i}\hat{j}}$ and introduce the $m \times m$ PTDF matrix $\boldsymbol{D} := (D_{e\hat{e}}, e, \hat{e} \in \mathcal{E})$.

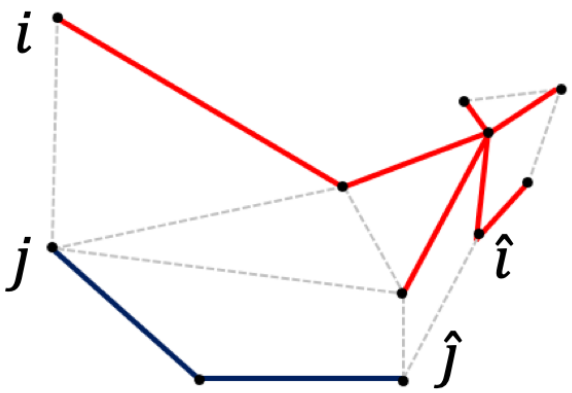

Figure 3.2: An example element in $\mathcal{T}(i\hat{i}, j\hat{j})$. The spanning trees containing $\{i, \hat{i}\}$ and $\{j, \hat{j}\}$ are highlighted as solid lines.

Corollary 3.3 summarizes how the PTDF matrix $\boldsymbol{D}$ can be expressed explicitly in terms of matrix A.

Corollary 3.3. *Assume $\mathcal{G}$ is connected. Then,*

1. $\boldsymbol{D} = \boldsymbol{B}\boldsymbol{C}^T\boldsymbol{A}\boldsymbol{C}$.
2. *For each line $e \in \mathcal{E}$, the corresponding diagonal entry of $\boldsymbol{D}$ is given by:*

$$D_{ee} = 1 - \frac{\sum_{H \in \mathcal{T}_{-e}} \beta(H)}{\sum_{H \in \mathcal{T}_{\mathcal{E}}} \beta(H)}.$$

Hence, $D_{ee} = 1$ if e is a bridge and $0 < D_{ee} < 1$ otherwise.

This corollary is a direct consequence of Theorem 3.2, and we omit its proof.

Line Outage Distribution Factor (LODF)

The line outage distribution factor (LODF) describes the impact of line outages on the power flows in the post-contingency network. We call the contingency a *non-cut (F) outage* if a non-cut set F of lines trip simultaneously, and a *non-bridge ($\hat{e}$) outage* when the non-cut set $F = \{\hat{e}\}$ is a singleton. We first study the impact of a non-bridge outage, and then generalize it to a non-cut set outage.

Non-bridge $\hat{e}$ outage

The line outage distribution factor (LODF) $K_{e\hat{e}}$ is defined to be the branch flow change Δf_e on a post-contingency surviving line e when a *single non-bridge* line $\hat{e}$

trips, normalized by the pre-contingency branch flow $f_{\hat{e}}$ over the tripped line:

$$K_{e\hat{e}} := \frac{\Delta f_e}{f_{\hat{e}}}, \quad e \neq \hat{e} \in \mathcal{E}, \text{ non-bridge line } \hat{e} \in \mathcal{E},$$

assuming that the injections remain unchanged since the network remains connected.

Writing $e = (i, j)$, $\hat{e} = (\hat{i}, \hat{j})$, $K_{e\hat{e}}$ can be calculated as [86]:

$$K_{e\hat{e}} = \frac{B_e \left(A_{i\hat{i}} + A_{j\hat{j}} - A_{i\hat{j}} - A_{j\hat{i}} \right)}{1 - B_{\hat{e}}(A_{\hat{i}\hat{i}} + A_{\hat{j}\hat{j}} - A_{\hat{i}\hat{j}} - A_{\hat{j}\hat{i}})} = \frac{D_{e\hat{e}}}{1 - D_{\hat{e}\hat{e}}}, \tag{3.1}$$

which is independent of the power injections. This formula only holds if the post-contingency graph $\tilde{\mathcal{G}} := (\mathcal{N}, \mathcal{E} \backslash \{\hat{e}\})$ is still connected, as otherwise its denominator is 0 by Corollary 3.3. Combining Theorem 3.2 and Corollary 3.3 immediately yields the following new formula for $K_{e\hat{e}}$.

Theorem 3.4. *Let $\hat{e} = (\hat{i}, \hat{j})$ be an edge such that $\tilde{\mathcal{G}} := (\mathcal{N}, \mathcal{E} \backslash \{\hat{e}\})$ is connected. Then, for any other edge $e = (i, j)$,*

$$K_{e\hat{e}} = \frac{B_e \left(\sum_{H \in \mathcal{T}(i\hat{i}, j\hat{j})} \beta(H) - \sum_{H \in \mathcal{T}(i\hat{j}, j\hat{i})} \beta(H) \right)}{\sum_{H \in \mathcal{T}_{-\hat{e}}} \beta(H)}. \tag{3.2}$$

As in Theorem 3.2, each term of (3.2) also carries clear graphical meanings: (a) The numerator of (3.2) quantifies the impact of tripping $\hat{e}$ propagating to e through all possible trees that connect $\hat{e}$ to e, counting orientation. (b) The denominator of (3.2) sums over all spanning trees of $\mathcal{G}$ that do not pass through $\hat{e} = (\hat{i}, \hat{j})$, and each tree of this type specifies an alternative path that power can flow through if line $\hat{e}$ is tripped. When there are more trees of this type, the network has a better ability to "absorb" the impact of line $\hat{e}$ being tripped, and the denominator of (3.2) precisely captures this effect by saying that the impact of $\hat{e}$ being tripped on other lines is inversely proportional to the sum of all alternative tree paths in the network. (c) The susceptance B_e in (3.2) captures the intuition that lines with smaller susceptance tend to be less sensitive to power flow changes from other parts of a power network.

Non-cut F outage

We now extend the results for LODFs from a non-bridge outage to a non-cut outage. Let $F \subsetneq \mathcal{E}$ be a non-cut set of lines that are disconnected simultaneously and $m_F := |F|$ be the number of disconnected lines. Denote by $-F := \mathcal{E} \setminus F$ the set of surviving lines and assume that the injections $\boldsymbol{p}$ remains unchanged. Partition the

susceptance matrix $\boldsymbol{B}$ and the incidence matrix $\boldsymbol{C}$ into submatrices corresponding to surviving lines in $-F$ and tripped lines in F:

$$\boldsymbol{B} =: \begin{bmatrix} \boldsymbol{B}_{-F} & \boldsymbol{0} \\ \boldsymbol{0} & \boldsymbol{B}_F \end{bmatrix}, \quad \boldsymbol{C} =: [\boldsymbol{C}_{-F} \ \ \boldsymbol{C}_F]. \tag{3.3}$$

Similarly, we can partition the PTDF matrix $\boldsymbol{D} = (D_{e\hat{e}}, e, \hat{e} \in \mathcal{E})$ into submatrices corresponding to non-outaged lines in $-F$ and outaged lines in F, possibly after permutations of rows and columns[2]:

$$\boldsymbol{D} = \begin{bmatrix} \boldsymbol{D}_{-F,-F} & \boldsymbol{D}_{-FF} \\ \boldsymbol{D}_{F,-F} & \boldsymbol{D}_{FF} \end{bmatrix}.$$

Since $\boldsymbol{D} = \boldsymbol{B}\boldsymbol{C}^T\boldsymbol{A}\boldsymbol{C}$ from Corollary 3.3, we have

$$\boldsymbol{D} = \begin{bmatrix} \boldsymbol{B}_{-F}\boldsymbol{C}_{-F}^T\boldsymbol{A}\boldsymbol{C}_{-F} & \boldsymbol{B}_{-F}\boldsymbol{C}_{-F}^T\boldsymbol{A}\boldsymbol{C}_F \\ \boldsymbol{B}_F\boldsymbol{C}_F^T\boldsymbol{A}\boldsymbol{C}_{-F} & \boldsymbol{B}_F\boldsymbol{C}_F^T\boldsymbol{A}\boldsymbol{C}_F \end{bmatrix}.$$

Similarly to the case of non-bridge outage, the post-contingency flow changes $\Delta\boldsymbol{f}_{-F} := (\Delta f_e, e \in -F)$ on the surviving lines depend linearly on the pre-contingency branch flows $\boldsymbol{f}_F := (f_{\hat{e}}, \hat{e} \in F)$ on the tripped lines. The sensitivities of $\Delta\boldsymbol{f}_{-F}$ to $\boldsymbol{f}_F$ implicitly define a $(m - m_F) \times m_F$ matrix $\boldsymbol{K}^F := \boldsymbol{K}^F_{-FF} := (K^F_{e\hat{e}}, e \in -F, \hat{e} \in F)$, called the *Generalized Line Outage Distribution Factor (GLODF)* with respect to a non-cut F outage, namely

$$\Delta\boldsymbol{f}_{-F} = \boldsymbol{K}^F\boldsymbol{f}_F, \quad \text{for non-cut set } F \subsetneq \mathcal{E}. \tag{3.4}$$

On the other hand, if we stack the LODF for single line outages into a matrix $\boldsymbol{K}_{-FF} := (K_{e\hat{e}}, e \in -F, \hat{e} \in F)$, $\boldsymbol{K}_{-FF}$ has the same dimension as the GLODF $\boldsymbol{K}^F$ for a non-cut F outage. Note that every element $K_{e\hat{e}}$ is the LODF when single non-bridge lines are tripped, as derived in (3.1). Equivalently, we can write $\boldsymbol{K}_{-FF}$ in the matrix form:

$$\boldsymbol{K}_{-FF} = \boldsymbol{D}_{-FF}\left(\boldsymbol{I} - \operatorname{diag}(\boldsymbol{D}_{FF})\right)^{-1}, \tag{3.5}$$

where $\operatorname{diag}(\boldsymbol{D}_{FF}) := \operatorname{diag}(D_{ee}, e \in F)$. In general $\boldsymbol{K}^F \neq \boldsymbol{K}_{-FF}$. However, they are related in the next result. Let $\boldsymbol{L}_{-F} := \boldsymbol{C}_{-F}\boldsymbol{B}_{-F}\boldsymbol{C}_{-F}^T$ be the Laplacian matrix of the *post*-contingency network. Let $\overline{\boldsymbol{L}}_{-F}$ be the submatrix of $\boldsymbol{L}_{-F}$ obtained by deleting its n-th row and column, and $\boldsymbol{A}_{-F} := \begin{bmatrix} (\overline{\boldsymbol{L}}_{-F})^{-1} & \boldsymbol{0} \\ \boldsymbol{0} & 0 \end{bmatrix}$.

[2]We also write $D_{F,\hat{F}}$ as $D_{F\hat{F}}$ when there is no confusion.

Theorem 3.5 (GLODF $\boldsymbol{K}^F$ for non-cut outage)**.** *Suppose a non-cut set $F \subsetneq \mathcal{E}$ of lines trip simultaneously so that the surviving graph $(\mathcal{N}, \mathcal{E}\setminus F)$ remains connected.*

1. *The GLODF $\boldsymbol{K}^F$ defined in* (3.4) *is given in terms of post-contingency network by:*

$$\boldsymbol{K}^F = \boldsymbol{B}_{-F}\boldsymbol{C}_{-F}^T\,\boldsymbol{A}_{-F}\,\boldsymbol{C}_F, \tag{3.6a}$$

2. *$\boldsymbol{K}^F$ is given in terms of pre-contingency inverses by:*

$$\boldsymbol{K}^F = \boldsymbol{D}_{-FF}\left(\boldsymbol{I} - \boldsymbol{D}_{FF}\right)^{-1}, \tag{3.6b}$$

   or, equivalently,

$$\boldsymbol{K}^F = \boldsymbol{B}_{-F}\boldsymbol{C}_{-F}^T\boldsymbol{A}\boldsymbol{C}_F\left(\boldsymbol{I} - \boldsymbol{B}_F\boldsymbol{C}_F^T\boldsymbol{A}\boldsymbol{C}_F\right)^{-1}. \tag{3.6c}$$

   The matrix $\boldsymbol{I} - \boldsymbol{D}_{FF} = \boldsymbol{I} - \boldsymbol{B}_F\boldsymbol{C}_F^T\boldsymbol{A}\boldsymbol{C}_F$ is invertible provided F is a non-cut set of disconnected lines.

3. *$\boldsymbol{K}^F$ is related to the LODF matrix $\boldsymbol{K}_{-FF}$ when single non-bridge lines are outaged through:*

$$\boldsymbol{K}^F = \boldsymbol{K}_{-FF}\left(\boldsymbol{I} - \operatorname{diag}(\boldsymbol{D}_{FF})\right)\left(\boldsymbol{I} - \boldsymbol{D}_{FF}\right)^{-1}. \tag{3.6d}$$

Theorem 3.5 is proved in Section 3.5. The formulae (3.6b)-(3.6c) generalize (3.1) from a non-bridge outage to a non-cut set outage. As mentioned earlier, $\boldsymbol{K}^F \neq \boldsymbol{K}_{-FF}$ unless $F = \{\hat{e}\}$ is a singleton and (3.6d) clarifies their relationship. This fact shows that the impact for multiple simultaneous line outages is not a simple superposition of the corresponding single line outages, as their effects are coupled by power flow physics and network topology.

In addition, Theorem 3.5 provides an alternative method to compute the GLODF over the post-contingency network. In particular, (3.6a) suggests that the GLODF $K_{e\hat{e}}^F$ equals to the PTDF $D_{e\hat{e}}^{(F)}$ over the post-contingency network $\tilde{\mathcal{G}} = (\mathcal{N}, \mathcal{E} \setminus F)$. In contrast to the aforementioned fact that the impact for multiple simultaneous line outages is not a simple superposition of the corresponding single line outages over the pre-contingency network, it can be computed directly from the flow changes caused by generation shifting over the *post*-contingency network:

$$\Delta f_e = \boldsymbol{K}_e^F\boldsymbol{f}_F = B_e\boldsymbol{C}_e^T\,\boldsymbol{A}_{-F}\,\boldsymbol{C}_F\boldsymbol{f}_F = \sum_{\hat{e}\in F} D_{e\hat{e}}^{(F)}C_{\hat{e}}f_{\hat{e}},$$

where $\boldsymbol{K}_e^F$ is the e-th row of $\boldsymbol{K}^F$ and $\boldsymbol{C}_e := (\boldsymbol{e}_i - \boldsymbol{e}_j)$ is the incidence vector for line $e = (i, j)$. As we will show later in this chapter, the perspective from post-contingency network can significantly simplify the analysis of GLODFs.

3.3 Line Failure Localization: Non-cut Outages

In this section, we first introduce the Simple Cycle Criterion that characterizes whether the branch flow on a surviving line is impacted by a non-bridge outage. We then use it to explain failure localizability of a power network: for a non-cut set outage, the impact is localized within each block where outages occur.

Simple Cycle Criterion

Theorem 3.4 shows that whether the tripping of a line $\hat{e}$ will impact another line e or not depends on how these two lines are connected by subtrees of $\mathcal{G}$. We now establish a simple criterion that can be directly verified on the network graph. It states that the outage of line $\hat{e}$ will impact the branch flow on line e, i.e., $K_{e\hat{e}} \neq 0$, only if there is a simple cycle in $\mathcal{G}$ that contains both lines (recall that a cycle in a graph $\mathcal{G}$ is called a *simple cycle* if it visits each vertex at most once except for the first/last vertex).

The converse holds "almost surely" in the following sense. Suppose the line susceptances are specified by a random vector $\boldsymbol{B} + \boldsymbol{w} := (B_e + w_e, e \in \mathcal{E})$ where the random vector $\boldsymbol{w} := (w_e, e \in \mathcal{E})$ is drawn from a multidimensional probability measure μ that is absolutely continuous with respect to the Lebesgue measure $\mathcal{L}_m$, i.e., for any measureable set X, $\mathcal{L}_m(X) = 0$ implies $\mu(X) = 0$. By the Radon-Nikodym Theorem [87], the probability measure μ is absolutely continuous with respect to $\mathcal{L}_m$ if and only if it has a probability density function. This essentially amounts to requiring the measure μ to not contain Dirac masses. In practice, such random vector $\boldsymbol{w}$ can model manufacturing, measurement, or modeling errors. For two predicates $s_1 := s_1(\boldsymbol{B} + \boldsymbol{w})$ and s_2 with s_1 dependent on the value of the random vector $\boldsymbol{B} + \boldsymbol{w}$, we say s_1 *"if" and only if* s_2 when s_1 implies s_2 and s_2 almost surely implies s_1, or mathematically, we have

$$s_1 \implies s_2 \quad \text{and} \quad s_2 \implies \mu(s_1(\boldsymbol{B} + \boldsymbol{w})) = 1.$$

With above notations, we establish the *Simple Cycle Criterion* in the following theorem (proved in Section 3.5) to characterize the LODF for single non-bridge failures. Specifically, for a non-bridge line failure $\hat{e}$ and a surviving line e, we have the LODF is non-zero, i.e., $K_{e\hat{e}} \neq 0$ only if there exists a simple cycle contains both

e and $\hat{e}$ in the pre-contingency network. On the other hand, if such a simple cycle exists, we can almost surely conclude that the LODF $K_{e\hat{e}}$ is non-zero.

Theorem 3.6 (Simple Cycle Criterion)**.** *For any $\hat{e} = (\hat{i}, \hat{j}) \in \mathcal{E}$ such that $\mathcal{G}' := (\mathcal{N}, \mathcal{E}\setminus\{\hat{e}\})$ is connected and $e = (i, j) \in \mathcal{E}$, we have $K_{e\hat{e}} \neq 0$ "if" and only if there exists a simple cycle in $\mathcal{G}$ that contains both e and $\hat{e}$.*

The following zero probability example shows that the *if* part does not follow.

Example 1. *Consider a complete graph on n vertices and pick $e = (i, j)$ and $\hat{e} = (\hat{i}, \hat{j})$ such that e and $\hat{e}$ do not share any common endpoints: $i \neq j \neq \hat{i} \neq \hat{j}$. Assume the line susceptances are all 1. By symmetry, it is eay to see that there is a bijective correspondence between $\mathcal{T}(i\hat{i}, j\hat{j})$ and $\mathcal{T}(i\hat{j}, j\hat{i})$, and thus*

$$\sum_{H\in\mathcal{T}(i\hat{i},j\hat{j})} \beta(H) - \sum_{H\in\mathcal{T}(i\hat{j},j\hat{i})} \beta(H) = 0.$$

By Theorem 3.4, we then have $K_{e\hat{e}} = 0$.

This example shows that even if there exists a simple cycle connecting e and $\hat{e}$, when the graph $\mathcal{G}$ is rich in symmetries, it is still possible that a failure of e does not impact line $\hat{e}$. Nevertheless, this issue is not critical as such symmetry almost never happens in practical systems because of heterogeneity in line susceptances. In fact, even if the system is originally symmetric, an infinitesimal change on the line susceptances is enough to break the symmetry, as stated in Theorem 3.6.

Localization of Non-bridge Outages

We now use Theorem 3.6 to explain failure localizability of the network graph $\mathcal{G}$ using its unique block decomposition (see Definition 3.1). Recall that two distinct edges are in the same block if and only if there is a simple cycle that contains both of them. Theorem 3.6 then implies the following failure localization property when a single non-bridge line $\hat{e}$ trips: only surviving lines in the same block as $\hat{e}$ may see their branch flows impacted. In particular, since a bridge is a block, a non-bridge outage will not impact the branch flow on any other bridge. Additionally, the PTDF matrix $\boldsymbol{D}$ has the same decoupling structure with the block decomposition as $D_{e\hat{e}} = K_{e\hat{e}}(1 - D_{\hat{e}\hat{e}})$ from (3.1). From these considerations, the following result readily follows.

Corollary 3.7 (Failure localization: non-bridge outage)**.** *Suppose a single non-bridge line $\hat{e} = (\hat{i}, \hat{j})$ trips so that the surviving graph $(\mathcal{N}, \mathcal{E}\backslash\{\hat{e}\})$ remains connected. For any surviving line $e = (i, j)$ the following statements hold:*

1. *LODF $K_{e\hat{e}} = 0$ if e and $\hat{e}$ are in different blocks of $\mathcal{G}$.*
2. *PTDF $D_{e\hat{e}} = 0$ if and only if $K_{e\hat{e}} = 0$.*

The converse part of the Simple Cycle Criterion asserts that $K_{e\hat{e}} \neq 0$ "if" there is a simple cycle that contains both e and $\hat{e}$. This immediately implies the converse of Corollary 3.7 that $K_{e\hat{e}} \neq 0$ "if" e and $\hat{e}$ are in the same block of $\mathcal{G}$.

Assume there is no bridge in the graph $\mathcal{G}$ and define the matrix $\boldsymbol{K} := (K_{e\hat{e}}, e \in \mathcal{E}, \hat{e} \in \mathcal{E})$ with $K_{ee} = 1$. Suppose the lines are ordered with blocks. Simple Cycle Criterion suggests that not only the matrix $\boldsymbol{K}$ is block-diagnonal, but also that almost surely with respect to μ, every entry of the diagonal blocks of $\boldsymbol{K}$ is non-zero. We formally state this result in the following Theorem.

Theorem 3.8 (Failure localization: non-bridge outage, converse)**.** *Suppose a single non-bridge line $\hat{e} = (\hat{i}, \hat{j})$ trips so that the surviving graph $(\mathcal{N}, \mathcal{E} \setminus \{\hat{e}\})$ remains connected. For any surviving line $e = (i, j)$, the LODF $K_{e\hat{e}} \neq 0$ "if" and only if e and $\hat{e}$ are in the same block of $\mathcal{G}$.*

Localization of Non-cut Outages

To extend failure localizability to the case of a non-cut F outage we use (3.6d) in Theorem 3.5 to express the GLODF $\boldsymbol{K}^F$ in terms of the LODF and PTDF submatrices $\boldsymbol{K}_{-FF}$ and $\boldsymbol{D}_{FF}$.

Corollary 3.7 implies a block-diagonal structure of $\boldsymbol{K}_{-FF}$ and $\boldsymbol{D}_{FF}$ which then translates into the same block-diagonal structure of the GLODF $\boldsymbol{K}^F$. Specifically, assume the set $\mathcal{E}$ of lines consists of b blocks $\mathcal{E}_k$ such that $\mathcal{E} = \mathcal{E}_1 \cup \cdots \cup \mathcal{E}_b$ and $\mathcal{E}_j \cap \mathcal{E}_k = \emptyset$ for $j \neq k$. Partition the set F of simultaneously outaged lines into b disjoint subsets $F_k := F \cap \mathcal{E}_k$, $k = 1, \ldots, b$, such that $F = \cup_k F_k$. Similarly partition the set $-F$ of surviving lines into b disjoint subsets $F_{-k} := -F \cap \mathcal{E}_k = \mathcal{E}_k \setminus F_k$, $k = 1, \ldots, b$, such that $-F = \cup_k F_{-k}$. Without loss of generality we assume that the lines are indexed so that the outaged lines in F_1 correspond to the first $|F_1|$ columns of $\boldsymbol{K}_{-FF}$, the outaged lines in F_2 correspond to the following $|F_2|$ columns of $\boldsymbol{K}_{-FF}$, so on and so forth, and the tripped lines in F_b correspond to the last $|F_b|$ columns of $\boldsymbol{K}_{-FF}$. Similarly, the surviving lines in F_{-1} correspond to the first $|F_{-1}|$ rows of

$\boldsymbol{K}_{-FF}$, and the surviving lines in F_{-b} correspond to the last $|F_{-b}|$ rows of $\boldsymbol{K}_{-FF}$. The ordering of rows and columns of $\boldsymbol{D}_{-FF}$ is the same as that for $\boldsymbol{K}_{-FF}$. Similarly the rows and columns of $\boldsymbol{D}_{FF}$ will be ordered according to F_k, $k = 1, \ldots, b$. Finally partition B and C according to the block structures of both $-F, F$ and $\mathcal{E}$:

$$\begin{aligned}
\boldsymbol{B} &= \begin{bmatrix} \boldsymbol{B}_{-F} & \boldsymbol{0} \\ \boldsymbol{0} & \boldsymbol{B}_F \end{bmatrix} \\
&=: \begin{bmatrix} \operatorname{diag}(\boldsymbol{B}_{-k}, k = 1, \ldots, b) & 0 \\ 0 & \operatorname{diag}(\boldsymbol{B}_k, k = 1, \ldots, b) \end{bmatrix}, \\
\boldsymbol{C} &= \begin{bmatrix} \boldsymbol{C}_{-F} & \boldsymbol{C}_F \end{bmatrix} \\
&=: \begin{bmatrix} \boldsymbol{C}_{-1} & \cdots & \boldsymbol{C}_{-b} & C_1 & \cdots & \boldsymbol{C}_b \end{bmatrix}.
\end{aligned}$$

Recall that $\boldsymbol{D}_{-FF} = \boldsymbol{B}_{-F}\boldsymbol{C}_{-F}^T\boldsymbol{A}\boldsymbol{C}_F$ and $\boldsymbol{D}_{FF} = \boldsymbol{B}_F\boldsymbol{C}_F^T\boldsymbol{A}\boldsymbol{C}_F$. Corollary 3.7 then implies that the PTDF submatrices $\boldsymbol{D}_{-FF}$ and $\boldsymbol{D}_{FF}$ decompose into diagonal structures corresponding to the blocks of $\mathcal{G}$:

$$\boldsymbol{D}_{-FF} =: \begin{bmatrix} \boldsymbol{D}_{-1} & 0 & \ldots & 0 \\ 0 & \boldsymbol{D}_{-2} & \ldots & 0 \\ \vdots & \vdots & \ddots & \vdots \\ 0 & 0 & \ldots & \boldsymbol{D}_{-b} \end{bmatrix}, \tag{3.7a}$$

where $\boldsymbol{D}_{-k} := \boldsymbol{B}_{-k}\boldsymbol{C}_{-k}^T\boldsymbol{A}\boldsymbol{C}_k$, $k = 1, \ldots, b$. Moreover,

$$\boldsymbol{D}_{FF} =: \begin{bmatrix} \boldsymbol{D}_1 & 0 & \ldots & 0 \\ 0 & \boldsymbol{D}_2 & \ldots & 0 \\ \vdots & \vdots & \ddots & \vdots \\ 0 & 0 & \ldots & \boldsymbol{D}_b \end{bmatrix}, \tag{3.7b}$$

where $\boldsymbol{D}_k := \boldsymbol{B}_k\boldsymbol{C}_k^T\boldsymbol{A}\boldsymbol{C}_k$, $k = 1, \ldots, b$. Here each $\boldsymbol{D}_{-k}$ is $|F_{-k}| \times |F_k|$ and each $\boldsymbol{D}_k$ is $|F_k| \times |F_k|$. They involve lines only in block $\mathcal{E}_k$ of $\mathcal{G}$. Since $\boldsymbol{K}_{-FF} = \boldsymbol{D}_{-FF}(\boldsymbol{I} - \operatorname{diag}(\boldsymbol{D}_{FF}))^{-1}$, the LODF submatrix $\boldsymbol{K}_{-FF}$ has the same block diagonal structure as $\boldsymbol{D}_{-FF}$:

$$\boldsymbol{K}_{-FF} =: \begin{bmatrix} \boldsymbol{K}_1 & 0 & \ldots & 0 \\ 0 & \boldsymbol{K}_2 & \ldots & 0 \\ \vdots & \vdots & \ddots & \vdots \\ 0 & 0 & \ldots & \boldsymbol{K}_b \end{bmatrix}, \tag{3.7c}$$

where $\boldsymbol{K}_k := \boldsymbol{D}_{-k}\left(\boldsymbol{I} - \mathrm{diag}(\boldsymbol{D}_k)\right)^{-1}$, $k = 1, \ldots, b$ and $\boldsymbol{D}_{-k}, \boldsymbol{D}_k$ are given in (3.7a), (3.7b). As for $\boldsymbol{D}_{-k}$, each $\boldsymbol{K}_k$ is $|F_{-k}| \times |F_k|$ and involves lines only in block $\mathcal{E}_k$ of $\mathcal{G}$. The invertibility of $\boldsymbol{I} - \mathrm{diag}(\boldsymbol{D}_k)$ follows from Corollary 3.3.

Even if $\boldsymbol{K}^F \neq \boldsymbol{K}_{-FF}$ in general, the next result shows that the GLODF $\boldsymbol{K}^F$ has the same block-diagonal structure as $\boldsymbol{K}_{-FF}$. This implies that even though the impacts of multiple simultaneous line outages are correlated through the network topology, such correlations are present only within each block. In particular, the impacts of a non-cut outage are also localized within blocks that contain outaged lines. It is proved by substituting (3.7) into Theorem 3.5.

Theorem 3.9 (Failure localization: non-cut set outage)**.** *Suppose a non-cut set F of lines trip simultaneously so that the surviving graph $(\mathcal{N}, \mathcal{E}\setminus F)$ remains connected. For any surviving line $e = (i, j)$:*

1. *GLODF $K^F_{e\hat{e}} = 0$ if e and $\hat{e}$ are in different blocks of $\mathcal{G}$.*
2. *$\boldsymbol{K}^F := \boldsymbol{K}^F_{-FF}$ has a block diagonal structure:*

$$\boldsymbol{K}^F =: \begin{bmatrix} \boldsymbol{K}^F_1 & 0 & \ldots & 0 \\ 0 & \boldsymbol{K}^F_2 & \ldots & 0 \\ \vdots & \vdots & \ddots & \vdots \\ 0 & 0 & \ldots & \boldsymbol{K}^F_b \end{bmatrix}, \tag{3.8a}$$

where for $k = 1, \ldots, b$ each $\boldsymbol{K}^F_k$ is $|F_{-k}| \times |F_k|$ and involves lines only in block $\mathcal{E}_k$ of $\mathcal{G}$, given by:

$$\begin{aligned} \boldsymbol{K}^F_k &:= \boldsymbol{D}_{-k}(\boldsymbol{I} - \boldsymbol{D}_k)^{-1} && (3.8b) \\ &= \boldsymbol{K}_k\left(\boldsymbol{I} - \mathrm{diag}(\boldsymbol{D}_k)\right)(\boldsymbol{I} - \boldsymbol{D}_k)^{-1}, && (3.8c) \end{aligned}$$

or in terms of $\boldsymbol{B}, \boldsymbol{C}$ and $\boldsymbol{A}$:

$$\boldsymbol{K}^F_k = \boldsymbol{B}_{-k}\boldsymbol{C}^T_{-k}\boldsymbol{A}\boldsymbol{C}_k\left(\boldsymbol{I} - \boldsymbol{B}_k\boldsymbol{C}^T_k\boldsymbol{A}\boldsymbol{C}_k\right)^{-1}. \tag{3.8d}$$

Again, since a bridge is a block, a non-cut outage does not impact the branch flow on any bridge. The invertibility of $\boldsymbol{I} - \boldsymbol{D}_k$ follows from Corollary 3.3 and the block-diagonal structure of D_{FF}. Theorem 3.9 subsumes Corollary 3.7 which corresponds

to the special case where $F = \{\hat{e}\}$. In that case, $\boldsymbol{K}^F = \boldsymbol{K}^{\hat{e}}$ is a size $m-1$ column vector. If $\hat{e} \in \mathcal{E}_1$, then $\boldsymbol{D}_{FF} = D_{\hat{e}\hat{e}}$ and

$$\boldsymbol{K}^{\hat{e}} \;=\; \begin{bmatrix} \boldsymbol{K}_1 \\ 0 \\ \vdots \\ 0 \end{bmatrix},$$

with $\boldsymbol{K}_1 := \boldsymbol{D}_{-1}(1 - D_{\hat{e}\hat{e}})^{-1}$ and $\boldsymbol{D}_{-1} := (D_{e\hat{e}}, e \neq \hat{e}, e \in \mathcal{E}_1)$.

The ability to characterize in terms of the GLODF $\boldsymbol{K}^F$ the localization of the impact of line outages within each block where outages occur is illustrated in the next example.

Example 2. *Consider a non-cut set $F := \{\hat{e}_1, \hat{e}_2\}$ and the $N-2$ event where lines $\hat{e}_1$ and $\hat{e}_2$ trip simultaneously. The branch flow change on a surviving line $e \in -F$ is given in terms of the GLODF $\boldsymbol{K}^F$ defined in* (3.4) *as:*

$$\tilde{f}_e - f_e \;=\; K^F_{e\hat{e}_1} f_{\hat{e}_1} \;+\; K^F_{e\hat{e}_2} f_{\hat{e}_2},$$

where $K^F_{e\hat{e}_i}$ is the $(e, \hat{e}_i)$-th entry of $\boldsymbol{K}^F$, $i = 1, 2$. There are two cases:

1. Lines $\hat{e}_1, \hat{e}_2$ are in the same block $\mathcal{E}_k$. *Then*

$$\tilde{f}_e - f_e \;=\; \begin{cases} 0 & \text{if } e \notin \mathcal{E}_k, \\ K^F_{e\hat{e}_1} f_{\hat{e}_1} + K^F_{e\hat{e}_2} f_{\hat{e}_2} & \text{if } e \in \mathcal{E}_k. \end{cases}$$

2. Lines $\hat{e}_1, \hat{e}_2$ are in different blocks, say $\hat{e}_i \in \mathcal{E}_i$. *Then*

$$\tilde{f}_e - f_e \;=\; \begin{cases} 0 & \text{if } e \notin \mathcal{E}_1 \cup \mathcal{E}_2, \\ K^F_{e\hat{e}_1} f_{\hat{e}_1} & \text{if } e \in \mathcal{E}_1, \\ K^F_{e\hat{e}_2} f_{\hat{e}_2} & \text{if } e \in \mathcal{E}_2. \end{cases}$$

   In this case, since there is a single non-bridge line that is outaged in each block, the decoupling of outages over different blocks means $K^F_{e\hat{e}} = K_{e\hat{e}}$ as if each of the outaged lines $\hat{e}_1$ and $\hat{e}_2$ is outaged separately.

□

Theorem 3.9 is a consequence of the Simple Cycle Criterion since $K_{e\hat{e}} \neq 0$ only if there is a simple cycle that contains both e and $\hat{e}$. The converse of the Simple Cycle

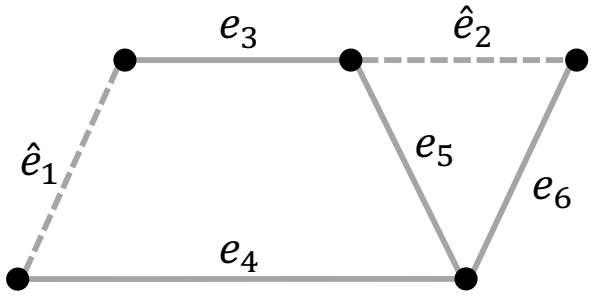

Figure 3.3: A counterexample with the lines in the non-cut set $F = \{\hat{e}_1, \hat{e}_2\}$ displayed as dashed.

Criterion asserts that $K_{e\hat{e}} \neq 0$ "if" there is a simple cycle that contains both e and $\hat{e}$. This immediately implies the converse of Corollary 3.7 that $K_{e\hat{e}} \neq 0$ "if" e and $\hat{e}$ are in the same block of $\mathcal{G}$. In other words, not only the submatrices $\boldsymbol{K}_{-FF}, \boldsymbol{D}_{-FF}, \boldsymbol{D}_{FF}$ are block-diagonal, but also that almost surely with respect to μ, *every* entry of the diagonal blocks $\boldsymbol{K}_k, \boldsymbol{D}_{-k}, \boldsymbol{D}_k$ in (3.7) is nonzero. This is only for the case when a single non-bridge line $\hat{e}$ trips. It does not directly imply the converse of Theorem 3.9, i.e., it is not clear whether every entry of $\boldsymbol{K}_k^F$ is nonzero (μ-almost surely) when multiple lines in a non-cut set F trip simultaneously. Even though every entry of $\boldsymbol{D}_{-k}, \boldsymbol{D}_k$ is nonzero (μ-almost surely), the issue is whether every entry of the product $\boldsymbol{K}_k^F = \boldsymbol{D}_{-k}(\boldsymbol{I} - \boldsymbol{D}_k)^{-1}$ from (3.8c) is still nonzero (μ-almost surely).

In fact, the following example shows that the converse of Theorem 3.9 does not hold, i.e., $\boldsymbol{K}_k^F$ can be zero with a non-zero probability when multiple lines trip simultaneously. Moreover, differently for the case of a single non-bridge failure in Corollary 3.7, the PTDFs and GLODFs are not always simultaneously zero. Specifically, when multiple lines trip simultaneously, the fact that GLODF $K_{e\hat{e}}^F = 0$ does not imply that the PTDF $D_{e\hat{e}} = 0$ or vice versa.

Example 3. *Consider the power grid in Fig. 3.3 where two dashed lines $\hat{e}_1$ and $\hat{e}_2$ trip simultaneously, i.e., $F = \{\hat{e}_1, \hat{e}_2\}$. Assuming all the lines have unit susceptance, the resulting absolute values of PTDF and GLODF are computed as in Table 3.1. In particular, $K_{e_6\hat{e}_1}^F = K_{e_3\hat{e}_2}^F = K_{e_4\hat{e}_2}^F = 0$, while the corresponding PTDFs are non-zero. Moreover, no matter how the susceptances change, the GLODFs $K_{e_6\hat{e}_1}^F$, $K_{e_3\hat{e}_2}^F$ and $K_{e_4\hat{e}_2}^F$ are always zero, even though all the lines belong to the same block in the pre-contingency network.*

$\hat{e}$ \ e	e_3	e_4	e_5	e_6
$\hat{e}_1$	3/11, 1	3/11, 1	2/11, 1	1/11, 0
$\hat{e}_2$	1/11, 0	1/11, 0	3/11, 1	4/11, 1

Table 3.1: The distribution factors for all the lines reported as pairs (PTDF $D_{e\hat{e}}$, GLODF $K^F_{e\hat{e}}$).

Such counterexamples may happen when the outage set F is such that the block decomposition of the surviving network has more blocks than the original network (in Example 3, they are 4 and 1, respectively). Recall the perspective from post-contingency network from (3.6a). We provide the localization result for non-cut failures based on the *post*-contingency network in the follwoing Theorem.

Theorem 3.10 (Failure localization: post-contingency network)**.** *Suppose a non-cut set F of lines trip simultaneously so that the surviving graph $(\mathcal{N}, \mathcal{E}\setminus F)$ remains connected. For any surviving line $e = (i, j)$, the GLODF $K^F_{e\hat{e}} \neq 0$ "if" and only if e and $\hat{e}$ are in the same block of network $\tilde{\mathcal{G}}' := (\mathcal{N}, \mathcal{E} \setminus F \cup \{\hat{e}\})$.*

3.4 Conclusion

In this chapter, we develop a spectral theory using the transmission network Laplacian matrix that precisely captures the Kirkhhoff's Law in terms of graphical structures. Our results show that the distributions of different families of subtrees play an important role in understanding power redistribution and enables us to derive algebraic properties using purely graphical arguments. We consider the scenario where the surviving network remains connected and explain how the localizability of line failures can be fully characterized using its block decomposition.

The results in this chapter can be extended in several directions. For example, injection disturbances such as loss of generators or loads can be readily incorporated into the same framework as initial failures. In addition, we explore ways to judiciously switch off a small number of transmission lines to create more blocks to enhance failure localization and develop real-time mitigation strategies in Chapter 6. This technique can be synergistically applied, or sometimes replace, controlled islanding (see e.g., [69, 71, 74, 88–92]) as a corrective action, in which an inter-connected power system will be partitioned into multiple blocks after a contingency that are connected by either bridges or cut vertices [67]. By not separating the system into multiple islands, more loads can potentially be supported in the emergency state,

more reliably, until restoration.

3.5 Proofs

Proof of Theorem 3.2

Recall in Chapter 2, Theorem 2.2 implies that

$$\begin{aligned}&\left(\sum_{H\in\mathcal{T}_{\mathcal{E}}}\beta(H)\right)\left(A_{i\hat{i}}+A_{j\hat{j}}-A_{i\hat{j}}-A_{j\hat{i}}\right)\\&=\sum_{H\in\mathcal{T}(i\hat{i},n)}\beta(H)+\sum_{H\in\mathcal{T}(j\hat{j},n)}\beta(H)\\&-\sum_{H\in\mathcal{T}(i\hat{j},n)}\beta(H)-\sum_{H\in\mathcal{T}(j\hat{i},n)}\beta(H).\end{aligned}\tag{3.9}$$

We can decompose the set $\mathcal{T}(i\hat{i},n)$ based on the tree to which node j belongs. This leads to the identity

$$\mathcal{T}(i\hat{i},n)=\mathcal{T}(ij\hat{i},n)\sqcup\mathcal{T}(i\hat{i},jn),$$

where $\sqcup$ denotes a disjoint union. Similarly, we also have

$$\mathcal{T}(j\hat{j},n)=\mathcal{T}(ij\hat{j},n)\sqcup\mathcal{T}(j\hat{j},in),$$

$$\mathcal{T}(i\hat{j},n)=\mathcal{T}(ij\hat{j},n)\sqcup\mathcal{T}(i\hat{j},jn),$$

$$\mathcal{T}(j\hat{i},n)=\mathcal{T}(ij\hat{i},n)\sqcup\mathcal{T}(j\hat{i},in).$$

Substituting the above decompositions into (3.9) and simplifying, we obtain

$$\begin{aligned}&\left(\sum_{H\in\mathcal{T}_{\mathcal{E}}}\beta(H)\right)\left(A_{i\hat{i}}+A_{j\hat{j}}-A_{i\hat{j}}-A_{j\hat{i}}\right)\\&=\sum_{H\in\mathcal{T}(i\hat{i},jn)}\beta(H)+\sum_{H\in\mathcal{T}(j\hat{j},in)}\beta(H)\\&-\sum_{H\in\mathcal{T}(i\hat{j},jn)}\beta(H)-\sum_{H\in\mathcal{T}(j\hat{i},in)}\beta(H).\end{aligned}\tag{3.10}$$

Furthermore, the following set of identities hold:

$$\begin{aligned}\mathcal{T}(i\hat{i},jn)&=\mathcal{T}(i\hat{i},jn\hat{j})\sqcup\mathcal{T}(i\hat{i}\hat{j},jn),\\\mathcal{T}(j\hat{j},in)&=\mathcal{T}(j\hat{j},in\hat{i})\sqcup\mathcal{T}(ji\hat{j},in),\\\mathcal{T}(j\hat{i},in)&=\mathcal{T}(j\hat{i},in\hat{j})\sqcup\mathcal{T}(ji\hat{j},in),\\\mathcal{T}(i\hat{j},jn)&=\mathcal{T}(i\hat{j},jn\hat{i})\sqcup\mathcal{T}(i\hat{i}\hat{j},jn).\end{aligned}$$

Substituting these into (3.10) and rearranging yields

$$\begin{aligned}&\left(\sum_{H\in\mathcal{T}_{\mathcal{E}}}\beta(H)\right)\left(A_{i\hat{i}}+A_{j\hat{j}}-A_{i\hat{j}}-A_{j\hat{i}}\right)\\&=\sum_{H\in\mathcal{T}(i\hat{i},jn\hat{j})}\beta(H)+\sum_{H\in\mathcal{T}(j\hat{j},in\hat{i})}\beta(H)\\&-\sum_{H\in\mathcal{T}(j\hat{i},in\hat{j})}\beta(H)-\sum_{H\in\mathcal{T}(i\hat{j},jn\hat{i})}\beta(H)\\&=\sum_{H\in\mathcal{T}(i\hat{i},j\hat{j})}\beta(H)-\sum_{H\in\mathcal{T}(j\hat{i},i\hat{j})}\beta(H),\end{aligned}$$

where the last equality follows from

$$\mathcal{T}(i\hat{i}, j\hat{j}) \;=\; \mathcal{T}(i\hat{i}, jn\hat{j}) \sqcup \mathcal{T}(j\hat{j}, in\hat{i})$$

and

$$\mathcal{T}(j\hat{i}, i\hat{j}) \;=\; \mathcal{T}(j\hat{i}, in\hat{j}) \sqcup \mathcal{T}(i\hat{j}, jn\hat{i}).$$

This completes the proof. □

Proof of Theorem 3.5

The first part is proved by analyzing the post-contingency network $\boldsymbol{A}_{-F}$, the second part is proved by analyzing the pre-contingency graph $\boldsymbol{A}$, and the third part is proved by relating $\boldsymbol{D}_{-FF}$ and $\boldsymbol{K}_{-FF}$.

Proof based on post-contingency $\boldsymbol{A}_{-F}$ The DC power flow equations (2.1) for the pre-contingency network are:

$$\boldsymbol{p} = \boldsymbol{C}\boldsymbol{f} = \boldsymbol{C}_{-F}\boldsymbol{f}_{-F} + \boldsymbol{C}_F\boldsymbol{f}_F, \quad \boldsymbol{f} = \boldsymbol{B}\boldsymbol{C}^T\boldsymbol{\theta}. \tag{3.11}$$

Let $(\tilde{\boldsymbol{f}}_{-F}, \tilde{\boldsymbol{\theta}})$ denote the post-contingency branch flows and phase angles. Given the assumption that the power injections remain the same, we have the following DC power flow equations for the post-contingency network:

$$\boldsymbol{p} = \boldsymbol{C}_{-F}\tilde{\boldsymbol{f}}_{-F}, \quad \tilde{\boldsymbol{f}}_F = \boldsymbol{B}_{-F}\boldsymbol{C}_{-F}^T\tilde{\boldsymbol{\theta}}. \tag{3.12}$$

Subtracting (3.11) from (3.12) gives

$$\boldsymbol{C}_{-F}(\tilde{\boldsymbol{f}}_{-F} - \boldsymbol{f}_{-F}) = \boldsymbol{C}_F\boldsymbol{f}_F, \quad \tilde{\boldsymbol{f}}_{-F} - \boldsymbol{f}_{-F} = \boldsymbol{B}_{-F}\boldsymbol{C}_{-F}^T(\tilde{\boldsymbol{\theta}} - \boldsymbol{\theta}).$$

Therefore, $(\Delta\boldsymbol{f}_{-F}, \Delta\boldsymbol{\theta}) := (\tilde{\boldsymbol{f}}_{-F} - \boldsymbol{f}_{-F}, \tilde{\boldsymbol{\theta}} - \boldsymbol{\theta})$ satisfies the DC power flow equations with injections $\boldsymbol{C}_F\boldsymbol{f}_F$ on the post-contingency network. The unique solution for $\Delta\boldsymbol{f}_{-F}$ is:

$$\Delta\boldsymbol{f}_{-F} = \underbrace{\boldsymbol{B}_{-F}\boldsymbol{C}_{-F}^T\boldsymbol{A}_{-F}\boldsymbol{C}_F}_{\boldsymbol{K}^F}\boldsymbol{f}_F,$$

which gives $\boldsymbol{K}^F$ in (3.6a).

Proof based on pre-contingency $\boldsymbol{A}$ In this part, we construct a fictitious network that mimics the impact of the non-cut F outage. Specifically, the network is the

same as the pre-contingency network, but with its injections changed from p to $\hat{\boldsymbol{p}} = \boldsymbol{p} + \Delta\boldsymbol{p}$. For this fictitious network, the DC power flow equations write:

$$\hat{\boldsymbol{p}} = \boldsymbol{C}\hat{\boldsymbol{f}} = \boldsymbol{C}_{-F}\hat{\boldsymbol{f}}_{-F} + \boldsymbol{C}_F\hat{\boldsymbol{f}}_F, \quad \hat{\boldsymbol{f}} = \boldsymbol{B}\boldsymbol{C}^T\hat{\boldsymbol{\theta}}. \tag{3.13}$$

We choose $\Delta\boldsymbol{p}$ so that it is carried entirely by the fictitious branch flows $\hat{\boldsymbol{f}}_F$ on lines in F that would have been disconnected, i.e., we pick

$$\Delta\boldsymbol{p} = \boldsymbol{C}_F\hat{\boldsymbol{f}}_F. \tag{3.14}$$

This additional injection $\Delta\boldsymbol{p}$ does satisfy $\mathbf{1}^T\Delta\boldsymbol{p} = 0$ and is thus balanced. Substituting (3.14) into (3.13) yields:

$$\boldsymbol{p} = \boldsymbol{C}_{-F}\hat{\boldsymbol{f}}_{-F}, \quad \hat{\boldsymbol{f}}_{-F} = \boldsymbol{B}_{-F}\boldsymbol{C}_{-F}^T\hat{\boldsymbol{\theta}}, \tag{3.15}$$

i.e., $(\hat{\boldsymbol{f}}_{-F}, \hat{\boldsymbol{\theta}})$ satisfies the same DC power flow equations (3.12) for the post-contingency network. Since the DC power flow equations have a unique branch flow solution, the post-contingency branch flows $\tilde{\boldsymbol{f}}_{-F}$ from (3.12) must coincide with the branch flows $\hat{\boldsymbol{f}}_{-F}$ in the fictitious network (3.13). This allows us to calculate the GLODF $\boldsymbol{K}^F$ by relating $\tilde{\boldsymbol{f}}_{-F}$ and $\boldsymbol{f}_F$ on two different networks through the relation between $\hat{\boldsymbol{f}}_{-F}$ and $\boldsymbol{f}_F$ on the same pre-contingency network. Considering the fictitious network, we have:

$$\hat{\boldsymbol{f}}_F = \boldsymbol{B}_F\boldsymbol{C}_F^T\hat{\boldsymbol{\theta}} = \boldsymbol{B}_F\boldsymbol{C}_F^T\boldsymbol{A}(\boldsymbol{p} + \Delta\boldsymbol{p}).$$

Substituting into (3.14) gives $\Delta\boldsymbol{p} = \boldsymbol{C}_F\hat{\boldsymbol{f}}_F = \boldsymbol{C}_F\boldsymbol{B}_F\boldsymbol{C}_F^T\boldsymbol{A}(\boldsymbol{p} + \Delta\boldsymbol{p})$. Hence,

$$\Delta\boldsymbol{p} = \left(\boldsymbol{I} - \boldsymbol{C}_F\boldsymbol{B}_F\boldsymbol{C}_F^T\boldsymbol{A}\right)^{-1}\boldsymbol{C}_F\boldsymbol{B}_F\boldsymbol{C}_F^T\boldsymbol{A}\boldsymbol{p}, \tag{3.16}$$

which yields the following expression for $\hat{\boldsymbol{f}}_{-F}$ in the fictitious network

$$\hat{\boldsymbol{f}}_{-F} = \boldsymbol{B}_{-F}\boldsymbol{C}_{-F}^T\boldsymbol{A}(\boldsymbol{p} + \Delta\boldsymbol{p}).$$

The pre-contingency line flows are given by

$$\boldsymbol{f}_{-F} = \boldsymbol{B}_{-F}\boldsymbol{C}_{-F}^T\boldsymbol{A}\boldsymbol{p}, \quad \boldsymbol{f}_F = \boldsymbol{B}_F\boldsymbol{C}_F^T\boldsymbol{A}\boldsymbol{p}.$$

Substituting these expressions, we have

$$\begin{aligned}\hat{\boldsymbol{f}}_{-F} &= \boldsymbol{f}_{-F} + \boldsymbol{B}_{-F}\boldsymbol{C}_{-F}^T\boldsymbol{A}\left(\boldsymbol{I} - \boldsymbol{C}_F\boldsymbol{B}_F\boldsymbol{C}_F^T\boldsymbol{A}\right)^{-1}\boldsymbol{C}_F\boldsymbol{f}_F \\ &= \boldsymbol{f}_{-F} + \underbrace{\boldsymbol{B}_{-F}\boldsymbol{C}_{-F}^T\boldsymbol{A}\boldsymbol{C}_F\left(\boldsymbol{I} - \boldsymbol{B}_F\boldsymbol{C}_F^T\boldsymbol{A}\boldsymbol{C}_F\right)^{-1}}_{\boldsymbol{K}^F}\boldsymbol{f}_F,\end{aligned}$$

where we use the identity $(\boldsymbol{I} + \boldsymbol{M}_1\boldsymbol{M}_2)^{-1}\boldsymbol{M}_1 = \boldsymbol{M}_1(\boldsymbol{I} + \boldsymbol{M}_2\boldsymbol{M}_1)^{-1}$ (provided the inverse exists) in the last equality. This identity follows from:

$$\begin{aligned}\boldsymbol{M}_1 &= \boldsymbol{M}_1(\boldsymbol{I} + \boldsymbol{M}_2\boldsymbol{M}_1)(\boldsymbol{I} + \boldsymbol{M}_2\boldsymbol{M}_1)^{-1} \\ &= (\boldsymbol{M}_1 + \boldsymbol{M}_1\boldsymbol{M}_2\boldsymbol{M}_1)(\boldsymbol{I} + \boldsymbol{M}_2\boldsymbol{M}_1)^{-1} \\ &= (\boldsymbol{I} + \boldsymbol{M}_1\boldsymbol{M}_2)\boldsymbol{M}_1(\boldsymbol{I} + \boldsymbol{M}_2\boldsymbol{M}_1)^{-1}.\end{aligned}$$

This gives the expression of $\boldsymbol{K}^F$ in (3.6b) and (3.6c).

Relation between $\boldsymbol{K}^F$ and $\boldsymbol{K}_{-FF}$ As shown in (3.5), we have $\boldsymbol{D}_{-FF} = \boldsymbol{K}_{-FF}(\boldsymbol{I} - \text{diag}(\boldsymbol{D}_F F))$. The $\boldsymbol{K}^F$ in terms of pre-contingency network A yields:

$$\begin{aligned}\boldsymbol{K}^F &= \boldsymbol{B}_{-F}\boldsymbol{C}_{-F}^T\boldsymbol{A}\boldsymbol{C}_F\left(\boldsymbol{I} - \boldsymbol{B}_F\boldsymbol{C}_F^T\boldsymbol{A}\boldsymbol{C}_F\right)^{-1} \\ &= \boldsymbol{D}_{-FF}\left(\boldsymbol{I} - \boldsymbol{D}_{FF}\right)^{-1} \\ &= \boldsymbol{K}_{-FF}(\boldsymbol{I} - \text{diag}(\boldsymbol{D}_F F))\left(\boldsymbol{I} - \boldsymbol{D}_{FF}\right)^{-1}.\end{aligned}$$

This gives the expression of $\boldsymbol{K}^F$ in (3.6d). □

Proof of Theorem 3.6

Theorem 3.4 implies that $K_{e\hat{e}}$ is proportional to the following polynomial in the susceptances $\boldsymbol{B}$:

$$g(\boldsymbol{B}) := \sum_{H\in\mathcal{T}(i\hat{i},j\hat{j})}\beta(H) - \sum_{H\in\mathcal{T}(j\hat{i},i\hat{j})}\beta(H).$$

If $K_{e\hat{e}} \neq 0$, then at least one of the sets $\mathcal{T}(i\hat{i}, j\hat{j})$ and $\mathcal{T}(i\hat{j}, j\hat{i})$ of spanning forests is nonempty. Suppose $\mathcal{T}(i\hat{i}, j\hat{j})$ is nonempty and contains a spanning forest H. The tree in H that contains buses i and $\hat{i}$ defines a path from i to $\hat{i}$, and the other tree that contains j and $\hat{j}$ defines a path from j to $\hat{j}$. These two paths are vertex-disjoint, i.e., they do not share any vertices. If we add the lines $e = (i, j)$ and $\hat{e} = (\hat{i}, \hat{j})$ to these two vertex-disjoint paths, we obtain a simple cycle that contains both e and $\hat{e}$.

Conversely, suppose there is a simple cycle that contains e and $\hat{e}$. Removing lines e and $\hat{e}$ from the simple cycle produces two vertex-disjoint paths, say, P_i that contains buses $i, \hat{i}$ and P_j that contains buses $j, \hat{j}$. Since $\mathcal{G}$ is connected, we can extend P_i and P_j into a spanning forest with exactly two disjoint trees. This spanning forest, denoted by H, is in $\mathcal{T}(i\hat{i}, j\hat{j})$. Furthermore H is not in $\mathcal{T}(i\hat{j}, j\hat{i})$ from the following claim:

$$\mathcal{T}(i\hat{i}, j\hat{j}) \cap \mathcal{T}(i\hat{j}, j\hat{i}) = \emptyset.$$

To show this, consider an element T_1 from $\mathcal{T}(i\hat{i}, j\hat{j})$, which consists of two trees $\mathcal{T}_1$ and $\mathcal{T}_2$ with $\mathcal{T}_1$ containing $i, \hat{i}$ and $\mathcal{T}_2$ containing $j, \hat{j}$. If $T_1 \in \mathcal{T}(i\hat{j}, j\hat{i})$, then $\mathcal{T}_1$ must also contain $\hat{j}$. However, this implies $\hat{j} \in \mathcal{T}_1 \cap \mathcal{T}_2$, and thus $\mathcal{T}_1$ and $\mathcal{T}_2$ are not disjoint, contradicting the definition of $\mathcal{T}(i\hat{j}, j\hat{i})$.

Therefore, $g(\boldsymbol{B})$ is not identically zero. This means $K_{e\hat{e}} = 0$ if and only if $\boldsymbol{B}$ is a root of the polynomial $g(\boldsymbol{B})$. It is a fundamental result that the root set of a polynomial which is not identically zero has Lebesgue measure zero. Therefore, since μ is absolutely continuous with respect to the Lebesgue measure $\mathcal{L}_m$, we have

$$\mu(g(\boldsymbol{B} + \boldsymbol{w}) = 0) = \mathcal{L}_m(g(\boldsymbol{B} + \boldsymbol{w}) = 0) = 0$$

i.e., $\mu(K_{e\hat{e}} \neq 0) = \mu(g(\boldsymbol{B} + \boldsymbol{w}) \neq 0) = 1$ if there is a simple cycle that contains e and $\hat{e}$. □

Chapter 4

FAILURES IN POWER SYSGTEMS: CUT SET OUTAGES

Chapter 3 establishes a spectral representation of power redistribution that precisely captures the Kirchhoff's Laws in terms of the distribution of different families of subtrees in the transmission network. This new representation enables us to characterize how non-cut line outages propagate.

In this chapter, we study cut set line outages and analytically characterize how such failures impact the remaining lines. Our results demonstrate how the impact of cut set outages propagates globally in a way that depends on both the power balancing rules and the network topological structure. This characterization, together with our results from Chapter 3, can be visualized in Fig. 4.1, where it becomes clear how the block decomposition of a network is linked to the sparsity of the LODF matrix $\boldsymbol{K} := (K_{e\hat{e}}, e, \hat{e} \in \mathcal{E})$. This new theory shows that the block decomposition yields an extremely useful representation of the distribution factors.

The formal characterization of single bridge outage is given by a Simple Path Criterion as Theorem 4.1 in Section 4.2, which shows that the relative positions of the nodes participating in load balancing fully determines how such failures propagate. This result applies to the scenario in which the post-contingency network is disconnected into two or more connected components, known as *islands*, and the original power injections need to be balanced in each island. We then formulate the concept of *participating block* and show that bridge outages typically propagate globally across the network and impact the branch flows on all transmission lines. In Section 4.3, we extend Theorem 4.1 to the case of a general cut set outage, and show that the aggregate impact of such failures can be decomposed into two terms: (a) a first term that captures the effect of power redistribution, which can be decomposed in accordance to the blocks where the failures occur and is fully characterized by our results in Chapter 3; and (b) a second term that describes the impact of the power balancing rule and generalizes the case of a single bridge failure, capturing how the system handles disconnected components.

Results in Chapters 3 and 4 provide a complete characterization of line failure propagation and is illustrated in Section 4.4 using IEEE 118-bus test network. In particular, we show that the LODF matrix has a clear block-diagonal structure

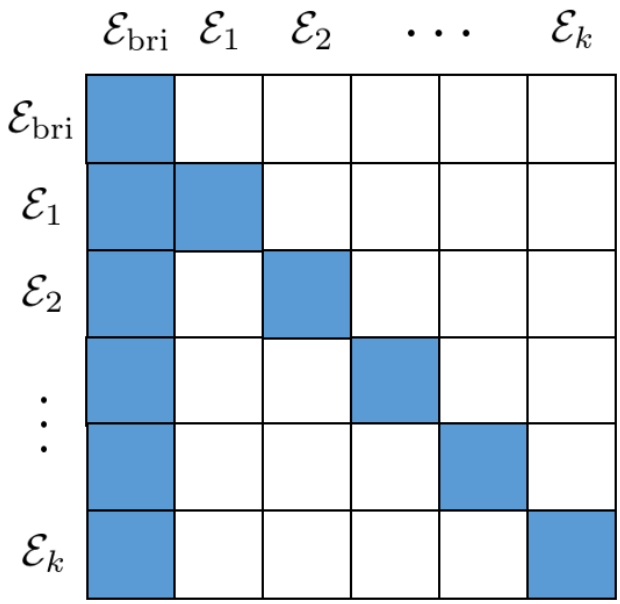

Figure 4.1: Non-zero entries of the $K_{e\hat{e}}$ matrix (depicted as the dark blocks) for a graph with non-bridge blocks $\{\mathcal{E}_1, \mathcal{E}_2, \cdots, \mathcal{E}_b\}$ and bridge set $\mathcal{E}_{\text{bri}}$.

predicted by our theory, even when using full AC power flow equations.

4.1 Islanding Model

In contrast to Chapter 3 where we focus on simultaneous line outages that do not disconnect the network, we consider now the case in which the set of initial line outages disconnects the network into two or more connected sub-networks, called *islands*. We refer to such contingency as a *cut set outage* and, in the special case in which the cut set consists of a single line, as a *bridge outage*. We remark that, in practice, such islands can be created accidentally by line outages, but also deliberately as a defensive action to prevent a disturbance/attack from propagating across the entire network infrastructure [71].

Islands and Cut Set Outages

We first present a detailed model for a single island that is necessary for our analysis of cut set outages in later sections. More specifically, we fully characterize the impact of a bridge outage in Section 4.2 and of a general cut set outage in Section 4.3.

We adopt the similar notations as in Chapter 3, which we now summarize. Let $\mathcal{G}' = (\mathcal{N}', \mathcal{E}')$ denote the pre-contingency network and consider a subset of lines $F' \subset \mathcal{E}'$ that is a cut set of $\mathcal{G}'$ and denote by $\mathcal{G}_1, \ldots, \mathcal{G}_k$ the multiple islands created

by the removal of lines in F'. Let us focus on one of these islands, say $\mathcal{G} = (\mathcal{N}, \mathcal{E})$, where $\mathcal{N} \subseteq \mathcal{N}'$ is the set of buses that belong to the island and $\mathcal{E} \subseteq \mathcal{E}'$ is the set of lines that, *pre-contingency*, have both endpoints inside the island. From the viewpoint of the island $\mathcal{G}$, the lines in the cut set F' can then be classified into three types, $F' = F_{\text{external}} \cup F_{\text{tie}} \cup F$, as follows:

- $F_{\text{external}} := \left\{\hat{e} = (\hat{i}, \hat{j}) \in F' : \hat{i} \notin \mathcal{N}, \hat{j} \notin \mathcal{N}\right\}$ is the set of tripped *external lines* with neither endpoints in the island $\mathcal{G}$;
- $F_{\text{tie}} := \left\{\hat{e} = (\hat{i}, \hat{j}) \in F' : \hat{i} \notin \mathcal{N}, \hat{j} \in \mathcal{N}\right\}$ is the set of tripped *tie lines* with exactly one endpoint (denoted by as $j(\hat{e})$) in the island $\mathcal{G}$;
- $F := \left\{\hat{e} = (\hat{i}, \hat{j}) \in F' : \hat{i} \in \mathcal{N}, \hat{j} \in \mathcal{N}\right\}$ is the set of tripped *internal lines* with both endpoints inside the island $\mathcal{G}$.

Note that the external line outages do not have a direct impact on the island $\mathcal{G}$ since the post-contingency operations and power flow equations are decoupled in each island and thus can be ignored. Therefore, without loss of generality, we henceforth assume $F' = F_{\text{tie}} \cup F$. Since the graph $\mathcal{G} = (\mathcal{N}, \mathcal{E})$ describes the pre-contingency topology of the island, its edge set $\mathcal{E}$ includes the tripped internal lines F, but not the tie lines F_{tie}. We refer to the lines that are still active in the island post-contingency as *surviving lines* and denote their collection as $-F := \mathcal{E} \setminus F$. The post-contingency island is thus fully described by the graph $(\mathcal{N}, \mathcal{E} \setminus F)$, which is connected by construction. In particular, the tripped internal lines F is a non-cut set of island $\mathcal{G}$.

Designate any bus in $\mathcal{N}$ to be the reference bus for $\mathcal{G}$ and, without loss of generality, assume it is bus n. Let $\boldsymbol{B}$ denote the susceptance matrix associated with the island $\mathcal{G}$, $\boldsymbol{C}$ its incidence matrix, $\boldsymbol{L} := \boldsymbol{C}\boldsymbol{B}\boldsymbol{C}^T$ its Laplacian matrix, and define $\boldsymbol{A}$ in terms of the reduced Laplacian matrix $\overline{\boldsymbol{L}}$ as in Chapter 2:

$$\boldsymbol{A} = \begin{bmatrix} \overline{\boldsymbol{L}}^{-1} & \boldsymbol{0} \\ \boldsymbol{0} & 0 \end{bmatrix}.$$

Let $\boldsymbol{f} := (f_{\hat{e}}, \hat{e} \in \mathcal{E})$ and $\boldsymbol{f}^{\text{tie}} := (f_{\hat{e}}, \hat{e} \in F_{\text{tie}})$ be the pre-contingency branch flows on the lines inside the island $\mathcal{G}$ and on the tie lines, respectively. We adopt the convention that $f_{\hat{e}} > 0$ for a line $\hat{e} = (\hat{i}, \hat{j})$ if power flows from bus $\hat{i}$ to bus $\hat{j}$ over line $\hat{e}$. In particular, for a tie line $\hat{e} \in F_{\text{tie}}$, $f_{\hat{e}} > 0$ implies that, before the line failure, the island imports power over line $\hat{e}$ and $f_{\hat{e}} < 0$ if it exports power over $\hat{e}$.

If the pre-contingency branch flow $f_{\hat{e}} = 0$ on any tie line or internal line $\hat{e} \in F'$, then its tripping has no impact on the post-contingency branch flows in this island, as modeled by the DC power flow equations. We therefore assume without loss of generality that the pre-contingency branch flows $f_{\hat{e}} \neq 0$ for all tripped lines $\hat{e} \in F'$ (otherwise, remove $\hat{e}$ from F' and the surviving island $\mathcal{G}$).

Pre-contingency Injections and Branch Flows

Let $\boldsymbol{p} := (p_k, k \in \mathcal{N})$ denote the pre-contingency injections in the buses of island $\mathcal{G}$. The effect of pre-contingency tie line branch flows on the island $\mathcal{G}$ can be modeled by additional injections $\boldsymbol{f}_{\hat{e}}$ at buses $j(\hat{e})$:

$$\Delta p_{\text{tie}} := \sum_{\hat{e} \in F_{\text{tie}}} f_{\hat{e}}\, \boldsymbol{e}_{j(\hat{e})}, \tag{4.1}$$

where $\boldsymbol{e}_{j(\hat{e})}$ is the standard unit vector of size $n := |\mathcal{N}|$ and $j(\hat{e})$ is the end node of line $\hat{e}$. Hence, for the purpose of computing pre-contingency branch flows in island $\mathcal{G}$, the injections can be taken to be $\boldsymbol{p} + \Delta \boldsymbol{p}_{\text{tie}}$. Let $\boldsymbol{f}_F := (f_{\hat{e}}, \hat{e} \in F)$ denote the pre-contingency branch flows on lines in F, $\boldsymbol{f}_{-F} := (f_e, e \in \mathcal{E} \setminus F)$ those on the surviving lines in $\mathcal{G}$, and $\boldsymbol{f} := (\boldsymbol{f}_{-F}, \boldsymbol{f}_F)$. Partition the matrices $(\boldsymbol{B}, \boldsymbol{C})$ according to the two sets of lines, F and $-F = \mathcal{E} \setminus F$, as follows:

$$\boldsymbol{B} =: \begin{bmatrix} \boldsymbol{B}_{-F} & \boldsymbol{0} \\ \boldsymbol{0} & \boldsymbol{B}_F \end{bmatrix}, \qquad \boldsymbol{C} =: \begin{bmatrix} \boldsymbol{C}_{-F}, & \boldsymbol{C}_F \end{bmatrix}.$$

From (4.1), it follows that $(\boldsymbol{f}, \boldsymbol{\theta})$ satisfies the DC power flow equations on the pre-contingency island $\mathcal{G} = (\mathcal{N}, \mathcal{E})$:

$$\boldsymbol{p} + \Delta \boldsymbol{p}_{\text{tie}} = \boldsymbol{C}\boldsymbol{f} = \boldsymbol{C}_{-F}\boldsymbol{f}_{-F} + \boldsymbol{C}_F \boldsymbol{f}_F, \tag{4.2a}$$

$$\boldsymbol{f} = \boldsymbol{B}\boldsymbol{C}^T \boldsymbol{\theta}, \tag{4.2b}$$

where $\boldsymbol{\theta}$ are the pre-contingency voltage angles.

Post-contingency Injections and Branch Flows

The effect of tie line outages F_{tie} on island $\mathcal{G}$ can be modeled as the loss of the injections $\Delta \boldsymbol{p}_{\text{tie}}$ at the endpoints of the tie lines. The pre-contingency injections are then unbalanced over the island $\mathcal{G}$ with a total imbalance equal to

$$\sum_{k \in \mathcal{N}} p_k = -\sum_{\hat{e} \in F_{\text{tie}}} f_{\hat{e}}.$$

Post contingency, there is a surplus if the island net exports power pre contingency and a shortage otherwise, depending on the sign of this total imbalance. A balancing

rule $\mathcal{R}$ is invoked to rebalance power in the island by adjusting injections (generators and/or loads) in response to the contingency. A popular balancing rule, which we name *proportional control*, prescribes how to share the imbalance proportionally among a set of participating buses. More specifically. a proportional control $\mathcal{R}_\alpha$ is defined by a nonnegative vector $\boldsymbol{\alpha} := (\alpha_k, k \in \mathcal{N})$ such that $\sum_{k\in\mathcal{N}} \alpha_k = 1$, with the interpretation that, post contingency, each bus $k \in \mathcal{N}$ adjusts its injection by the amount:

$$\mathcal{R}_\alpha : \quad \Delta p_k := -\alpha_k \sum_{k\in\mathcal{N}} p_k = \alpha_k \sum_{\hat{e}\in F_{\text{tie}}} f_{\hat{e}}, \quad k \in \mathcal{N}. \tag{4.3}$$

We call a bus k *participating* if $\alpha_k > 0$. By design, all participating buses adjust their injections in the same direction. Examples of proportional control $\mathcal{R}_\alpha$ include participation factors used in automatic generation control or economic dispatch [93, Chapter 3.8], or equal sharing of total imbalance among participating buses [9, 38]; see also [9, 39, 94]. In this chapter, we focus solely on proportional control $\mathcal{R}_\alpha$. For a different class of balancing rules in which the post-contingency injections are determined as a solution of an optimization problem to minimize the number of buses involved, see Chapters 6 and 7.

Under $\mathcal{R}_\alpha$, the vector of injection adjustments are then

$$\Delta\boldsymbol{p}_\alpha := (\Delta p_k, k \in \mathcal{N}) := \sum_{\hat{e}\in F_{\text{tie}}} f_{\hat{e}} \sum_{k\in\mathcal{N}} \alpha_k \boldsymbol{e}_k, \tag{4.4}$$

where $\boldsymbol{e}_k$ is the standard unit vector in $\mathbb{R}^n$. The post-contingency injections are thus $\boldsymbol{p} + \Delta\boldsymbol{p}_\alpha$. Since $\sum_{k\in\mathcal{N}} \alpha_k = 1$, the identity $\sum_{k\in\mathcal{N}}(p_k + \Delta p_k) = 0$ holds for any initial injection vector $\boldsymbol{p}$, which means that post-contingency power injections are always rebalanced under the proportional control $\mathcal{R}_\alpha$.

Let $(\tilde{\boldsymbol{f}}_{-F}, \tilde{\boldsymbol{\theta}})$ denote the post-contingency branch flows and voltage angles, which satisfy the DC power flow equations on the post-contingency network $(\mathcal{N}, \mathcal{E}\setminus F)$:

$$\boldsymbol{p} + \Delta\boldsymbol{p}_\alpha = \boldsymbol{C}_{-F}\tilde{\boldsymbol{f}}_{-F}, \tag{4.5a}$$

$$\tilde{\boldsymbol{f}}_{-F} = \boldsymbol{B}_{-F}\boldsymbol{C}_{-F}^T\tilde{\boldsymbol{\theta}}. \tag{4.5b}$$

For post-contingency network, we denote the Laplacian matrix by $\boldsymbol{L}_{-F} := \boldsymbol{C}_{-F}\boldsymbol{B}_{-F}\boldsymbol{C}_{-F}^T$ and define the matrix $\boldsymbol{A}_{-F}$ correspondingly in terms of the reduced Laplacian matrix $\overline{\boldsymbol{L}}_{-F}$.

In the next two sections, we use this island model to analyze line outage localization within the island $\mathcal{G}$ under the proportional control $\mathcal{R}_\alpha$.

4.2 Bridge Outage

In this section, we focus on the case of a single bridge $\hat{e}$ outage, i.e., $F_{\text{tie}} = \{\hat{e}\}$, and no internal line outages, i.e., $F = \emptyset$. In the next section, we will then extend the results to a cut set outage where the post-contingency branch flows in island $\mathcal{G}$ are impacted by both internal line outages in $F \subset \mathcal{E}$ and by tie line outages in F_{tie}. Since F is not a cut set in $\mathcal{G}$, we study this impact by combining the analysis of a non-cut outage in Chapter 3 of the thesis and that of a bridge outage.

Consider a single bridge $\hat{e}$ outage with pre-contingency branch flow $f_{\hat{e}}$ that disconnects the network into two islands. Focus on one of them, say $\mathcal{G}$. Let $\hat{j} := j(\hat{e})$ be the endpoint of $\hat{e}$ in island $\mathcal{G}$. In this case,

$$\Delta \boldsymbol{p}_{\text{tie}} = f_{\hat{e}}\, \boldsymbol{e}_{\hat{j}}. \tag{4.6}$$

Post contingency, the injections are changed from $\boldsymbol{p} + \Delta \boldsymbol{p}_{\text{tie}}$ to $\boldsymbol{p} + \Delta \boldsymbol{p}_{\alpha}$ under the proportional control $\mathcal{R}_{\alpha}$ as defined in (4.4). Note that since $F = \emptyset$, we have $-F = \mathcal{E}$, $\boldsymbol{C}_{-F} = \boldsymbol{C}$, $\boldsymbol{B}_{-F} = \boldsymbol{B}$ and $\boldsymbol{A}_{-F} = \boldsymbol{A}$. Therefore, the post-contingency branch flows $\tilde{\boldsymbol{f}}$ in the island $\mathcal{G}$ are given by

$$\begin{aligned} \tilde{\boldsymbol{f}} &= \boldsymbol{B}\boldsymbol{C}^T\boldsymbol{A}\,(\boldsymbol{p} + \Delta \boldsymbol{p}_{\alpha}) \\ &= \boldsymbol{B}\boldsymbol{C}^T\boldsymbol{A}\,(\boldsymbol{p} + \Delta \boldsymbol{p}_{\text{tie}} + \Delta \boldsymbol{p}_{\alpha} - \Delta \boldsymbol{p}_{\text{tie}}) \\ &= \boldsymbol{f} + \boldsymbol{B}\boldsymbol{C}^T\boldsymbol{A}\,(\Delta \boldsymbol{p}_{\alpha} - \Delta \boldsymbol{p}_{\text{tie}})\,. \end{aligned} \tag{4.7}$$

Using (4.4), (4.6), and the fact that $\sum_{k\in\mathcal{N}} \alpha_k = 1$, we get

$$\begin{aligned} \Delta \boldsymbol{p}_{\alpha} - \Delta \boldsymbol{p}_{\text{tie}} &= f_{\hat{e}} \sum_{k\in\mathcal{N}} \alpha_k \boldsymbol{e}_k - f_{\hat{e}}\, \boldsymbol{e}_{\hat{j}} \sum_{k\in\mathcal{N}} \alpha_k \\ &= f_{\hat{e}} \sum_{k\in\mathcal{N}} \alpha_k \left(\boldsymbol{e}_k - \boldsymbol{e}_{\hat{j}}\right). \end{aligned} \tag{4.8}$$

Substituting this expression in (4.7) gives

$$\tilde{\boldsymbol{f}} - \boldsymbol{f} = f_{\hat{e}} \sum_{k\in\mathcal{N}} \alpha_k\, \boldsymbol{B}\boldsymbol{C}^T\boldsymbol{A} \left(\boldsymbol{e}_k - \boldsymbol{e}_{\hat{j}}\right).$$

Recalling that $f_{\hat{e}} \neq 0$ by assumption, for any line $e = (i, j) \in \mathcal{E}$ we obtain

$$\begin{aligned} \frac{\tilde{f}_e - f_e}{f_{\hat{e}}} &= \sum_{k\in\mathcal{N}} \alpha_k\, B_e \left(A_{ik} + A_{j\hat{j}} - A_{i\hat{j}} - A_{jk}\right) \\ &= \sum_{k:\alpha_k>0} \alpha_k\, D_{e,k\hat{j}}, \end{aligned}$$

where $D_{e,k\hat{j}}$ is the power transfer distribution factor (PTDF) for island $\mathcal{G}$ defined in Chapter 3. Therefore, the branch flow change on line e is the superposition of impacts due to injecting $\alpha_k f_{\hat{e}}$ at participating buses $k \in \mathcal{N}$ and withdrawing them at bus $\hat{j}$. We can thus extend the definition of line outage distribution factor (LODF) $K_{e\hat{e}}$ to allow bridge outages as follows: given a bridge outage $\hat{e}$, under the proportional control $\mathcal{R}_\alpha$ for all $e \in \mathcal{E}$ we have

$$K_{e\hat{e}} := \frac{\tilde{f}_e - f_e}{f_{\hat{e}}} = \sum_{k:\alpha_k>0} \alpha_k \, D_{e,k\hat{j}}. \tag{4.9}$$

Note that $\hat{e} \notin \mathcal{E}$ in the island model that we consider here.

The next result is analogous to the Simple Cycle Criterion (see Theorem 3.6) for non-bridge outages. It states that all (μ-almost surely), and only, lines on a simple path[1] between bus $\hat{j}$ and a participating bus $k \in \mathcal{N}$ with $\alpha_k > 0$ will be impacted by the bridge $\hat{e}$ outage.

Theorem 4.1 (Simple Path Criterion: bridge outage)**.** *For a single bridge $\hat{e}$ outage, under the proportional control $\mathcal{R}_\alpha$, for every line e in the island $\mathcal{G}$, $K_{e\hat{e}} \neq 0$ "if" and only if there exists a simple path in $\mathcal{G}$ that contains e from $\hat{j}$ to a participating bus $k \in \mathcal{N}$.*

See Section 4.6 for a proof. Note that if $\hat{j}$ (the endpoint of $\hat{e}$ in $\mathcal{G}$) is the only participating bus, then $K_{e\hat{e}} = 0$ for all $e \in \mathcal{E}$.

Denote by $\mathcal{E}_1, \ldots, \mathcal{E}_b$ the unique block decomposition of $\mathcal{G}$.[2] We say a block $\mathcal{E}_k$ is *on a simple path between bus $\hat{j}$ and a participating bus $i \in \mathcal{N}$* if there is a simple path between bus $\hat{j}$ and bus i with $\alpha_i > 0$ that contains a line $e \in \mathcal{E}_k$. From Theorem 4.1 we can deduce the following localization property after a single bridge $\hat{e}$ outage in terms of the block structure of the island $\mathcal{G}$.

Corollary 4.2 (Bridge outage)**.** *Under the proportional control $\mathcal{R}_\alpha$ (4.3), for any block $\mathcal{E}_k$ of the island $\mathcal{G}$ the following statement hold:*

1. *$\tilde{f}_e = f_e$ for all lines e in block $\mathcal{E}_k$ if $\mathcal{E}_k$ is not on a simple path between bus $\hat{j}$ and a participating bus.*
2. *Conversely, $\tilde{f}_e \neq f_e$ for all lines e in $\mathcal{E}_k$ "if" $\mathcal{E}_k$ is on a simple path between bus $\hat{j}$ and a participating bus.*

[1] A simple path is a path that visits each node at most once.

[2] See Section 3.1 for the formal definition of network block decomposition.

Corollary 4.2 shows that the positions of participating buses play an important role in distributing the power imbalance across the network. In particular, the proportional control $\mathcal{R}_\alpha$ almost surely changes the branch flow on every line that lies in a path from the failure endpoint $\hat{j}$ to the set of participating buses. As a result, if e is a bridge connecting two sub-networks $\mathcal{G}_1$ and $\mathcal{G}_2$ post contingency (each of which contains one or more blocks), assuming $\hat{j} \in \mathcal{G}_1$, then $\Delta f_e \neq 0$ "if" and only if there is a participating bus in $\mathcal{G}_2$ since a path from $\hat{j}$ to any node in $\mathcal{G}_2$ must pass through the bridge e. If e is not a bridge, i.e., e belongs to a non-bridge block, then we can devise a simple sufficient condition for $\Delta f_e \neq 0$ using *participating blocks*, defined as follows:

Definition 4.3. *Consider an island $\mathcal{G}$ with block decomposition $\mathcal{E}_1, \mathcal{E}_2, \ldots, \mathcal{E}_b$ operating under proportional control $\mathcal{R}_\alpha$ with a set $\mathcal{N}_\alpha := \{i \in \mathcal{N} : \alpha_i > 0\}$ of participating buses. A non-bridge block is said to be a* **participating block** *if there is a non-cut vertex in this block that is a participating bus.*

If all generators participate in automatic generation control (AGC) and load-side participation is implemented at all load buses, then every node in the network is a participating bus and, hence, every block is participating.

The following result, whose proof is presented in Section 4.6, shows that if a non-bridge block is participating, then all lines inside it are impacted when the original bridge $\hat{e}$ is disconnected.

Corollary 4.4. *Consider a bridge outage $\hat{e}$ with non-zero branch flow $f_{\hat{e}} \neq 0$ and let the block decomposition of island $\mathcal{G}$ be $\mathcal{E}_1, \ldots, \mathcal{E}_b$. If $\mathcal{E}_k$ is a participating block, then $\Delta f_e \neq 0$ μ-almost surely for any $e \in \mathcal{E}_k$, i.e., $\mu(\Delta f_e \neq 0) = 1$.*

4.3 Cut Set Outage

We now extend our results to a cut set outage F'. Consider an island $\mathcal{G} = (\mathcal{N}, \mathcal{E})$ and, as before, partition the tripped lines into tie lines and internal lines, i.e., $F' = F \cup F_{\text{tie}}$.

The impact on post-contingency branch flows is a superposition of the impact of internal line outages in F, weighted by generalized line outage distribution factor (GLODF) with multiple tripped lines $\boldsymbol{K}^F$, and the impact of tie line outages in F_{tie}, weighted by the proportional control $\mathcal{R}_\alpha$ as well as PTDF of the post-contingency network, as stated in the following theorem (proved in Section 4.6).

Theorem 4.5. *Given an island $\mathcal{G} = (\mathcal{N}, \mathcal{E})$ with a cut set outage F', under the proportional control $\mathcal{R}_\alpha$* (4.4) *the branch flow changes on the surviving lines in*

$-F = \mathcal{E} \setminus F$ are given by

$$\Delta \boldsymbol{f}_{-F} = \boldsymbol{K}^F \boldsymbol{f}_F + \sum_{\hat{e} \in F_{tie}} f_{\hat{e}} \sum_{k \in \mathcal{N}} \alpha_k \hat{\boldsymbol{D}}^F \left(\boldsymbol{e}_k - \boldsymbol{e}_{j(\hat{e})} \right), \tag{4.10}$$

where $\boldsymbol{K}^F := \boldsymbol{B}_{-F} \boldsymbol{C}_{-F}^T \boldsymbol{A} \boldsymbol{C}_F \left(\boldsymbol{I} - \boldsymbol{B}_F \boldsymbol{C}_F^T \boldsymbol{A} \boldsymbol{C}_F \right)^{-1}$ is the GLODF[3] of island $\mathcal{G}$ with a non-cut outage F, and $\hat{\boldsymbol{D}}^F$ is the PTDF for the post-contingency network $(\mathcal{N}, \mathcal{E} \setminus F)$ defined as

$$\hat{\boldsymbol{D}}^F := \boldsymbol{B}_{-F} \boldsymbol{C}_{-F} \boldsymbol{A}_{-F}, \tag{4.11a}$$

which can equivalently be expressed in terms of the pre-contingency island $\mathcal{G}$ as

$$\hat{\boldsymbol{D}}^F = \left(\boldsymbol{B}_{-F} \boldsymbol{C}_{-F}^T + \boldsymbol{K}^F \boldsymbol{B}_F \boldsymbol{C}_F^T \right) \boldsymbol{A}. \tag{4.11b}$$

The theorem reduces to (4.9) for a single bridge $\hat{e}$ outage, that is when $F = \emptyset$ and $F_{\text{tie}} = \{\hat{e}\}$. When the cut set outage contains both internal line outages in F and tie line outages in F_{tie}, the post-contingency branch flows depend on both types of outages in an intricate way. Our theorem makes this relationship explicit and precise:

1. The first term on the right-hand side of (4.10) represents the impact of the outage of a non-cut set F of internal lines in $\mathcal{G}$ through the GLODF $\boldsymbol{K}^F$ of island $\mathcal{G}$. If there are no tie line outages $F_{\text{tie}} = \emptyset$, then the formula reduces to the GLODF for a non-cutset outage as discussed in Chapter 3.

2. The second term on the right-hand side of (4.10) represents the impact of the proportional control $\mathcal{R}_\alpha$ in response to tie line outages in F_{tie}. If there are no internal line outages $F = \emptyset$, then the formula reduces to

$$\Delta \boldsymbol{f}_{-F} = \sum_{\hat{e} \in F_{\text{tie}}} f_{\hat{e}} \sum_{k \in \mathcal{N}} \alpha_k \hat{\boldsymbol{D}}^F \left(\boldsymbol{e}_k - \boldsymbol{e}_{j(\hat{e})} \right),$$

   which generalizes (4.9) from a single bridge $\hat{e}$ outage to a cut set F_{tie} outage with multiple tripped tie lines. In this case the impact of simultaneous outage of a set F_{tie} of tie lines is simply the sum of the impacts of single-bridge outages *as if* $\hat{e}$ is a bridge incident on $\mathcal{G}$. The expressions for $\hat{\boldsymbol{D}}^F$ (4.11a) and (4.11b) in terms of pre- and post-contingency network trivially coincide when $F = \emptyset$.

[3] See Chapter 3 for more details on GLODFs.

3. When both $F \neq \emptyset$ and $F_{\text{tie}} \neq \emptyset$, the effect of their outages on post-contingency branch flows can be interpreted in terms of either the pre-contingency network $\boldsymbol{A}$ or the post-contingency network $\boldsymbol{A}_{-F}$, through the expressions for both $\boldsymbol{K}^F$ and $\hat{\boldsymbol{D}}^F$. In particular the expression for $\hat{\boldsymbol{D}}^F$ in terms of the pre-contingency network $\boldsymbol{A}$ has two components. The first component $\boldsymbol{B}_{-F}\boldsymbol{C}_{-F}^T\boldsymbol{A}$ says that the injection adjustments due to the proportional control α_k will change the branch flows on the surviving lines in $-F$ according to PTDF. The second component $\boldsymbol{K}^F\boldsymbol{B}_F\boldsymbol{C}_F^T\boldsymbol{A}$ says that the injection adjustments are first mapped to flow changes on lines in F through PTDF $\boldsymbol{B}_F\boldsymbol{C}_F^T\boldsymbol{A}\left(\boldsymbol{e}_k - \boldsymbol{e}_{j(\hat{e})}\right)$ in the *pre-contingency* network, and they are then mapped to flow changes on surviving lines in $-F$ through $\boldsymbol{K}^F$ when lines in the non-cut set F are disconnected.

4. According to the expression (4.11a) for $\hat{\boldsymbol{D}}^F$, the post-contingency network integrates both effects: changes to post-contingency branch flows are the sum of the impact of injection adjustments under proportional control factor α_k through PTDF $\boldsymbol{B}_{-F}\boldsymbol{C}_{-F}^T\boldsymbol{A}_{-F}\left(\boldsymbol{e}_k - \boldsymbol{e}_{j(\hat{e})}\right)$ on the *post-contingency* network.

Considering a surviving line $e \in -F$, the flow change is given by, in terms of pre-contingency island $\mathcal{G}$:

$$\begin{aligned}
\Delta f_e &= \sum_{\tilde{e}\in F} K^F_{e\tilde{e}} f_{\tilde{e}} \\
&\quad + \sum_{\hat{e}\in F_{\text{tie}}} f_{\hat{e}} \sum_{k\in\mathcal{N}} \alpha_k \Big(D_{e,kj(\hat{e})} + \sum_{\tilde{e}\in F} K^F_{e\tilde{e}} D_{\tilde{e},kj(\hat{e})} \Big) \\
&= \sum_{\tilde{e}\in F} K^F_{e\tilde{e}} \Big(f_{\tilde{e}} + \sum_{\hat{e}\in F_{\text{tie}}} \sum_{k\in\mathcal{N}} \alpha_k D_{\tilde{e},kj(\hat{e})} f_{\hat{e}} \Big) \\
&\quad + \sum_{\hat{e}\in F_{\text{tie}}} f_{\hat{e}} \sum_{k\in\mathcal{N}} \alpha_k D_{e,kj(\hat{e})}. \qquad (4.12)
\end{aligned}$$

From Theorem 3.10 (which covers the case of a non-cut outage), it follows that the first term is zero if e is not in the same block as any disconnected internal line $\hat{e} \in F$ (since $K^F_{e\hat{e}} = 0$) of the island $\mathcal{G}$. Applying the Simple Path Criterion in Theorem 4.1 implies that the second term is zero if, for every tie line $\hat{e} \in F_{\text{tie}}$ and every participating bus $k \in \mathcal{N}$ with $\alpha_k > 0$, l does not lie on any simple path in $\mathcal{G}$ connecting $j(\hat{e})$ and k. We can thus derive the following localization property in terms of the block decomposition of $\mathcal{G}$.

Corollary 4.6 (Cut set outage)**.** *For a cut set F' outage, under the proportional control $\mathcal{R}_\alpha$ (4.4), for any surviving line $e \in -F$ in the island $\mathcal{G}$, $\Delta f_e = 0$ if the unique block $\mathcal{E}_k$ containing e satisfies both the following conditions:*

- *$\mathcal{E}_k$ contains no disconnected internal line $\hat{e} \in F$; and*
- *For every tie line $\hat{e} \in F_{tie}$ and every participating bus $i \in \mathcal{N}$ with $\alpha_i > 0$, $\mathcal{E}_k$ is not on a simple path in $\mathcal{G}$ between $j(\hat{e})$ and k.*

The converse in general is false because, even when both terms in (4.12) are nonzero, they may cancel with each other, resulting in $\Delta f_e = 0$.

4.4 Case Studies

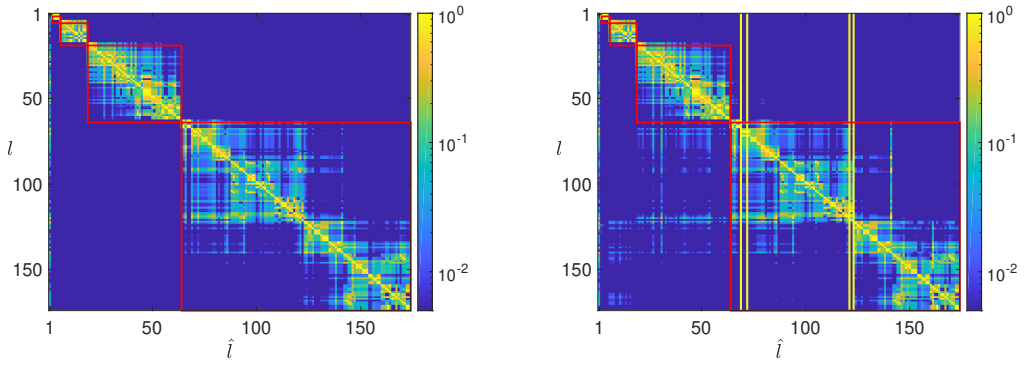

(a) DC (b) AC

Figure 4.2: The LODF matrix (reporting the absolute values of the distribution factors) of IEEE 118-bus network calculated under (a) DC and (b) AC power flow model. The four yellow solid line in (b) represent four transmission lines whose failure lead to non-convergent AC power flow equations. The red rectangles indicate blocks of the network.

Theorem 3.5 and Theorem 4.5 summarize the mathematical theory that characterizes the patterns of line failure propagation in power systems. More specifically, the failure localizability depends critically on the block decomposition of a power network. In this section, we demonstrate these localizability properties through simulations using the IEEE 118-bus test network.

IEEE 118-bus Network

This IEEE test network consists of 118 nodes and 186 edges and has a block decomposition with two non-bridge blocks: one giant block with 164 edges, and a smaller one with 13 edges. There are trivial “dangling" appendages each of which connects a single node to the giant block[4]. For a clearer demonstration, we remove

[4]It should be mentioned that many detailed models of transmission networks have a meshed core with “dangling” appendages like IEEE 118-bus system.

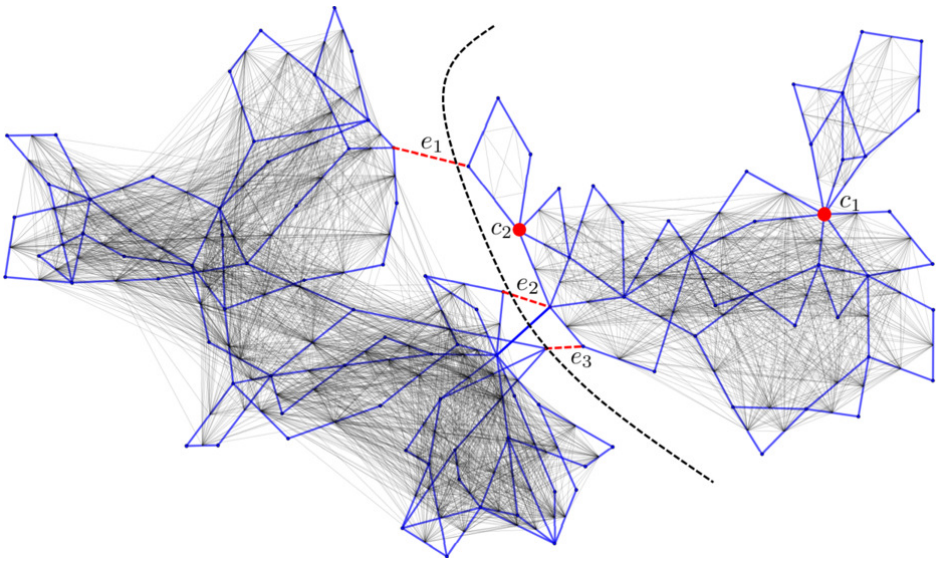

Figure 4.3: Influence graphs on the IEEE 118-bus test network after switching off lines e_1, e_2 and e_3. Blue edges represent physical transmission lines and grey edges represent connections in the influence graph. The black dashed line and the red solid points indicate the failure propagation boundary defined by the blocks.

these dangling bridges and replace them by power injections at the corresponding endpoints in the giant block that equal the power flows on these bridges. In addition, we switch off three transmission lines to create more non-bridge blocks to better illustrate the block diagonal structure of the LODF matrix. The resulting network is composed of 4 non-bridge blocks with 4, 13, 45 and 110 edges, connected by one bridge block and two cut vertices.

In Chapter 6, we explore ways to judiciously switch off a small number of transmission lines to create more blocks for localizing failures. In this section, however, we focus on characterizing the intrinsic properties of a power network itself rather than the design for network reconfiguration and dynamic controller.

LODF Matrix

In our experiments, the system parameters are taken from the Matpower Package [95] and we calculate the LODF matrix $\boldsymbol{K} = (K_{e\hat{e}}, e \in \mathcal{E}, \hat{e} \in \mathcal{E})$ that describes the impact on other lines of a single line outage. For non-bridge outages, we directly calculate the LODF as defined in (3.1). For bridge outages that create islands, we adopt the proportional control and assume all nodes are participating with the same participating factor $\alpha_k = \alpha$ for all k.

We visualize the magnitude of LODF matrix in Fig. 4.2a by means of a heatmap,

in which we reorder the lines based on the block they belong to. Specifically, we stack bridge blocks first, followed by non-bridge blocks in nondecreasing order of the block size. In addition, we set a color limit for better visualization so that $|K_{e\hat{e}}| \leq 0.005$ maps to dark blue and $|K_{e\hat{e}}| \geq 1$ maps to yellow. In Fig. 4.2b, we plot the same heatmap under the AC power flow equations (the four yellow solid line represent four transmission lines whose failure lead to non-convergent AC power flow equations), where the LODF is computed directly from its definition $K_{e\hat{e}} = \frac{\Delta f_e}{f_{\hat{e}}}$.

In both the DC and AC case, the global effect of a bridge failure is clearly visible in the first column (since only one line is a bridge) of the LODF matrices in Fig. 4.2. Since almost all the entries of that column are non-zero, almost all surviving lines will be impacted by the failure of that bridge. For non-bridge failures, the LODF matrix in the DC case exhibits a clear block diagonal structure. In the AC case, however, the cross-block entries are not necessary zero, but they are relatively small. Moreover, the LODF within a block are similar for both cases, indicating that the LODF computed from DC model can be a good approximation for AC model. We further remark that the LODFs within a block can be small, but they are strictly nonzero in all cases, confirming our result in Theorem 3.8.

Influence Graph

We now visualize the transmission line failure propagation patterns using an *influence graph*. Despite being similar in concept to that of [2, 96], unlike these influence graphs which are based on a probabilistic failure models, our influence graph is simply a visualization of the LODFs $K_{e\hat{e}}$ that we superimpose on the original network topology. The IEEE 118-bus network topology is depicted in blue in Fig. 4.3. The corresponding influence graph has these transmission lines (in blue) as nodes and connect any two transmission lines e and $\hat{e}$ in the influence graph (with a grey edge) if the corresponding LODF satisfies $|K_{e\hat{e}}| \geq 0.005$. As Fig. 4.3 shows, the impact a non-bridge outages are "blocked" by cut-vertices or bridges. Specifically, there are no edges connecting transmission lines that belong to different blocks, as predicted by our theory.

4.5 Conclusion

In this chapter, we make use of the spectral representation of power redistribution developed in Chapter 3 to provide a characterization of line failure localizability when the initial failure disconnects the original network. This, together with our results in Chapter 3, establishes a mathematical theory that covers all initial failure

scenarios and reveals how a general power system responds to such disturbances. A case study on the IEEE 118-bus test network corroborates the block-diagonal structure predicted by our theory, even when the system is under full AC power flow equations.

Our results in Chapters 3 and 4 can be further built upon in several ways: (a) Some practical power systems have been operating in partitioned mode. However, their tie-lines are high voltage DC (HVDC) transmission lines. One major feature of HVDC lines is that they are sensitive to voltage disturbances [97] so outages inside a block can cause HVDC outages, and further triggering outages in other blocks. More study is needed to fully understand line failure localizability for such systems. (b) The network block decomposition has potential application in power systems planning. It can also be used as a corrective action immediately after a contingency, similar to controlled islanding, to prevent failure propagation; see [67] for a recent paper exploring this possibility. It would be interesting to understand the tradeoffs of post-contingency corrective block configuration and controlled islanding and how they can be synergistically integrated for failure mitigation. (c) Our model builds upon DC power flow dynamics, which are accurate for small deviations but less so under large disruptions. Yet, our preliminary simulations suggest a strong underlying structure that connects the gap between DC and AC models in the context of line failures. It would be interesting to understand this structure and develop bounds on the distance between DC and AC predictions. (d) It is possible to integrate fast-timescale frequency control into our framework to provide a control strategy with provably optimal localization and mitigation properties. In Chapter 6, we integrate the network block decomposition with the frequency control algorithm to achieve better failure mitigation and localization performance.

4.6 Proofs

Proof of Theorem 4.1

The proof is similar to that for the Simple Loop Criterion in Theorem 3.6. Recall from Chapter 3 that the PTDF $D_{e,k\hat{j}}$ at participating buses in (4.9) is given by:

$$\frac{B_e}{\sum_{H\in\mathcal{T}_\mathcal{E}}\beta(H)}\left(\sum_{H\in\mathcal{T}(ik,j\hat{j})}\beta(H) \;-\; \sum_{H\in\mathcal{T}(i\hat{j},jk)}\beta(H)\right).$$

Note that the spanning forests H in $\mathcal{T}_\mathcal{E}$, $\mathcal{T}(ik, j\hat{j})$ and $T(i\hat{j}, jk)$ are spanning forests of the pre-contingency network, not just the post-contingency island.

Suppose $D_{e,k\hat{j}} \neq 0$. Then either $\mathcal{T}(ik, j\hat{j})$ or $\mathcal{T}(i\hat{j}, jk)$ or both is nonempty. Suppose without loss of generality that there is a spanning forest $H \in \mathcal{T}(ik, j\hat{j})$. Then there is a path in H from buses $\hat{j}$ to j and another vertex-disjoint path from buses i to k. Joining these two paths with the line $e = (i, j)$ creates a simple path from $\hat{j}$ to k that contains line e, as desired.

Conversely suppose there is a simple path in $\mathcal{G}$ from $\hat{j}$ to a participating bus $k' \in \mathcal{N}$ that contains $e = (i, j)$. We will show that $g(\boldsymbol{B}) := \sum_k D_{e,k\hat{j}}(\boldsymbol{B})\alpha_k$ in (4.9) as a polynomial in the susceptances $\boldsymbol{B}$ of *all* lines in the pre-contingency network is not identically zero, and hence $\mu(g(\boldsymbol{B} + \boldsymbol{w}) = 0) = 0$. Since the pre-contingency network is connected the simple path in the island $\mathcal{G}$ from buses $\hat{j}$ to k' that contains $e = (i, j)$ can be extended into a spanning tree of the pre-contingency network. Suppose without loss of generality that, on this spanning tree, the path from $\hat{j}$ to i contains j, i.e., the path from k' to $\hat{j}$ is of the form $k' \rightsquigarrow i \rightarrow j \rightsquigarrow \hat{j}$. Then removing the edge e from this spanning tree creates a spanning forest H in $\mathcal{T}(ik', j\hat{j})$ that contains exactly two trees, denoted by $H_{ik'}$ connecting buses i, k' and $H_{j\hat{j}}$ connecting buses $j, \hat{j}$. Following a similar argument in our proof for the Simple Cycle Criterion, for $H \notin \mathcal{T}(i\hat{j}, jk')$ the term $\beta(H)$ is not canceled by a negative term in $D_{e,k'\hat{j}}$. Moreover we claim that $H \notin \mathcal{T}(i\hat{j}, jk)$ for all other participating buses k and therefore $\beta(H)$ is not canceled by negative terms from other $D_{e,k\hat{j}}$ in $g(\boldsymbol{B})$ either. To see this, if $H \in \mathcal{T}(i\hat{j}, jk)$ for a participating bus k, then there must be a path in H connecting buses i to $\hat{j}$, but this path then connects tree $H_{ik'}$ to tree $H_{j\hat{j}}$ into a spanning tree. This contradicts that the spanning forest $H \in \mathcal{T}(ik', j\hat{j})$ consists of two distinct trees. Hence $g(\boldsymbol{B})$ is not a zero polynomial and $K_{e\hat{e}} \neq 0$ μ-almost surely. □

Proof of Corollary 4.2

Let $\overline{C}$ be the block that contains e. Since $\mathcal{E}_k$ is a participating region, we know there exists a bus within C, say n_1, that participates the power balance and is not a cut vertex. Note that any path from $j(\hat{e})$ to C must go through a common cut vertex in C, say n_e. Now by adding an edge between n_e and n_1 (if such edge did not originally exist), the resulting block C' is still 2-connected. Thus there exists a simple cycle in C' that contains the edge (n_e, n_1) and $e := (i, j)$, which implies we can find two disjoint paths P_1 and P_2 connecting the endpoints of these two edges. Without loss of generality, assume P_1 connects n_e to i and P_2 connects n_1 to j. By concatenating the path from $j(\hat{e})$ to n_e, we can extend P_1 to a path $\tilde{P}_1$ from $j(\hat{e})$ to i, which is still disjoint from P_2. Now, by adjoining $\hat{e}$ to $\tilde{P}_1$ and P_2, we can construct a

path from $j(\hat{e})$ to n_1 that passes through e. The Simple Path Criterion then implies $\mu(\Delta f_{\hat{e}} \neq 0) = 1$. □

Proof of Theorem 4.5

The first part of Theorem 4.5 is proved by analyzing the post-contingency network $(\mathcal{N}, \mathcal{E} \setminus F)$ using the matrix $\boldsymbol{A}_{-F}$, while the second part leverages the relation between the matrices A for the pre- and post-contingency networks. Similar to our analysis of GLODF, taking the difference between (4.5b) and (4.2b) shows that the branch flow changes $\Delta \boldsymbol{f}_{-F} := \tilde{\boldsymbol{f}}_{-F} - \boldsymbol{f}_{-F}$ satisfy the post-contingency DC power flow equations:

$$\begin{aligned} \boldsymbol{C}_F \boldsymbol{f}_F + (\Delta \boldsymbol{p}_\alpha - \Delta \boldsymbol{p}_{\text{tie}}) &= \boldsymbol{C}_{-F} \Delta \boldsymbol{f}_{-F}, \\ \Delta \boldsymbol{f}_{-F} &= \boldsymbol{B}_{-F} \boldsymbol{C}_{-F}^T \left(\tilde{\boldsymbol{\theta}} - \boldsymbol{\theta} \right). \end{aligned}$$

Recall that $\boldsymbol{A}_{-F}$ is defined in terms of the inverse of the reduced Laplacian matrix $\boldsymbol{L}_{-F} = \boldsymbol{C}_{-F} \boldsymbol{B}_{-F} \boldsymbol{C}_{-F}^T$ for the post-contingency network. The branch flow changes are given by

$$\begin{aligned} \Delta \boldsymbol{f}_{-F} &= \boldsymbol{B}_{-F} \boldsymbol{C}_{-F}^T \boldsymbol{A}_{-F} \left(\boldsymbol{C}_F \boldsymbol{f}_F + \Delta \boldsymbol{p}_\alpha - \Delta \boldsymbol{p}_{\text{tie}} \right) \\ &= \underbrace{\boldsymbol{B}_{-F} \boldsymbol{C}_{-F}^T \boldsymbol{A}_{-F} \boldsymbol{C}_F}_{\boldsymbol{K}^F} \boldsymbol{f}_F \\ &\quad + \underbrace{\boldsymbol{B}_{-F} \boldsymbol{C}_{-F}^T \boldsymbol{A}_{-F}}_{\hat{\boldsymbol{D}}^F} \left(\Delta \boldsymbol{p}_\alpha - \Delta \boldsymbol{p}_{\text{tie}} \right), \end{aligned}$$

where the GLODF $\boldsymbol{K}^F = \boldsymbol{B}_{-F} \boldsymbol{C}_{-F}^T \boldsymbol{A}_{-F} \boldsymbol{C}_F$ is defined by Theorem 3.5 and $\hat{\boldsymbol{D}}^F$ is defined in (4.11a). From (4.4) and (4.1) it follows that

$$\Delta \boldsymbol{p}_\alpha - \Delta \boldsymbol{p}_{\text{tie}} = \sum_{\hat{e} \in F_{\text{tie}}} f_{\hat{e}} \sum_{k \in \mathcal{N}} \alpha_k \left(\boldsymbol{e}_k - \boldsymbol{e}_{j(\hat{e})} \right). \tag{4.13}$$

Hence the branch flow changes are the sum of the impacts of internal line outages in F and tie line outages in F_{tie}:

$$\Delta \boldsymbol{f}_{-F} = \underbrace{\boldsymbol{K}^F \boldsymbol{f}_F}_{\text{int. line } F \text{ outage}} + \underbrace{\sum_{\hat{e} \in F_{\text{tie}}} f_{\hat{e}} \sum_{k \in \mathcal{N}} \alpha_k \hat{\boldsymbol{D}}^F \left(\boldsymbol{e}_k - \boldsymbol{e}_{j(\hat{e})} \right)}_{\text{tie line } F_{\text{tie}} \text{ outage}}.$$

This proves identity (4.10) of Theorem 4.5.

We now show that (4.11b) is an alternative representation of (4.11a). To do so, we express the matrix $\hat{\boldsymbol{D}}^F$ in terms of the matrices of the pre-contingency network. In

particular, we relate A_{-F} with A using matrix inversion lemma as follows:

$$\begin{aligned}
\hat{\boldsymbol{D}}^F &= \boldsymbol{B}_{-F}\boldsymbol{C}_{-F}^T\boldsymbol{A}_{-F} \\
&= \boldsymbol{B}_{-F}\boldsymbol{C}_{-F}^T\boldsymbol{A} \\
&\quad +\boldsymbol{B}_{-F}\boldsymbol{C}_{-F}^T\boldsymbol{A}\boldsymbol{C}_F\left(\boldsymbol{I}-\boldsymbol{B}_F\boldsymbol{C}_F^T\boldsymbol{A}\boldsymbol{C}_F\right)^{-1}\boldsymbol{B}_F\boldsymbol{C}_F\boldsymbol{A} \\
&= \boldsymbol{B}_{-F}\boldsymbol{C}_{-F}^T\boldsymbol{A}+\boldsymbol{K}^F\boldsymbol{B}_F\boldsymbol{C}_F\boldsymbol{A}.
\end{aligned}$$

□

Chapter 5

INTERFACE NETWORKS AND FAILURE LOCALIZATION

An interconnected power system comprises sub-grids that are usually individually managed by independent system operators (ISOs). It is desirable to localize failure impact within the sub-grid where the failure happens while leaving other sub-grids unaffected. In Chapters 3 and 4, we show that non-cut failures are localized if sub-grids are connected in a tree structure and that, if sub-grids are connected by multiple lines, failures cannot be completely localized. This suggests switching off certain transmission lines in order to leave only one line between sub-grids.

However, maintaining a tree structure at the sub-grid level is at odds with the $N-1$ security standard. Further, a tree-connected power network significantly reduces the power transmission capacity between the sub-grids, increasing the cost of power dispatch. It is therefore desirable to have multiple lines between sub-grids to ensure there is no single-point vulnerabilities and to increase the power transmission capacity.

These contrasting views lead to an important open question: *Is it possible to provably localize failures within sub-grids without creating a single point of failure?*

In this chapter, we continue to investigate the LODFs as a metric to quantify the localization of line failures. In particular, we extend our localization results to the cases when the sub-grids are connected by different interface networks with robust connectivity, rather than a tree structure. Specifically, we consider a power network consisting of two sub-grids and propose three alternative *interface networks* to connect them, as shown in Fig. 5.1. We prove, in Theorems 5.4 and 5.5, that the LODFs are not increasing if the sub-grids are connected by a series (Fig. 5.1b) or a parallel (Fig. 5.1c) interface network. We further provide an upper bound for the LODF if the sub-grids are connected by a 2×2 complete bipartite network (Fig. 5.1d) in Theorem 5.6. By carefully designing the line susceptances of the interface network, the complete bipartite interface network can eliminate failure propagation to other sub-grids while keeping the impact on surviving lines in the same sub-grid unchanged. We validate the efficacy of the proposed interface networks on the IEEE 118-bus test network under both DC and AC power flow models. All three interface networks decrease the LODF for lines in different sub-grids, with the complete

bipartite network achieving the best localization.

There have been extensive efforts toward understanding the localizability of failures in power systems to network topological structures. Most papers focus on summarizing empirical results. For example, [38] observes the LODF decreases as the distance from the tripped line increases, and [54] defines another distance metric that better captures such decay. There are only a few papers presenting analytical results on failure localization. Following our work in Chapter 3 on the topological representation for the LODF and the characeterization on LODF being zero if sub-grids are connected in a tree structure, tree-partitioning has been proposed to replace controlled islanding as a defense mechanism to arrest cascading failure in [67]. However, a power network with tree-connected sub-grids is less practical as it creates a single point of failure. In [98], authors propose to connect the sub-grids by a complete bipartite interface, the network isolator, to suppress the failure spreading. However, they require the adjacency matrix (weighted by line susceptance) of the interface network to be exactly rank-1 which can be difficult to satisfy in practice. To the best of our knowledge, our result is the first to mathematically characterize the LODF with sub-grids connected by interface networks beyond the rank-1 setting.

5.1 Power Redistribution

When a line failure occurs, the power will redistribute over the post-contingency network, and line flows can both increase or decrease, sometimes even reversing their directions. The power transfer (PTDF) and the line outage (LODF) distribution factors are commonly used to describe the post-contingency line flows, as discussed in Chapters 3 and 4.

Consider a non-bridge line failure $\hat{e} = (\hat{i}, \hat{j})$ and a surviving transmission line $e \in \mathcal{E} \setminus \{\hat{e}\}$. Recall that the PTDF and LODF can be computed with the pre-contingency network[1]:

$$D_{e,\hat{i}\hat{j}} = B_e(\boldsymbol{e}_i - \boldsymbol{e}_j)^T \boldsymbol{L}^\dagger(\boldsymbol{e}_{\hat{i}} - \boldsymbol{e}_{\hat{j}}), \tag{5.1a}$$

$$K_{e\hat{e}} = \frac{B_e(\boldsymbol{e}_i - \boldsymbol{e}_j)^T \boldsymbol{L}^\dagger(\boldsymbol{e}_{\hat{i}} - \boldsymbol{e}_{\hat{j}})}{1 - B_{\hat{e}}(\boldsymbol{e}_{\hat{i}} - \boldsymbol{e}_{\hat{j}})^T \boldsymbol{L}^\dagger(\boldsymbol{e}_{\hat{i}} - \boldsymbol{e}_{\hat{j}})}, \tag{5.1b}$$

where $\{\boldsymbol{e}_k\}_{k=1,\ldots,n}$ is the standard vector basis. In Chapter 3, we show that the PTDFs

[1] Note that we have $(\boldsymbol{e}_i - \boldsymbol{e}_j)^T \boldsymbol{L}^\dagger(\boldsymbol{e}_{\hat{i}} - \boldsymbol{e}_{\hat{j}}) = (\boldsymbol{e}_i - \boldsymbol{e}_j)^T \boldsymbol{A}(\boldsymbol{e}_{\hat{i}} - \boldsymbol{e}_{\hat{j}})$ for any nodes $i, j, \hat{i}, \hat{j}$.

and LODFs are related as in (3.1):

$$K_{e\hat{e}} = \frac{D_{e,\hat{i}\hat{j}}}{1 - D_{\hat{e},\hat{i}\hat{j}}}.$$

This expression suggests that the power redistribution after line failures can be emulated by introducing fictitious injections over the pre-contingency network [48]. In fact, the power redistribution can be analyzed over the post-contingency network as well. Recall in Chapter 3, we relate the LODFs for the pre-contingency network and the PTDF for the post-contingency network. For convenience, we summarize the result as follows:

Lemma 5.1. *Consider a network $\mathcal{G} = (\mathcal{N}, \mathcal{E})$ and a non-bridge transmission line $\hat{e}$ failure*[2]*. Let $K_{e\hat{e}}$ denote the LODF for the pre-contingency network $\mathcal{G}$, and let $D^{\hat{e}}_{e,\hat{i}\hat{j}}$ denote the PTDF for the post-contingency network $\tilde{\mathcal{G}} = (\mathcal{N}, \mathcal{E} \setminus \hat{e})$. We have $K_{e\hat{e}} = D^{\hat{e}}_{e,\hat{i}\hat{j}}$.*

Lemma 5.1 suggests that the impact of a transmission line $\hat{e} = (\hat{i}, \hat{j})$ failure is equivalent to the power flows when the pre-contingency flow $f_{\hat{e}}$ is injected at bus $\hat{i}$ and withdrawn from bus $\hat{j}$ over the post-contingency network. This post-contingency perspective allows us to convert the calculation of LODF into the calculation of PTDF, relating the failure impact directly to the network topology.

We remark that the above result holds also in the case of multiple line failures. Consider a set F of lines that are simultaneously disconnected and suppose the post-contingency network remains connected. The generalized LODF $K^F_{e\hat{e}}$ equals the PTDF for line e with the pair of buses $\hat{i}, \hat{j}$ of the post-contingency network $\tilde{\mathcal{G}} = (\mathcal{N}, \mathcal{E} \setminus F)$, i.e., $K^F_{e\hat{e}} = D^F_{e,\hat{i}\hat{j}}$, as proven in Theorem 3.5. To simplify the presentation, we restrict ourself to the case of single non-bridge failures in the rest of this chapter.

Decomposition of the PTDF

A power grid usually consists of several interconnected sub-grids and it is of interest to decompose the calculation of distribution factors accordingly. In this section, we introduce such a decomposition for certain network structures of PTDFs. Specifically, suppose a connected network $\mathcal{G} = (\mathcal{N}, \mathcal{E})$ can be decomposed into two sub-grids: $\mathcal{G}_1 = (\mathcal{N}_1, \mathcal{E}_1)$ and $\mathcal{G}_2 = (\mathcal{N}_2, \mathcal{E}_2)$ such that:

[2] A non-bridge line is a transmission line whose deletion does not increase the network's number of connected components. Otherwise it is a bridge.

- The line sets do not overlap: $\mathcal{E}_1 \cap \mathcal{E}_2 = \emptyset$, $\mathcal{E}_1 \cup \mathcal{E}_2 = \mathcal{E}$;
- The bus sets overlap with only 2 buses: $\mathcal{N}_1 \cap \mathcal{N}_2 = \{s, t\}$, $\mathcal{N}_1 \cup \mathcal{N}_2 = \mathcal{N}$.

Given a pair of buses i, j of the network $\mathcal{G}$ (not necessarily adjacent to each other), we define *effective susceptance* between i, j to be

$$B_{ij}^{(e)} = \frac{1}{(\boldsymbol{e}_i - \boldsymbol{e}_j)^T \boldsymbol{L}^\dagger (\boldsymbol{e}_i - \boldsymbol{e}_j)}. \tag{5.2}$$

The effective susceptance summarizes the network effect between a pair of buses by a single line [59].

The following proposition demonstrates how $D_{e,\hat{i}\hat{j}}$, the PTDF for line e and a pair of buses $\hat{i}, \hat{j}$ in different sub-grids, can be decomposed.

Proposition 5.2. *Consider a network $\mathcal{G}$ and its decomposition $\mathcal{G}_1$, $\mathcal{G}_2$. Let $\hat{\mathcal{G}}_1 = (\mathcal{N}_1, \mathcal{E}_1 \cup (s,t))$ be a graph by adding a fictitious line (s,t) to the sub-grid $\mathcal{G}_1$, with susceptance equaling the effective susceptance between buses s, t of the sub-grid $\mathcal{G}_2$:*

$$B_{st}^{(e)} = \frac{1}{(\boldsymbol{e}_s - \boldsymbol{e}_t)^T \boldsymbol{L}_2^\dagger (\boldsymbol{e}_s - \boldsymbol{e}_t)},$$

where $\boldsymbol{L}_2$ is the Laplacian matrix of $\mathcal{G}_2$. For any pair of buses $\hat{i}, \hat{j} \in \mathcal{N}_1$ and any line $e \in \mathcal{E}_2$, the PTDF $D_{e,\hat{i}\hat{j}}$ can be computed as:

$$D_{e,\hat{i}\hat{j}} = \hat{D}_{(s,t),\hat{i}\hat{j}} \cdot \bar{D}_{e,st},$$

where $\hat{D}_{(s,t),\hat{i}\hat{j}}$ is the PTDF for the fictitious line (s,t) and the pair of buses $\hat{i}, \hat{j}$ of $\hat{\mathcal{G}}_1$, and $\bar{D}_{e,st}$ is the PTDF for line e and the pair of buses s, t of $\mathcal{G}_2$.

Proof (sketch). Since a DC power network is a linear network and the sub-grids are only joined by buses s and t, the effect of $\mathcal{G}_2$ can be equivalently represented as a fictitious transmission line (s,t) with the effective susceptance between buses s, t of the sub-grid $\mathcal{G}_2$. Using Kron reduction [60], we can decompose the PTDF as above. □

We remark that this result is in fact a special case of the Kron reduction [60] for linear networks.

Monotonicity of the PTDF

The next result describes the dependence of the PTDF for a line e on its susceptance B_e and network topology.

Proposition 5.3. *Consider a connected network $\mathcal{G}$. For any line e and any pair of buses $\hat{i}, \hat{j}$, the absolute value of PTDF $D_{e,\hat{i}\hat{j}}$ can be expressed as:*

$$|D_{e,\hat{i}\hat{j}}| = \frac{T_1 B_e}{T_2 B_e + T_3}, \tag{5.3}$$

where $T_i \geq 0$ is a constant independent of the susceptance B_e for $i = 1, 2, 3$.

Proof. The PTDF can be computed as a quotient of different spanning trees of the network, as shown in Theorem 3.2 in Chapter 3:

$$D_{e,\hat{i}\hat{j}} = \frac{B_e \left(\sum_{H \in \mathcal{T}(i\hat{i}, j\hat{j})} \beta(H) - \sum_{H \in \mathcal{T}(i\hat{j}, j\hat{i})} \beta(H) \right)}{\sum_{H \in \mathcal{T}_{\mathcal{E}}} \beta(H)}.$$

Specifically, the numerator involves a subset of spanning trees that must pass through line e. The denominator involves all spanning trees, including those that pass through line e, accounted for in the term $T_2 B_e$, and those that do not, giving rise to the term T_3. □

This proves that the absolute value of PTDF for a line e and a pair of nodes $\hat{i}, \hat{j}$ is non-decreasing in its susceptance. This monotonicity result is aligned with the intuition that lines with larger admittances (thus smaller impedances) tend to "attract" more power to flow through.

5.2 Interface Networks and LODFs

The sub-grids that make up an interconnected power system operate relatively independently. It is thus desirable to localize the impact of failures within the sub-grid to prevent large-scale blackouts. Failures in power systems, however, are known to propagate non-locally. In Chapter 3, we investigate the block decomposition of the power networks and demonstrates that non-cut failures are localized if the sub-grids are connected in a tree structure. In practice, however, designing a power system with tree-connected sub-grids creates bridges and thus introduces single-point vulnerabilities. Therefore, it is crucial to localize failures while maintaining connectivity of the grid.

In this section, we consider a power network with two interconnected sub-grids $\mathcal{G}_1, \mathcal{G}_2$ joined by two buses s and t and propose three interface networks, as shown

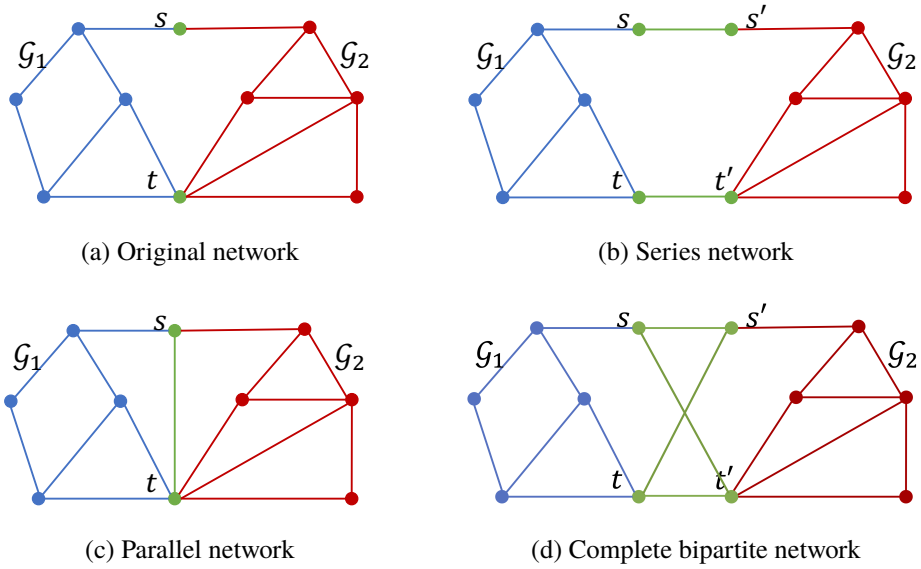

(a) Original network

(b) Series network

(c) Parallel network

(d) Complete bipartite network

Figure 5.1: Two sub-grids (a) are interconnected by (b) series, (c) parallel and (d) complete bipartite interface networks.

in Fig. 5.1. In contrast to the tree-connected sub-grids proposed in Chapter 3, our design does not decrease the connectivity or introduce any single point of failure into the original network. We show that all three interface networks can achieve failure localization by carefully designing the susceptances. Note that in this chapter we focus on the interface networks of the power grid where sub-grids are joined by two buses. Larger interface networks require special topological structures of the sub-grids to guarantee failure localization. For this reason we leave this as a challenging topic for future work.

To quantify the benefit of the interface networks in Fig. 5.1, we compare the LODF $K_{e\hat{e}}$ of the original network and that of the modified network with various interface networks. The tripped line $\hat{e}$ and the monitored line e are in different sub-grids. Without loss of generality, we assume that $\hat{e} \in \mathcal{G}_1$ and $e \in \mathcal{G}_2$. We assume that buses s, t are not directly connected (i.e., not adjacent to each other) in the original network to simplify our discussion. We use the superscript $(\cdot)^{(m)}$ to denote variables corresponding to the modified network.

Series Interface Network

We first introduce the 2×2 *series* interface network where we split the buses s, t and connect (s, s') and (t, t') as additional transmission lines, as shown in Fig. 5.1b. Intuitively, the series interface network increases the topological distance between

the tripped line $\hat{e}$ and the monitored line e. It is thus likely to reduce the failure impact across the sub-grids. As characterized by the following theorem, the LODF $K^{(m)}_{e\hat{e}}$ for the modified grid with a series interface network is guaranteed not to increase.

Theorem 5.4. *If $\mathcal{G}_1$ and $\mathcal{G}_2$ are connected by a series network, then $|K^{(m)}_{e\hat{e}}| \leq |K_{e\hat{e}}|$.*

Proof. With Lemma 5.1 and Proposition 5.2, we can write the LODF for the original network as:

$$K_{e\hat{e}} = \hat{D}_{(s,t),\hat{i}\hat{j}} \cdot \bar{D}_{e,st}.$$

We use $\hat{D}_{(s,t),\hat{i}\hat{j}}$ to denote the PTDF for the fictitious line (s,t) of the *post*-contingency sub-grid of $\hat{\mathcal{G}}_1$, with susceptance being the effective susceptance $B^{(e)}_{st}$ of the sub-grid $\mathcal{G}_2$. $\bar{D}_{e,st}$ represents the PTDF for line e of the sub-grid $\mathcal{G}_2$.

For the modified network $\mathcal{G}^{(m)}$, let $\mathcal{G}^{(m)}_1 = \mathcal{G}_1$ and $\mathcal{G}^{(m)}_2 = (\mathcal{N}_2 \cup \{s', t'\}, \mathcal{E}_2 \cup \{(s,s'),(t,t')\})$. The LODF can be decomposed similarly as:

$$K^{(m)}_{e\hat{e}} = \hat{D}^{(m)}_{(s,t),\hat{i}\hat{j}} \cdot \bar{D}^{(m)}_{e,st}.$$

Note that $\bar{D}^{(m)}_{e,st} = \bar{D}_{e,st}$ since line (s,s') and (t,t') are bridges of $\mathcal{G}^{(m)}_2$. The effective susceptance for the fictitious line $B^{(m)}_{st} = (1/B_{ss'} + 1/B_{tt'} + 1/B^{(e)}_{st})^{-1} < B^{(e)}_{st}$, so we have $|\hat{D}^{(m)}_{(s,t),\hat{i}\hat{j}}| \leq |\hat{D}_{(s,t),\hat{i}\hat{j}}|$ from Proposition 5.3. Therefore we conclude $|K^{(m)}_{e\hat{e}}| \leq |K_{e\hat{e}}|$. □

We remark that many empirical studies show that the LODF decreases as the distance from the initial failure increases [38, 99]. Theorem 5.4 provides theoretical support for such observations. Furthermore, the LODF $|K^{(m)}_{e\hat{e}}|$ is a non-decreasing function in the susceptance of lines (s,s') and (t,t'). Therefore, we can design the series interface network to achieve different levels of failure localizability.

Parallel Interface Network

We now consider the *parallel* interface network where we connect the buses s and t, as shown in Fig. 5.1c. Effectively, the line (s,t) provides an alternative path to redistribute power without passing through the other sub-grid $\mathcal{G}_2$. Therefore we expect the line failures to be less impactful on the other sub-grid. Indeed, the following theorem shows that the LODF is guaranteed not to increase after connecting buses s,t.

Theorem 5.5. *If $\mathcal{G}_1$ and $\mathcal{G}_2$ are connected by a parallel network, then $|K^{(m)}_{e\hat{e}}| \leq |K_{e\hat{e}}|$.*

Proof. Similar to the proof of Theorem 5.4, we can write the LODF for the original network and modified network as:

$$K_{e\hat{e}} = \hat{D}_{(s,t),\hat{i}\hat{j}} \cdot \bar{D}_{e,st},\ K^{(m)}_{e\hat{e}} = \hat{D}^{(m)}_{(s,t),\hat{i}\hat{j}} \cdot \bar{D}^{(m)}_{e,st},$$

where we define $\mathcal{G}_1^{(m)} = \mathcal{G}_1, \mathcal{G}_2^{(m)} = (\mathcal{N}_2, \mathcal{E}_2 \cup \{(s,t)\})$. From Proposition 5.3, we have

$$|\hat{D}_{(s,t),\hat{i}\hat{j}}| = \frac{T_1 B^{(e)}_{st}}{T_2 B^{(e)}_{st} + T_3},\ |\hat{D}^{(m)}_{(s,t),\hat{i}\hat{j}}| = \frac{T_1 B^{(m)}_{st}}{T_2 B^{(m)}_{st} + T_3},$$

where $B^{(m)}_{st} = x + B^{(e)}_{st}$ with x being the susceptance of the newly added parallel line (s,t). On the other hand, a simple circuit analysis shows that $\bar{D}^{(m)}_{e,st} = \frac{B^{(e)}_{st}}{B^{(m)}_{st}} \bar{D}_{e,st}$.

Therefore, we can conclude that

$$\begin{aligned} |K^{(m)}_{e\hat{e}}| &= \frac{T_1 B^{(m)}_{st}}{T_2 B^{(m)}_{st} + T_3} \cdot \frac{B^{(e)}_{st}}{B^{(m)}_{st}} |\bar{D}_{e,st}| \\ &= \frac{T_1 B^{(e)}_{st}}{T_2 B^{(m)}_{st} + T_3} |\bar{D}_{e,st}| \\ &\leq \frac{T_1 B^{(e)}_{st}}{T_2 B^{(e)}_{st} + T_3} |\bar{D}_{e,st}| = |K_{e,\hat{e}}|. \end{aligned}$$

□

We remark that the LODF $|K^{(m)}_{e\hat{e}}|$ is non-increasing in the susceptance of the parallel line (s,t). We can thus increase the susceptance of line (s,t) to improve the failure localizability. On the other hand, the LODF for the parallel line (s,t) may increase as the susceptance increases according to Proposition 5.3. Thus we need to systematically design the susceptance of the line (s,t).

Complete Bipartite Network

We now introduce the 2×2 *complete bipartite* interface network with two buses on each side, where we split the buses s, t and connect (s,s'), (s,t'), (t,s') and (t,t'), respectively. This design is similar to the Wheatstone bridge in circuit analysis literature. We show in the following theorem that the LODF for lines across sub-grids can be upper bounded. In particular, the impact of failures can be completely eliminated under the condition $B_{ss'}B_{tt'} = B_{st'}B_{ts'}$, where B_{pq} denotes the susceptance of line (p,q). We remark that this specific interface network has been proposed in [98] as the *network isolator* and shown to provide localization if a rank-1 condition holds

on the weighted adjacency matrix of the interface network. The rank-1 condition is equivalent to $B_{ss'}B_{tt'} = B_{st'}B_{ts'}$ for the 2×2 complete bipartite network. Our result generalizes the failure localization properties of a network isolator to the case in which the rank-1 condition does not hold for the four-node bipartite network.

Theorem 5.6. *If $\mathcal{G}_1$ and $\mathcal{G}_2$ are connected by a complete bipartite network, then we have*

$$|K^{(m)}_{e\hat{e}}| \leq \frac{|B_{ss'}B_{tt'} - B_{st'}B_{ts'}|}{(B_{ss'} + B_{st'})(B_{tt'} + B_{ts'})},$$

where B_{pq} is the susceptance for line (p, q). In particular, if $B_{ss'}B_{tt'} = B_{st'}B_{ts'}$, then $K^{(m)}_{e\hat{e}} = 0$.

Proof. We have

$$K^{(m)}_{e\hat{e}} = \hat{D}^{(m)}_{(s,t),\hat{i}\hat{j}} \cdot \bar{D}^{(m)}_{e,st},$$

where $\mathcal{G}_1^{(m)} = \mathcal{G}_1$ and $\mathcal{G}_2^{(m)} = (\mathcal{N}_2 \cup \{s', t'\}, \mathcal{E}_2 \cup \{(s, s'), (t, t'), (s, t'), (t, s')\})$. Since the PTDF is guaranteed to be within $[-1, 1]$, we first bound $|\hat{D}^{(m)}_{(s,t),\hat{i}\hat{j}}|$ by 1 and focus on the second term. Moreover, we can further decompose $\mathcal{G}_2$ into $\mathcal{G}_2^1 = (\{s, s', t, t'\}, \{(s, s'), (t, t'), (s, t'), (t, s')\})$ and $\mathcal{G}_2^2 = (\mathcal{N}_2 \cup \{s', t'\}, \mathcal{E}_2)$. Therefore, we have

$$|K^{(m)}_{e,\hat{e}}| \leq |\bar{D}^{(m)}_{e,st}| = |\hat{D}^{1}_{(s',t'),st}| \cdot |\bar{D}^{2}_{e,s't'}| \leq |\hat{D}^{1}_{(s',t'),st}|.$$

Now all we need is to provide an upper bound for the right hand side, which is the PTDF for the fictitious line (s', t') with effective susceptance $B^{(e)}$ for $\hat{\mathcal{G}}_2^1 = (\{s, s', t, t'\}, \{(s, s'), (t, t'), (s, t'), (t, s'), (s', t')\})$. We can compute the PTDF as in (5.1a):

$$\begin{aligned}
\hat{D}^{1}_{(s',t'),st} \;=\; & B^{(e)}(B_{ss'}B_{tt'} - B_{st'}B_{ts'})/ \\
& [(B_{ss'}B_{st'}B_{ts'} + B_{ss'}B_{st'}B_{tt'} + B_{ss'}B_{ts'}B_{tt'} + \\
& B_{st'}B_{ts'}B_{tt'}) + (B_{ss'}B_{st'})(B_{ts'} + B_{tt'})B^{(e)}].
\end{aligned}$$

Therefore, we conclude an upper bound for the LODF:

$$|K^{(m)}_{e\hat{e}}| \leq |\hat{D}^{1}_{(s',t'),st}| \leq \frac{|B_{ss'}B_{tt'} - B_{st'}B_{ts'}|}{(B_{ss'} + B_{st'})(B_{tt'} + B_{ts'})}.$$

□

Note that the bound depends only on the susceptance of the transmission lines for the complete bipartite network, and hence, is valid for every pair of the tripped line $\hat{e}$ and the monitored line e in different sub-grids. In practice, the actual LODF under

the complete bipartite interface network is usually much lower than the theoretical bound due to the internal connectivity of the network. Therefore, the complete bipartite network can provide strong failure localization.

We remark that the complete bipartite interface network can be designed not only to eliminate the impact outside the sub-grid where the failure happens, but to maintain the same level of robustness within the sub-grid. Specifically, as stated in the following theorem, the LODF remains the same as the original network if the lines are in the same sub-grids, while the LODF is zero if the lines are in different sub-grids.

Theorem 5.7. *Consider a network $\mathcal{G}$ consisting of two sub-grids $\mathcal{G}_1, \mathcal{G}_2$ joined by two buses s and t, and the modified network with the 2×2 complete bipartite interface network. Suppose the effective susceptances between buses s and t for the two sub-grids $\mathcal{G}_1, \mathcal{G}_2$ is $B_1^{(e)}$ and $B_2^{(e)}$, respectively. If the susceptances of the lines in the complete bipartite network satisfies the following condition:*

$$B_{tt'} < \min(B_1^{(e)}, B_2^{(e)}) \text{ or } B_{tt'} > \max(B_1^{(e)}, B_2^{(e)}),$$
$$B_{ss'} = \frac{B_1^{(e)} B_2^{(e)}}{B_{tt'}},\ B_{st'} = \frac{B_2^{(e)}(B_1^{(e)} - B_{tt'})}{B_2^{(e)} - B_{tt'}},\ B_{ts'} = \frac{B_1^{(e)}(B_2^{(e)} - B_{tt'})}{B_1^{(e)} - b_{tt'}},$$

then we have

$$K_{e\hat{e}}^{(m)} = \begin{cases} K_{e\hat{e}}, \text{ if the lines } e, \hat{e} \text{ are in the same sub-grid,} \\ 0, \text{ if the lines } e, \hat{e} \text{ are in different sub-grids.} \end{cases}$$

Proof (sketch). This result can be proved using the fact that the effective susceptance between buses (s, t) and (s', t') remains the same if the conditions are satisfied. □

Comments

The theoretical analysis presented in this section focuses on non-bridge line failures where post-contingency power injections are assumed to remain constant. In practice, however, the injections might change due to the real-time automatic controls of the power grid. The situation is even more complicated when islanding occurs due to bridge line failures. Even if a detailed model of these situations is beyond the scope of this work, the three interface networks presented here are capable of localizing the impact of injection fluctuations, as it can be seen through a similar analysis of the PTDF.

We remark that the sensitivity factors PTDF and LODF we considered in this chapter are independent of the power injections and transmission line capacities and, in fact, are known to only depend on the topological structure of the power grid. Therefore, our analysis sheds light on how the power grid can be optimized by possibly re-designing the network through line switching or bus splitting for planning purposes. If the pre-contingency system state and the line capacities are known, our analysis on LODF can be helpful to identify possible successive failures, for which corrective control actions can then be performed.

5.3 Case Study

In this section, we evaluate the failure localization performance of the three interface networks studied in the previous section for the IEEE 118-bus network. We start with the DC model, and then extend it to the AC model.

Experimental Setup

We split the IEEE 118-bus network into two sub-grids connected by four tie-lines as shown in Fig. 5.1. Note that the sub-grids are not connected by the cut vertices as in Fig. 5.1a. Therefore we modify the tie-lines connecting the sub-grids to create interface networks as follows. For a series interface network, we switch off the two dashed blue lines and keep the two solid blue lines as in Fig. 5.2a. A parallel interface network is built on top of the series network, where we add the purple line as in Fig. 5.2b. The complete bipartite interface network is achieved by connecting the end-points of solid blue lines as the solid purple lines in Fig. 5.1c. We then calculate the LODF as a metric to quantify the failure impact for each interface network.

Experimental Results

DC Model We start with evaluating failure localization under the DC power flow model. The DC LODF is well-defined and can be computed as (5.1b) if the tripped line does not disconnect the network.

We first compare the failure localizability across the sub-grids under various interface networks. Specifically, we compute the LODF for all pairs of tripped lines e and monitored lines $\hat{e}$ in different sub-grids and demonstrate the complementary cumulative distribution function (CCDF) of the absolute LODF in Fig. 5.2a. Note that the x-axis is in logarithmic scale, and we set the LODF $|K_{e\hat{e}}| \leq 10^{-8}$ as zero. The vertical dashed line represents the theoretical bound of the LODF for the complete

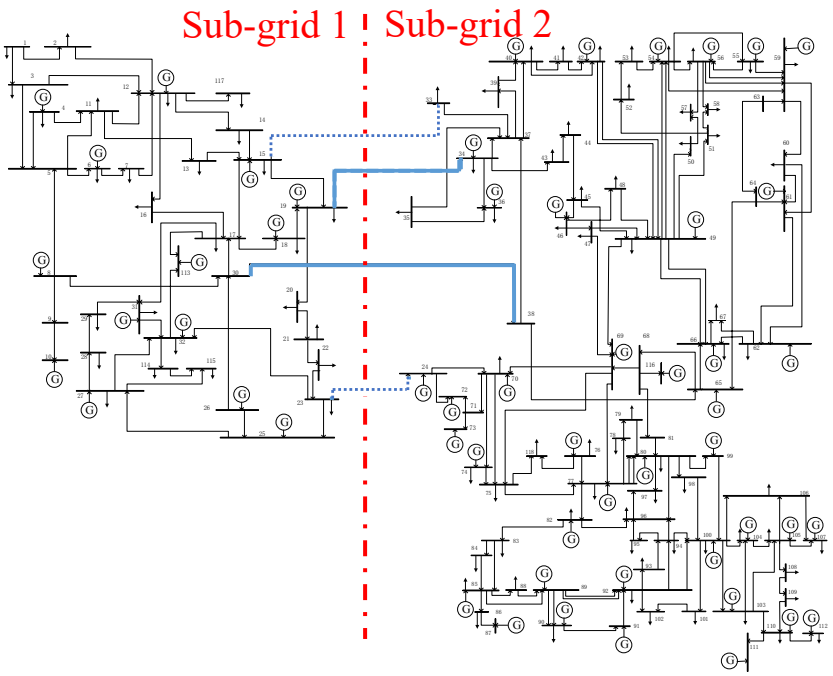

(a) Series interfacing network

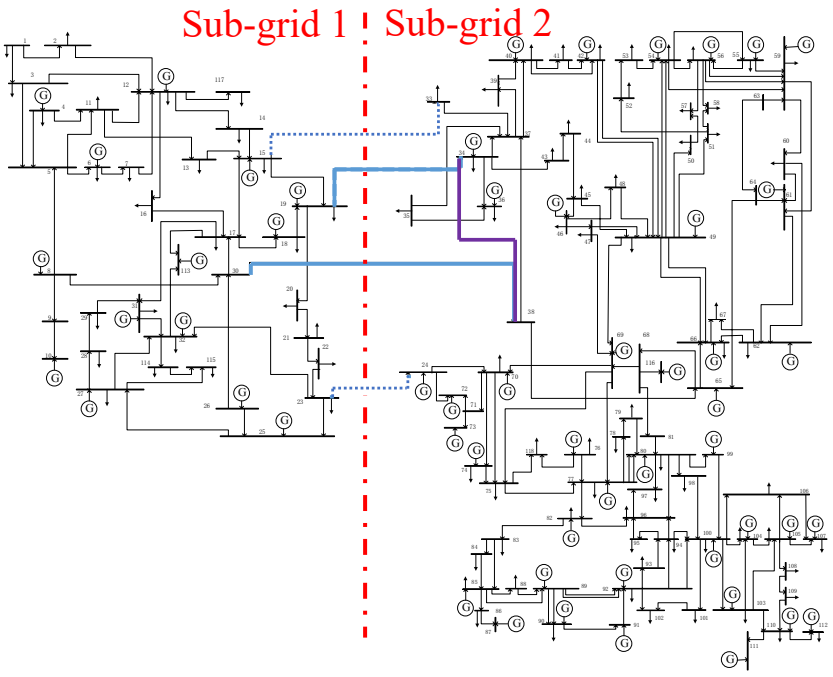

(b) Parallel interfacing network

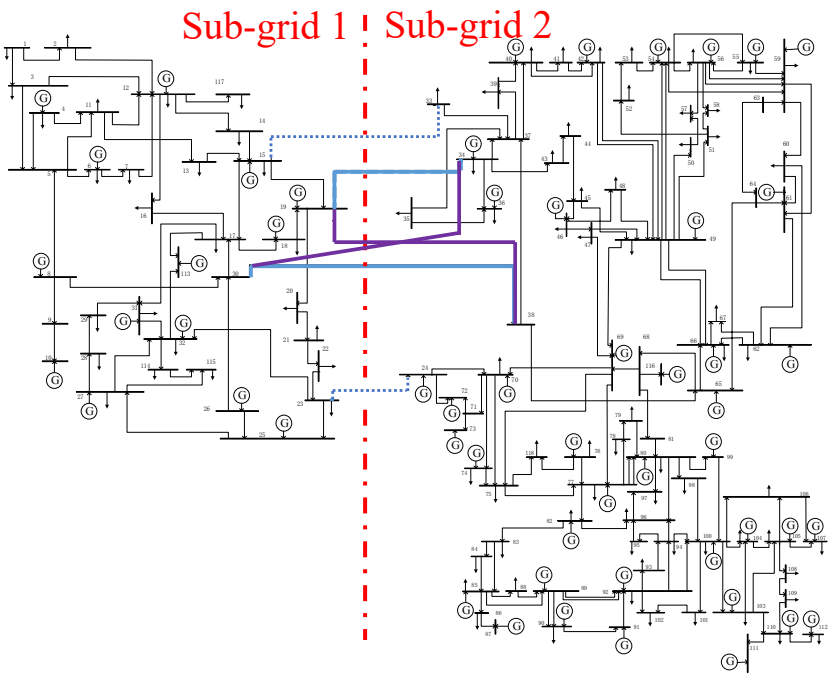

(c) Complete bipartite network

Figure 5.1: Two sub-grids are connected by 4 blue lines in the original IEEE 118-bus network. (a) Two dashed lines are switched off to create the series interface network. (b) One purple line is added to create the parallel interface network. (c) Two purple lines are added to create the complete bipartite network.

bipartite network. We observe that all three interface networks reduce the LODF across the sub-grids. For the original 118-bus network, there are roughly 10% pairs of lines with the absolute LODF greater than 0.01, while those cases are negligible (1%) with the series interface network. As expected, adding a parallel interface network on top of the series network further decreases the LODF. The complete bipartite interface network achieves the best localization performance, even though the susceptance does not satisfy the rank-1 condition to completely localize the failure within the sub-grid, i.e., $B_{ss'}B_{tt'} \neq B_{st'}B_{ts'}$.

It is crucial to analyze the impact within the same sub-grid where the line failure happens as well. In Fig. 5.2c, we show the CCDF of the absolute LODF for the pairs of tripped line and monitored line within the same sub-grid. We observe that the distributions of LODF within the sub-grid for the series, parallel and complete bipartite interface networks are very similar, all lower than the original network. Therefore, introducing the proposed interface networks properly will not decrease the robustness for the sub-grids against failures.

We remark that the two sub-grids of IEEE 118-bus network does not follow the

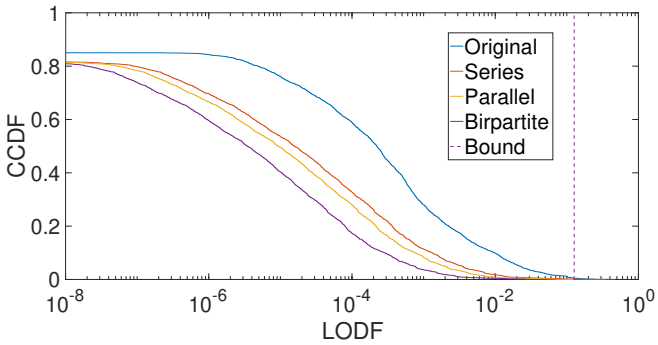

(a) DC LODF for lines in different sub-grids.

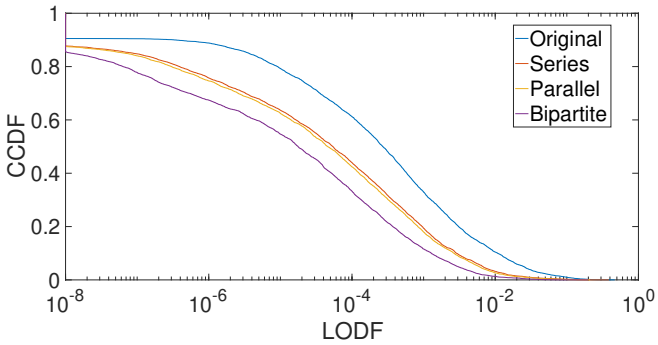

(b) AC LODF for lines in different sub-grids.

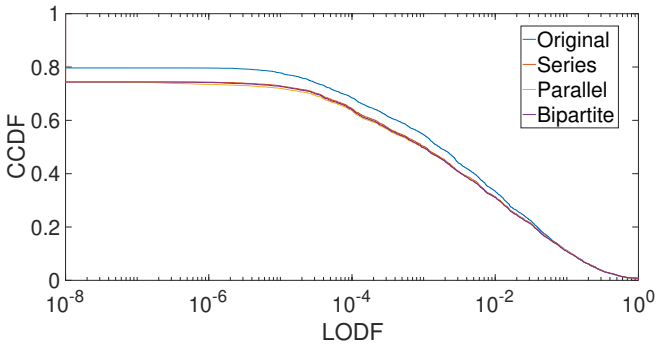

(c) DC LODF for lines in the same sub-grid.

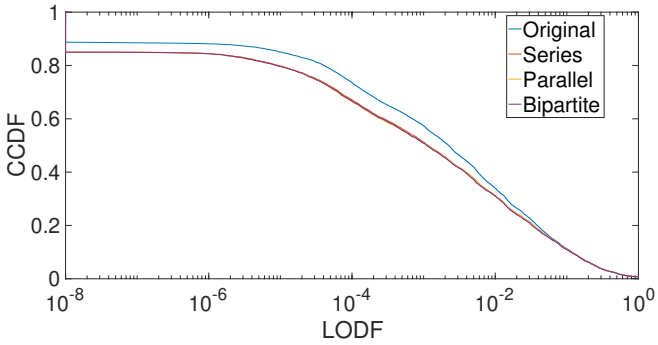

(d) AC LODF for lines in the same sub-grid.

Figure 5.2: The CCDF of LODF for monitored line e and tripped line $\hat{e}$ under DC (a,c) and AC (b,d) models. (a,b) $e, \hat{e}$ are in different sub-grids. (c,d) $e, \hat{e}$ are in the same grid.

definition of original network in Section 5.2: they are connected by four tie-lines instead of only two buses. Nevertheless, the LODF for the modified networks with all three interface network decreases. It suggests a broader range of applicability and stronger failure localizability for the interface networks. This, however, requires a proper selection on which transmission lines to keep, and we leave it as a future direction to explore.

AC model We further evaluate the localization performance under AC model. Since there is no closed-form expression for AC LODF, we calculate the LODF directly using the definition. Specifically, we adopt the line parameters and the nominal power injections from [100] as the pre-contingency operating status. For every non-bridge transmission line $\hat{e}$, we compute the post-contingency flow with AC power flow equations when line $\hat{e}$ trips, assuming that the post-contingency injections remain the same. The LODF is thus computed as $K_{e\hat{e}} = \frac{\Delta f_e}{f_{\hat{e}}}$, where Δf_e is the flow change over line e and $f_{\hat{e}}$ is the pre-contingency flow over line $\hat{e}$.

The CCDF of LODF for all pairs of the monitored line and the tripped line are shown in Fig. 5.2b and Fig. 5.2d. We notice that the network in which the sub-grids are connected by any of the three interface networks achieves higher failure localizability similarly to the DC model. It should be noted that the LODF is not zero for the complete bipartite network under the AC model, even when the susceptances are designed to satisfy the rank-1 condition. Nevertheless, all interface networks reduce failure impact across sub-grids, while maintaining similar robustness within the sub-grid.

5.4 Conclusion

In this chapter, we propose three interface networks connecting sub-grids to achieve stronger failure localization while maintaining robust network connectivity. Both theoretical analysis and case studies validate our proposed method. There are a number of important directions for future exploration of this topic. The most important and challenging extension is to consider larger interface networks. In this chapter, we have considered 2×2 interface networks, but larger networks have the potential to provide even more robust connections between sub-grids. However, it is quite challenging to characterize the LODF for larger interface networks without assuming very specific topological properties and thus to ensure localization of failures for such interface networks.

Chapter 6

FAILURE MITIGATION: ADAPTIVE NETWORK RESPONSE

In Chapters 3, 4, and 5, we investigate the failure propagation patterns under the steady-state DC model. In particular, we assume that injections remain unchanged after a line failure if the post-contingency network remains connected (and are changed only after a bridge failure according to a generic balancing rule that re-balances power in each island). Since tertiary control can take effect 5 minutes to more than an hour after the disturbance, most literature on cascading failure analysis adopts this assumption [9, 38, 94, 101]. However, it is unrealistic and tends to be pessimistic: it does not take into account frequency control mechanisms that adjust injections of controllable generators and loads immediately in response to line outages, on a faster timescale than that of post-contingency line tripping.

In this chapter, we augment the existing steady-state cascading failure models with frequency control dynamics that affect power flow redistribution in the new equilibrium post contingency. We adopt the integrated failure model proposed in Chapter 2 which is not only more realistic, but also offers additional means to mitigate cascading failure through better design of the frequency control mechanism. Our proposed control strategy builds upon this extra freedom and reacts to line outages on a timescale of minutes. Specifically, *we integrate a distributed frequency control strategy with a tree-partitioned network to provide provable failure mitigation and localization guarantees on line failures.* This strategy operates on a different timescale and supplements current practice, improving both grid reliability and operation efficiency. To the best of our knowledge, this is the first attempt to leverage results from the frequency regulation literature in the context of cascading failures, bringing new perspectives and insights to both literature. Our proposed strategy guarantees that (a) whenever it is feasible to avoid it, line failures do not propagate, and (b) the impact of line failures is localized as much as possible in a manner configurable by the system operator.

We introduce the main idea of this new mitigation strategy in Section 6.2, which makes use of the so-called *Unified Controller (UC)*, a recent mechanism developed in the frequency regulation literature [3, 41–43, 81]. We specifically leverage the ability of UC to enforce line limits on a faster timescale than thermal line failure

dynamics whenever possible. Our design revolves around the properties that emerge when the balancing areas that UC manages are connected in a tree structure. More specifically, in Section 6.3, we characterize how UC responds to an initial failure, and prove that any *non-critical failure* is automatically mitigated and localized. Later, in Section 6.4, we discuss how the system operator can configure its mitigation strategy to minimize the impact of *critical failures*, and show that UC can be extended to detect such scenarios as part of its normal operation.

In Section 6.6, we compare the proposed control strategy with classical Automatic Generation Control (AGC) using the IEEE 118-bus and 2736-bus test networks. We demonstrate that by switching off only a small number of transmission lines and adopting UC as the frequency controller, one can significantly improve overall grid reliability in terms of the $N - k$ security standard. Moreover, in a majority of the load profiles that are examined, our control strategy localizes the impact of initial failures to the balancing area where they occur, leaving the operating points of all other areas unchanged. This decoupling across balancing areas is important in practice. Lastly, we highlight that when load shedding is necessary, the proposed strategy incurs significantly smaller load loss.

6.1 The Bridge-block Decomposition and the Unified Controller

The bridge-block decomposition and the unified controller have recently emerged as two important tools for grid reliability [3, 102, 103]. The two concepts operate on different timescales to improve the power system robustness: the bridge-block decomposition aims to localize the failure propagation, while the unified controller aims to stabilize a disturbed system. In this section, we review these concepts and elaborate on how they can be integrated as a novel control framework for failure localization and mitigation.

Bridge-block Decomposition

Given a power network $\mathcal{G} = (\mathcal{N}, \mathcal{E})$, a *partition* of $\mathcal{G}$ is defined as a finite collection $\mathcal{P} = \{\mathcal{N}_1, \mathcal{N}_2, \cdots, \mathcal{N}_k\}$ of nonempty and disjoint subsets of $\mathcal{N}$ such that $\bigcup_{i=1}^{k} \mathcal{N}_i = \mathcal{N}$. For a partition $\mathcal{P}$, each edge can be classified as either a *tie-line* if the two endpoints belong to different subsets of $\mathcal{N}$ or an *internal line* otherwise.

We define an equivalence relation on $\mathcal{N}$ such that two nodes are in the same equivalence class if and only if there are two edge-disjoint paths connecting them. For this specific partition, the tie-lines connecting different components are exactly the *bridges* (cut-edges) of the graph. We thus refer to this partition as *bridge-block*

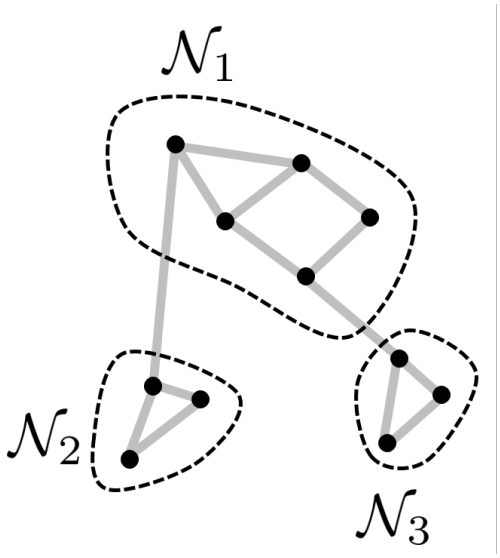

Figure 6.1: Bridge-block decomposition of a graph.

decomposition $\mathcal{P}^{\mathrm{BB}}$ of the power network (see Fig. 6.1 for an example).

We show in Chapter 3 that each graph has a unique bridge-block decomposition, which can be found in linear time. In particular, the bridge-block decomposition encodes rich information on failure propagation.

Unified Controller (UC)

Before we introduce the unified controller, we first summarize the integrated failure model proposed in Chapter 2. We describe the cascading failure process by the set of outaged lines $\mathcal{B}(\mathfrak{n}) \subset \mathcal{E}$ over stages $\mathfrak{n} \in \{1, 2, \ldots, N\}$. For each stage $\mathfrak{n}$, the system evolves according to the fast-timescale dynamics on the topology $\mathcal{G}(\mathfrak{n}) := (\mathcal{N}, \mathcal{E}(\mathfrak{n}))$ where $\mathcal{E}(\mathfrak{n}) := \mathcal{E} \setminus \mathcal{B}(\mathfrak{n})$ and converges to an equilibrium point. When it eventually converges to an equilibrium, we compare the branch flow with the steady-state thermal capacity π_e for the surviving transmission line e. Overloaded lines are then tripped and the cycle repeats, i.e., $\mathcal{B}(\mathfrak{n}+1) = \mathcal{B}(\mathfrak{n}) \cup \{e : |f_e(\mathfrak{n})| > \pi_e, e \in \mathcal{E}(\mathfrak{n})\}$.

We adopt the linearized frequency dynamics as the fast-timescale dyanmics after line failures:

$$\dot{\theta}_j = \omega_j, \quad j \in \mathcal{N} \tag{6.1a}$$

$$M_j \dot{\omega}_j = r_j + d_j - D_j \omega_j - \sum_{e \in \mathcal{E}} C_{je} f_e, \quad j \in \mathcal{N} \tag{6.1b}$$

$$f_{ij} = B_{ij}(\theta_i - \theta_j), \quad (i,j) \in \mathcal{E}. \tag{6.1c}$$

UC is a control approach recently proposed in the frequency regulation literature [3,

41–43, 81]. Compared to classical droop control or AGC [82], UC simultaneously integrates primary control, secondary control, and congestion management on a fast timescale. The key feature of UC is that the *closed-loop* equilibrium of (6.1) under UC solves the following optimization problem on the *post*-contingency network:

$$\min_{\boldsymbol{\theta},\boldsymbol{\omega},\boldsymbol{d},\boldsymbol{f}} \quad \sum_{j\in\mathcal{N}} c_j(d_j) \tag{6.2a}$$

$$\text{s.t.} \quad \boldsymbol{\omega} = \mathbf{0}, \tag{6.2b}$$

$$\boldsymbol{r} + \boldsymbol{d} - \boldsymbol{C}\boldsymbol{f} = \mathbf{0}, \tag{6.2c}$$

$$\boldsymbol{f} = \boldsymbol{B}\boldsymbol{C}^T\boldsymbol{\theta}, \tag{6.2d}$$

$$\boldsymbol{E}\boldsymbol{C}\boldsymbol{f} = \mathbf{0}, \tag{6.2e}$$

$$\underline{f}_e \le f_e \le \overline{f}_e, \quad e \in \mathcal{E}, \tag{6.2f}$$

$$\underline{d}_j \le d_j \le \overline{d}_j, \quad j \in \mathcal{N}, \tag{6.2g}$$

where $c_j(\cdot)$'s are associated cost functions that penalize deviations from the last optimal dispatch (and hence attain minimum at $d_j = 0$), (6.2b) ensures secondary frequency regulation is achieved, (6.2c) guarantees power balance at each bus, (6.2d) is the DC power flow equation, (6.2e) enforces zero area control error [82], (6.2f) and (6.2g) are the flow and control limits. The matrix $\boldsymbol{E}$ encodes balancing area information as follows. Given a partition $\mathcal{P}^{\mathrm{UC}} = \{\mathcal{N}_1, \mathcal{N}_2, \cdots, \mathcal{N}_k\}$ of $\mathcal{G}$ that specifies the balancing areas for secondary frequency control, $\boldsymbol{E} \in \{0,1\}^{|\mathcal{P}^{\mathrm{UC}}|\times n}$ is defined by $E_{lj} = 1$ if bus j is in balancing area $\mathcal{N}_l$ and $E_{lj} = 0$ otherwise. As a result, the l-th row of $\boldsymbol{E}\boldsymbol{C}\boldsymbol{f} = \mathbf{0}$ ensures that the branch flow deviations on the tie-lines connected to balancing area $\mathcal{N}_l$ sum to zero.

UC is designed so that its controller dynamics, combined with the system dynamics (6.1), form a variant of projected primal-dual algorithms to solve (6.2). It is shown in [3, 41–43, 81] that when the optimization problem (6.2) is feasible, under mild assumptions, the closed-loop equilibrium under UC is globally asymptotically stable and it is an optimal point of (6.2). Such an optimal point is unique (up to a constant shift of $\boldsymbol{\theta}$) if the cost functions $c_j(\cdot)$ are strictly convex. This means that, after a (cut or non-cut) failure, the post-contingency system is driven by UC to an optimal solution of (6.2) (under appropriate assumptions). We refer the readers to [3, 41–43, 81] for specific controller designs and their analysis.

Connecting UC and the Bridge-Block Decomposition

We have introduced two partitions of a power network: the bridge-block decomposition $\mathcal{P}^{\mathrm{BB}}$ and the balancing area partition $\mathcal{P}^{\mathrm{UC}}$, which in general are different from

each other. However, when they do coincide, the underlying power grid inherits analytical properties from both bridge-block decomposition and UC, making the system particularly robust against failures. Our proposed control strategy leverages precisely this feature, as we present in Section 6.2.

In practice, the balancing areas over which UC operates are usually connected by multiple tie-lines in a mesh structure. However, in order to align with the bridge-block decomposition, we may have to switch off a few tie-lines of $\mathcal{P}^{\mathrm{UC}}$. The selection of these tie-lines can be systematically optimized, e.g., to minimize line congestion or inter-area flows on the resulting network; see Section 6.2 for more details. We henceforth assume that $\mathcal{P}^{\mathrm{BB}} = \mathcal{P}^{\mathrm{UC}}$. We refer to such a network as the *tree-partitioned* network since the balancing areas are connected in a tree structure prescribed by its bridge-block decomposition.

Definition 6.1. *Given a cascading failure process described by* $\mathcal{B}(\mathfrak{n})$*, with* $\mathfrak{n} \in \{1, 2, \ldots, N\}$*, the set* $\mathcal{B}(1)$ *is said to be its* **initial failure**. *An initial failure* $\mathcal{B}(1)$ *is said to be* **critical** *if the UC optimization* (6.2) *is infeasible over* $\mathcal{G}(1) := (\mathcal{N}, \mathcal{E} \setminus \mathcal{B}(1))$*, or* **non-critical** *otherwise.*

To formally state our localization result, we define the following concept to clarify the precise meaning of an area being "local" with respect to an initial failure.

Definition 6.2. *Given an initial failure* $\mathcal{B}(1)$*, we say that a tree-partitioned balancing area* $\mathcal{N}_l$ *is* **associated** *with* $\mathcal{B}(1)$ *if there exists an edge* $e = (i, j) \in \mathcal{B}(1)$ *such that either* $i \in \mathcal{N}_l$ *or* $j \in \mathcal{N}_l$*.*

As we discuss below, our control strategy possesses a strong localization property for both non-critical and critical failures in the sense that only the operation of the associated areas are adjusted whenever possible.

6.2 Proposed Control Strategy: Summary

Our strategy consists of two phases: a planning phase in which tree-partitioned networks are created and an operation phase during which UC actively monitors and autonomously reacts to line failures during its operation.

Planning Phase: Align Bridge-blocks and Balancing Areas

Each balancing area of a multi-area power network is managed by an independent system operator (ISO). Although these areas exchange power with each other as

prescribed by economic dispatch, their operations are relatively independent. This is usually achieved via the zero area control error constraint in secondary frequency control [82], which is enforced by UC with (6.2e). As mentioned in previous sections, such balancing areas typically do not form bridge-blocks, as redundant lines are believed to be critical in maintaining $N-1$ security of grid [21, 82, 101].

We propose to create bridge-blocks whose components coincide with the balancing areas over which UC operates. This can be done by switching off a small subset of the tie-lines so that areas are connected in a tree structure.

More specifically, consider a grid $\mathcal{G} = (\mathcal{N}, \mathcal{E})$ with balancing areas described by a partition $\mathcal{P} = \{\mathcal{N}_1, \cdots, \mathcal{N}_k\}$. We denote $\mathcal{L} := \{(s,t) \in \mathcal{E} | s \in \mathcal{N}_i^{\mathrm{UC}}, t \in \mathcal{N}_j^{\mathrm{UC}}, i \neq j\}$ as the set of all tie lines connecting different balancing areas. The reduced graph $\mathcal{G}_{\mathcal{P}}(\mathcal{E})$ under partition $\mathcal{P}$ is a graph obtained from $\mathcal{G}$ by collapsing each area $\mathcal{N}_i$ into a "super node" and adding an edge between super nodes $\mathcal{N}_i$ and $\mathcal{N}_j$ for each tie line connecting them. Note that the redundancy-based design of a power grid usually leads to a non-simple (i.e., there are multiple lines between two super nodes) or cyclic reduced graph. Our method aims to select a subset of tie lines $T \subset \mathcal{L}$ to switch off, such that the balancing areas of the remaining network are connected in a tree topology, i.e., the reduced graph $\mathcal{G}_{\mathcal{P}}(\mathcal{E} \setminus T)$ is a tree. This implies that $|\mathcal{L}| - k + 1$ tie lines will be switched off, where k is the number of balancing areas of the grid.

Similarly to line failures, tie line switching actions change the system operating point as power flows redistribute in the new network topology. Let $\boldsymbol{p}$ denote the nominal injection for topology design purpose. We choose the set T of candidate lines to minimize *network congestion level* $\gamma(T)$ defined as:

$$\gamma(T) = \max_{e \in \mathcal{E} \setminus T} |f_e(T)| / \pi_e,$$

where $f_e(T)$ is the line flow on line e after the lines in T are switched off and π_e is the line capacity. We are therefore interested in solving the optimization problem:

$$\min_{T \subset \mathcal{L}} \quad \gamma(T) \tag{6.3a}$$

$$\text{s.t.} \quad \mathcal{G}_{\mathcal{P}}(\mathcal{E} \setminus T) \text{ is a tree.} \tag{6.3b}$$

The complexity of the optimization (6.3) originates from finding all possible subsets T of all tie lines $\mathcal{L}$ to switch off. Solving the above optimization problem often becomes intractable for large-scale power grids. An approximate but faster algorithm

is proposed in [104] where tree-connected areas are created by recursively splitting the existing ones, yielding very good results for most application scenarios.

We remark that it is not guaranteed that $\gamma(T^*) \leq 1$, where T^* is an optimal selection, implying that some transmission lines may become overloaded after switching actions. This may be alleviated if one has the flexibility to design the control areas of the grid. We refer interested readers to [104] for optimal partitioning of the grid using network modularity clustering algorithms. However, $\gamma(T^*) < 1$ indeed holds for most practical scenarios simulated in [104], especially when the original grid is not heavily congested.

The switching actions only need to be carried out in the planning phase, as line failures that occur during the operating phase do not affect the bridge-blocks already in place.[1] It is interesting to notice that when the subset of lines to switch off is chosen carefully, the tree-partitioned network not only localizes the impact of line failures, but can also *improves* overall reliability. This seemingly counter-intuitive phenomenon is illustrated by our case studies in Section 6.6.

It is actually natural to match bridge-blocks to balancing areas in transmission systems. First, there are typically small number of tie-lines between areas. Switching off those tie-lines is less likely to cause severe congestion to the grid. Second, each balancing area is supposed to balance its own power and the primary goal of failure mitigation is to prevent, as much as possible, a failure from impact other areas. This reconciles with the area control error (ACE) in traditional secondary frequency control.

Operating Phase: Extending Unified Controller

Once the tree-partitioned areas are formed, the power network operates under UC as a closed-loop system and responds to disturbances such as line failures or loss of generator/load in an autonomous manner. Unlike traditional secondary frequency control, UC is distributed and reacts continuously to any disturbances as part of normal operation. There is no explicit termination of UC primal-dual dynamics. We assume that UC can detect line failures in real-time and thus react to the post-contingency network accordingly. In normal conditions where the system disturbances caused by line failures are small, UC always drives the power network back to an equilibrium point that can be interpreted as an optimal solution of (6.2).

[1] In fact, line failures can lead to a "finer" bridge-block decomposition, as more bridge blocks are potentially created when lines are removed from service.

This is the case, for instance, when non-critical failures (see Definition 6.1) happen, and therefore such failures are always successfully mitigated.

However, in extreme scenarios where a major disturbance (e.g., a critical failure) happens, the optimization problem (6.2) can be infeasible. In other words, it is physically impossible for UC to achieve all of its control objectives after such a disturbance. This makes UC unstable (see Proposition 6.7) and may lead to successive failures. There is therefore a need to extend the version of UC proposed in [3, 41–43, 81] with two features: (a) a detection mechanism that monitors the system state and detects critical failures promptly; and (b) a constraint-lifting mechanism that responds to critical failures by proactively relaxing certain constraints of (6.2) to ensure system stability can be reached at minimal cost.

Our technical results in Section 6.4 suggest a way to implement both components as part of the normal operation of UC. System operators can prioritize different balancing areas by specifying the sequence of constraints to lift in response to extreme events. This allows the non-associated areas to be progressively involved and coordinated in a systematic fashion when mitigating critical failures. We discuss some potential schemes in Section 6.4.

Guaranteed Mitigation and Localization

We show in detail in Sections 6.3 and 6.4 that the proposed strategy provides strong guarantees in the mitigation and localization of both non-critical and critical failures. Specifically, it ensures that the cascading process is always stopped (a) after a non-critical failure by the associated areas, and the operating points of non-associated areas are not impacted in equilibrium or (b) after a critical failure when constraints in (6.2) are lifted in a progressive manner specified by the system operator. Thus the proposed strategy can always prevent successive failures, while localizing the impact of the initial failures as much as possible.

We remark that our strategy can maintain the $N-1$ security standard even though the balancing areas are connected in a tree structure. Unlike other classical approaches where failures that disconnect the network tend to incur more severe impact, our strategy can mitigate such failures as much as possible by autonomously adjusting the injections to rebalance and stabilize the system in each of the surviving component. In fact, our fast-timescale control can significantly improve the grid reliability in $N-k$ sense as we show in the numerical experiments in Section 6.6.

6.3 Localizing Non-critical Failures

In this section, we consider non-critical failures, as defined in Section 6.1, and prove that such failures are always fully mitigated within the associated balancing areas.

We first characterize how the system operating point shifts in response to such failures. Recall that if an initial failure $\mathcal{B}(1)$ is non-critical, the UC optimization (6.2) is feasible and thus the new operating point $\boldsymbol{x}^*(1) := (\boldsymbol{\theta}^*(1), \boldsymbol{\omega}^*(1), \boldsymbol{d}^*(1), \boldsymbol{f}^*(1))$ satisfies all the constraints in (6.2). In particular, none of the line limits is violated at $\boldsymbol{x}^*(1)$ by (6.2f), i.e., $\boldsymbol{x}^*(1)$ is a secure operating point and the cascade stops. Moreover the power flows on bridges remain unchanged in equilibrium from their pre-contingency values, as the next result says.

Lemma 6.3. *Given a non-critical initial failure $\mathcal{B}(1)$, the new operating point $\boldsymbol{x}^*(1)$ prescribed by the UC satisfies $f_e^*(1) = 0$ for every bridge e of the network.*

Proof. To simplify the notation, we drop the stage index (1) from $\boldsymbol{x}^*$ and denote $\boldsymbol{x}^* = (\boldsymbol{\theta}^*, \boldsymbol{\omega}^*, \boldsymbol{d}^*, \boldsymbol{f}^*)$. Given a bridge $e = (j_1, j_2)$ of $\mathcal{G}$, removing e partitions $\mathcal{G}$ into two connected components, say C_1 and C_2. Without loss of generality, assume $j_1 \in C_1$ and $j_2 \in C_2$. For an area $\mathcal{N}_v$ from the partition $\mathcal{P}$, we say $\mathcal{N}_v$ is within C_1 if for any $j \in \mathcal{N}_v$ we have $j \in C_1$. It is easy to check from the definition of a tree-partitioned network that any area $\mathcal{N}_v$ from $\mathcal{P}$ is either within C_1 or within C_2, and that e is the only edge in $\mathcal{G}$ that has one endpoint in C_1 and the other endpoint in C_2.

Let $\mathcal{P}'$ be the subset of areas within C_1 from $\mathcal{P}$, and let $\mathbf{1}_{\mathcal{P}'} \in \{0,1\}^{|\mathcal{P}|}$ be its characteristic vector (that is, the l-th component of $\mathbf{1}_{\mathcal{P}'}$ is 1 if $\mathcal{N}_l \in \mathcal{P}'$ and 0 otherwise). Given two buses i and j, we denote $i \to j$ if $(i,j) \in \mathcal{E}$ and $j \to i$ if $(j,i) \in \mathcal{E}$.

Note that (6.2e) ensures the injections are balanced for all areas. We can thus sum over all areas within C_1:

$$0 \;=\; \mathbf{1}_{\mathcal{P}'}^T \boldsymbol{E}\boldsymbol{C}\boldsymbol{f}^*.$$

Following the definition of matrices $\boldsymbol{E}, \boldsymbol{C}$ and the above notations, we can rewrite the above equations as:

$$\begin{aligned} 0 \;&=\; \sum_{l:\mathcal{N}_l \in \mathcal{P}'} \sum_{i \in \mathcal{N}_l} \Big(\sum_{j:j\to i} f_{ji}^* - \sum_{j:i\to j} f_{ij}^* \Big) \\ &=\; \sum_{i:i\in C_1} \Big(\sum_{j:j\to i} f_{ji}^* - \sum_{j:i\to j} f_{ij}^* \Big). \end{aligned} \tag{6.4}$$

Mathematically, $\left(\sum_{j:j\to i} f^*_{ji} - \sum_{j:i\to j} f^*_{ij}\right) + r_i + d^*_i = 0$ is the flow conservation for node i. Therefore, the right hand side of equation (6.4) calculates the summation of injections over all nodes within the connected component C_1, which should be zero enforced by (6.2e).

Now, consider the node j_1 and the bridge $e = (j_1, j_2)$. For all other transmission lines (i, j) within component C_1, the flow will be counted twice (for nodes i and j, respectively) with opposite direction in (6.4) and thus gets cancelled out. Only the flow of bridge e is counted once for node j_1. Therefore, we conclude that the flow on the bridge must be zero, i.e., $f^*_e = 0$. Since the bridge e is arbitrary, we have thus proved the desired result. □

This lemma shows that tree-partitioned areas enable UC to achieve more than what it was originally designed for in [3, 41–43, 81]: the extended UC not only enforces zero area control errors through (6.2e), it also guarantees zero flow deviations on all bridges.

The following proposition is another result of this type, which clarifies how the tree-partitioned network induces a localization property under UC.

Proposition 6.4. *Assume $c_j(\cdot)$ is strictly convex and achieves its minimum at $d_j = 0$ for all $j \in \mathcal{N}$. Given a non-critical initial failure $\mathcal{B}(1)$, if an area $\mathcal{N}_l$ is not associated with $\mathcal{B}(1)$, then at equilibrium $\boldsymbol{x}^*(1)$ we have $d^*_j(1) = 0$ for all $j \in \mathcal{N}_l$.*

Proof. To simplify the notation, we drop the stage index from the equilibrium $\boldsymbol{x}^*$ and write $x^* = (\boldsymbol{\theta}^*, \boldsymbol{\omega}^*, \boldsymbol{d}^*, \boldsymbol{f}^*)$ and $\boldsymbol{p}^* = \boldsymbol{r} + \boldsymbol{d}^*$.

First, we construct a different point $\tilde{\boldsymbol{x}}^* = (\tilde{\boldsymbol{\theta}}^*, \tilde{\boldsymbol{\omega}}^*, \tilde{\boldsymbol{d}}^*, \tilde{\boldsymbol{f}}^*)$ by changing certain entries of $\boldsymbol{x}^*$ within a non-associated area $\mathcal{N}_l$ as follows: (a) replace d^*_j with $\tilde{d}^*_j = 0$ for all $j \in \mathcal{N}_l$; (b) replace f^*_e with $\tilde{f}^*_e = 0$ for $e \in \mathcal{E}$ that have both endpoints in $\mathcal{N}_l$; and (c) replace $\boldsymbol{\theta}^*$ by a solution $\tilde{\boldsymbol{\theta}}^* = \boldsymbol{L}^\dagger \tilde{\boldsymbol{p}}^*$ obtained from solving the DC power flow equations with injections $\tilde{\boldsymbol{p}}^* = \boldsymbol{r} + \tilde{\boldsymbol{d}}^*$. All other entries of $\boldsymbol{x}^*$ remain unchanged in $\tilde{\boldsymbol{x}}^*$. Since $c_j(\cdot)$ attains its minimum at $d_j = 0$, $\tilde{\boldsymbol{x}}^*$ achieves at most the same objective value (6.2a) as $\boldsymbol{x}^*$. Thus $\tilde{\boldsymbol{x}}^*$ must be an optimal point of (6.2), provided it is feasible.

When the cost functions $c_j(\cdot)$ are strictly convex, the optimal solution to (6.2) is unique in $\boldsymbol{d}^*$ and $\boldsymbol{f}^*$ ($\boldsymbol{\theta}^*$ is also unique up to an arbitrary reference angle). As a result, if the constructed point $\tilde{\boldsymbol{x}}^*$ is feasible, We can then conclude that $\tilde{\boldsymbol{x}}^* = \boldsymbol{x}^*$ (up to an arbitrary reference angle).

We now prove the feasibility of $\tilde{\boldsymbol{x}}^*$. The construction of $\tilde{\boldsymbol{x}}^*$ ensures that (6.2e)-(6.2g) are satisfied. If we can show that $\tilde{\boldsymbol{f}}^* = \boldsymbol{B}\boldsymbol{C}^T\tilde{\boldsymbol{\theta}}^*$, then since $\tilde{\boldsymbol{\theta}}^*$ is obtained by solving the DC power flow equations from $\boldsymbol{C}\boldsymbol{B}\boldsymbol{C}^T\tilde{\boldsymbol{\theta}}^* = \tilde{\boldsymbol{p}}^*$, constraints (6.2c) and (6.2d) are also satisfied, proving the feasibility of $\tilde{\boldsymbol{x}}^*$. It thus suffices to show $\tilde{\boldsymbol{f}}^* = \boldsymbol{B}\boldsymbol{C}^T\tilde{\boldsymbol{\theta}}^*$. To do so, we first establish the following lemma:

Lemma 6.5. *For any tree-partitioned area $\mathcal{N}_z$ in $\mathcal{P}$, we have $\sum_{j\in\mathcal{N}_z} p_j^* = \sum_{j\in\mathcal{N}_z} \tilde{p}_j^* = 0$.*

Proof. Let $\mathbf{1}_{\mathcal{N}_z} \in \mathbb{R}^{|\mathcal{N}|}$ be the characteristic vector of $\mathcal{N}_z$, that is, the j-th component of $\mathbf{1}_{\mathcal{N}_z}$ is 1 if $j \in \mathcal{N}_z$ and 0 otherwise. Summing (6.2c) over $j \in \mathcal{N}_z$, we have: $\sum_{j\in\mathcal{N}_z} p_j^* = \mathbf{1}_{\mathcal{N}_z}^T \boldsymbol{C}\boldsymbol{f} = (\boldsymbol{E}\boldsymbol{C}\boldsymbol{f})_z = 0$, where $(\boldsymbol{E}\boldsymbol{C}\boldsymbol{f})_z$ is the z-th row of $\boldsymbol{E}\boldsymbol{C}\boldsymbol{f}$. If $\mathcal{N}_z = \mathcal{N}_l$, we have $\tilde{p}_j^* = 0$ for $j \in \mathcal{N}_l$ by construction and hence $\sum_{j\in\mathcal{N}_z} \tilde{p}_j^* = 0$. For $\mathcal{N}_z \neq \mathcal{N}_l$, we have $\tilde{p}_j^* = p_j^*$ for any $j \in \mathcal{N}_z$ by construction. Thus, $\sum_{j\in\mathcal{N}_z} \tilde{p}_j^* = 0$, completing the proof. □

Consider now an area $\mathcal{N}_w$ that is different from $\mathcal{N}_l$. In this case, we do not change the injections from $\boldsymbol{x}^*$ when constructing $\tilde{\boldsymbol{x}}^*$, thus $p_j^* - \tilde{p}_j^* = 0$ for all $j \in \mathcal{N}_w$. From Lemma 6.5, we see that $\sum_{j\in\mathcal{N}_z} \left(p_j^* - \tilde{p}_j^*\right) = 0$ for all z. Since both $(\boldsymbol{p}^*, \boldsymbol{\theta}^*)$ and $(\tilde{\boldsymbol{p}}^*, \tilde{\boldsymbol{\theta}}^*)$ satisfy the DC power flow equations, we have $\boldsymbol{C}\boldsymbol{B}\boldsymbol{C}^T(\boldsymbol{\theta}^* - \tilde{\boldsymbol{\theta}}^*) = \boldsymbol{p}^* - \tilde{\boldsymbol{p}}^*$.

Lemma 6.6. *Let $\mathcal{P} = \{\mathcal{N}_1, \mathcal{N}_2, \cdots, \mathcal{N}_k\}$ be the tree-partitioned areas of $\mathcal{G}$ and consider a vector $\boldsymbol{p} \in \mathbb{R}^n$ such that $p_j = 0$ for all $j \in \mathcal{N}_1$ and $\sum_{j\in\mathcal{N}_z} p_j = 0$ for $z \neq 1$. Then the Laplacian equation $\boldsymbol{C}\boldsymbol{B}\boldsymbol{C}^T\boldsymbol{\theta} = \boldsymbol{p}$ is solvable, and any solution $\boldsymbol{\theta}$ satisfies $\theta_i = \theta_j$ for all $i, j \in \overline{\mathcal{N}}_1$, where $\overline{\mathcal{N}}_1 := \{j : \exists\, i \in \mathcal{N}_1 \text{ s.t. } (i,j) \in \mathcal{E} \text{ or } (j,i) \in \mathcal{E}\}$.*

Proof. In Chapter 2, we show that the Laplacian matrix $\boldsymbol{L} := \boldsymbol{C}\boldsymbol{B}\boldsymbol{C}^T$ of a connected graph $\mathcal{G} = (\mathcal{N}, \mathcal{E})$ has rank $|\mathcal{N}| - 1$, and $\boldsymbol{L}\boldsymbol{\theta} = \boldsymbol{p}$ is solvable if and only if $\mathbf{1}^T\boldsymbol{p} = 0$, where $\mathbf{1}$ is the vector with proper dimension that consists of ones. Moreover, the kernel of $\boldsymbol{L}$ is given by span($\mathbf{1}$).

If $\mathcal{N}_1$ is the only area in $\mathcal{P}$, then $\boldsymbol{p} = 0$ since $p_j = 0$ for all $j \in \mathcal{N}_1$. We thus know the solution space to $\boldsymbol{L}\boldsymbol{\theta} = \boldsymbol{p}$ is exactly the kernel of $\boldsymbol{L}$, and the desired result holds.

If $\mathcal{N}_1$ is not the only area in $\mathcal{P}$, we can show that $f_e = 0$ for every bridge e connecting different areas. To see this, we start from a leaf area $\mathcal{N}_z$ of the tree-partitioned network. Since $\sum_{j\in\mathcal{N}_z} p_j = 0$, we have that the only bridge connecting the leaf area will carry zero flow. Therefore, the area $\mathcal{N}_z$ is decoupled from other areas and the Laplacian equation can be decomposed. We can iteratively use the

above statement and decompose the Laplacian equation with respect to each area. With the previous result, we know $\theta_i = \theta_j$ for all $i, j \in \mathcal{N}_1$ since $p_j = 0$ for all $j \in \mathcal{N}_1$. Together with the fact that bridges carry zero flow, we have $\theta_i = \theta_j$ for all $i, j \in \overline{\mathcal{N}}_1$. □

By Lemma 6.6, we then have $\theta_j^* - \tilde{\theta}_j^*$ is a constant over $\overline{\mathcal{N}}_l$, and thus $\tilde{\theta}_i^* - \tilde{\theta}_j^* = \theta_i^* - \theta_j^*$ for all $i, j \in \overline{\mathcal{N}}_l$. This in particular implies $\tilde{f}_e^* = f_e^* = B_e(\theta_i^* - \theta_j^*) = B_e(\tilde{\theta}_i^* - \tilde{\theta}_j^*)$ for all $e = (i, j)$ such that $i \in \mathcal{N}_w$ or $j \in \mathcal{N}_w$.

Finally, consider the area $\mathcal{N}_l$. We have $\tilde{p}_j^* = 0$ by construction. From Lemma 6.5, we have $\sum_{j \in \mathcal{N}_z} \tilde{p}_j^* = 0$ for all z. Since $\boldsymbol{C}\boldsymbol{B}\boldsymbol{C}^T\tilde{\boldsymbol{\theta}}^* = \tilde{\boldsymbol{p}}^*$, we know $\tilde{\theta}_i^* = \tilde{\theta}_j^*$ for all $i, j \in \overline{\mathcal{N}}_l$. This implies that for any edge $e = (i, j)$ within $\mathcal{N}_l$, we have $\tilde{f}_e^* = 0 = B_e(\tilde{\theta}_i^* - \tilde{\theta}_j^*)$. and therefore $\tilde{f}_e^* = B_e(\tilde{\theta}_i^* - \tilde{\theta}_j^*)$ for all $e \in \mathcal{E}$, concluding the proof. □

Proposition 6.4 reveals that with the proposed control strategy, after a non-critical failure, the injections and power flows in non-associated areas remain unchanged at equilibrium, even though they fluctuate during transient according to (6.1). Our control scheme guarantees that non-critical failures in a balancing area do not impact the operations of other areas, achieving stronger balancing area independence than that ensured by zero area control error alone.

Furthermore, traditional control strategies usually treat failures that disconnects the system differently, i.e., the post-contingency injections normally stay constant, but can be changed if the system are disconnected due to the line failures [38]. Under our scheme, failures that disconnect the system are treated in exactly the same way as failures that do not, provided that they are non-critical. Moreover, the impact of a failure that disconnects the system is localized and properly mitigated to the associated areas as well. This is in stark contrast with the global and severe impact of a bridge failure discussed in Chapter 4 and is the key benefit of integrating UC with the bridge-block decomposition.

6.4 Controlling Critical Failures

We now consider the case where the initial failure is critical. This may happen when a major generator or transmission line is disconnected from the grid.

Unified Controller under Critical Failures

Since UC is a concept that has emerged from the frequency regulation literature, the underlying optimization (6.2) is always assumed to be feasible in existing studies

[3, 41–43, 81]. As such, little is known about the behavior of UC if this assumption is violated when a critical failure happens. We now characterize the limiting behavior of UC in this setting.

In order to do this, we first formulate the exact controller dynamics of UC. Unfortunately, there is no standard way to do this as multiple designs of UC have been proposed in the literature [3, 41–43, 81], each with its own strengths and weaknesses. Nevertheless, all of the proposed controller designs are (approximately) projected primal-dual algorithms for the optimization problem (6.2) satisfying two assumptions that we now state. Let λ_i, for $i \in \left\{1, 2, \cdots, n + 3m + \left|\mathcal{P}^{\mathrm{UC}}\right|\right\}$, be the dual variables corresponding to the constraints (6.2c)-(6.2f).

UC1: For all $j \in \mathcal{N}$, $\underline{d}_j \leq d_j(t) \leq \overline{d}_j$ is satisfied for all t. This is achieved either via a projection operator that maps $d_j(t)$ to this interval or by requiring the cost function $c_j(\cdot)$ to approach infinity near these boundaries.

UC2: The primal variables $\boldsymbol{f}, \boldsymbol{\theta}$ and the dual variables λ_i are updated by a primal-dual algorithm[2] to solve (6.2).

Proposition 6.7. *Assume UC1 and UC2 hold. If* (6.2) *is infeasible, then there exists a dual variable λ_i such that* $\limsup_{t\to\infty} |\lambda_i(t)| = \infty$.

Proof. First, collect in the vector $\boldsymbol{x} = (\boldsymbol{\theta}, \boldsymbol{\omega}, \boldsymbol{d}, \boldsymbol{f}) \in \mathbb{R}^{3n+m}$ all the decision variables of the UC optimization (6.2) and rewrite it in a more standard form as

$$\min_{\underline{\boldsymbol{d}} \leq \boldsymbol{d} \leq \overline{\boldsymbol{d}}} \quad c(\boldsymbol{d}) \quad \text{s.t.} \quad \boldsymbol{A}\boldsymbol{x} \leq \boldsymbol{g},\ \boldsymbol{C}\boldsymbol{x} = \boldsymbol{h} \tag{6.5}$$

where $\boldsymbol{A}, \boldsymbol{C}, \boldsymbol{g}, \boldsymbol{h}$ are matrices (vectors) of proper dimensions that can be recovered from the full formulation in (6.2). Let $\boldsymbol{\lambda}_1, \boldsymbol{\lambda}_2$ be the corresponding dual variables, and set $\boldsymbol{\lambda} := [\boldsymbol{\lambda}_1; \boldsymbol{\lambda_2}]$ ($[\cdot;\cdot]$ here means matrix concatenation as a column). We can then write the Lagrangian for (6.5) as

$$\mathcal{L}(\boldsymbol{x}, \boldsymbol{\lambda}) = c(\boldsymbol{d}) + \boldsymbol{\lambda}_1^T(\boldsymbol{A}\boldsymbol{x} - \boldsymbol{g}) + \boldsymbol{\lambda}_2^T(\boldsymbol{C}\boldsymbol{x} - \boldsymbol{h}).$$

By the assumption UC2, we know that:

$$\dot{\boldsymbol{\lambda}}_1 = [\boldsymbol{A}\boldsymbol{x} - \boldsymbol{g}]^+_{\boldsymbol{\lambda_1}}, \quad \dot{\boldsymbol{\lambda}}_2 = \boldsymbol{C}\boldsymbol{x} - \boldsymbol{h}$$

with the projection operator $[\cdot]^+_{\boldsymbol{a}}$ defined component-wise by $\left([\boldsymbol{x}]^+_{\boldsymbol{a}}\right)_i = x_i$ if $x_i > 0$ or $(a)_i > 0$, and $\left([\boldsymbol{x}]^+_{\boldsymbol{a}}\right)_i = 0$ otherwise. Consider two closed convex sets $S_1 =$

[2] We do not consider the specific variants of primal-dual algorithms that are proposed in different designs of UC, since the standard primal-dual algorithm is often a good approximation.

$\{\boldsymbol{x} \mid \boldsymbol{A}\boldsymbol{x} \leq \boldsymbol{g}, \boldsymbol{C}\boldsymbol{x} = \boldsymbol{h}\}$ and $S_2 = \{\boldsymbol{x} \mid \underline{\boldsymbol{d}} \leq \boldsymbol{d} \leq \overline{\boldsymbol{d}}\}$. If the optimization (6.2) is infeasible, then $S_1 \cap S_2 = \emptyset$. As a result, we can find a hyper-plane that separates S_1 and S_2: more specifically, there exists $\boldsymbol{q} \in \mathbb{R}^{3n+m}$, $q_0 \in \mathbb{R}$ such that

$$\boldsymbol{q}^T\boldsymbol{x} > q_0, \ \forall\, \boldsymbol{x} \in S_1 \ \text{ and } \ \boldsymbol{q}^T\boldsymbol{x} \leq q_0, \ \forall\, \boldsymbol{x} \in S_2.$$

This fact then implies that the system $\left\{\boldsymbol{A}\boldsymbol{x} \leq \boldsymbol{g}, \quad \boldsymbol{C}\boldsymbol{x} = \boldsymbol{h}, \quad \boldsymbol{q}^T\boldsymbol{x} \leq q_0\right\}$ is not solvable. By Farkas' Lemma, we can thus find vectors $\boldsymbol{w}_1, \boldsymbol{w}_2, w_3$ such that $\boldsymbol{w}_1 \geq \boldsymbol{0}, w_3 \geq 0$, $\boldsymbol{A}^T\boldsymbol{w}_1 + \boldsymbol{C}^T\boldsymbol{w}_2 + \boldsymbol{q}w_3 = \boldsymbol{0}$, and $\boldsymbol{g}^T\boldsymbol{w}_1 + \boldsymbol{h}^T\boldsymbol{w}_2 + q_0 w_3 = -\epsilon < 0$. Define $\boldsymbol{z} = [\boldsymbol{w}_1; \boldsymbol{w}_2]$. We then see that under the UC controller, we have for any t:

$$\begin{aligned}
\boldsymbol{z}^T\dot{\boldsymbol{\lambda}}(t) &= \boldsymbol{w}_1^T[\boldsymbol{A}\boldsymbol{x}(t) - \boldsymbol{g}]_{\boldsymbol{\lambda}}^+ + \boldsymbol{w}_2^T(\boldsymbol{C}\boldsymbol{x}(t) - \boldsymbol{h}) \\
&\geq \boldsymbol{w}_1^T[\boldsymbol{A}\boldsymbol{x}(t) - \boldsymbol{g}]_{\boldsymbol{\lambda}}^+ + \boldsymbol{w}_2^T(\boldsymbol{C}\boldsymbol{x}(t) - \boldsymbol{h}) + \ w_3(\boldsymbol{q}^T\boldsymbol{x}(t) - q_0) \qquad (6.6a) \\
&\geq \boldsymbol{w}_1^T(\boldsymbol{A}\boldsymbol{x}(t) - \boldsymbol{g}) + \boldsymbol{w}_2^T(\boldsymbol{C}\boldsymbol{x}(t) - \boldsymbol{h}) + \ w_3(\boldsymbol{q}^T\boldsymbol{x}(t) - q_0) \qquad (6.6b) \\
&= \left(\boldsymbol{A}^T\boldsymbol{w}_1 + \boldsymbol{C}^T\boldsymbol{w}_2 + \boldsymbol{q}w_3\right)\boldsymbol{x}(t) - \left(\boldsymbol{w}_1^T\boldsymbol{g} + \boldsymbol{w}_2^T\boldsymbol{h} + w_3 q_0\right) \\
&= 0 + \epsilon > 0
\end{aligned}$$

where (6.6a) follows from $w_3 \geq 0$ and assumption UC1, which ensures $\boldsymbol{x}(t) \in S_2$ and thus $\boldsymbol{q}^T\boldsymbol{x}(t) - q_0 \leq 0$, and (6.6b) comes from $\boldsymbol{w}_1 \geq \boldsymbol{0}$ and the fact that $[\boldsymbol{x}]_{\boldsymbol{\lambda}}^+ \geq \boldsymbol{x}$ for all $\boldsymbol{x}$ (the inequality is component-wise). Consequently, $\boldsymbol{z}^T\boldsymbol{\lambda}(t) - \boldsymbol{z}^T\boldsymbol{\lambda}(0) > \epsilon t$ and thus $\lim_{t\to\infty} \boldsymbol{z}^T\boldsymbol{\lambda}(t) = \infty$. Finally, by noting $\lim_{t\to\infty} \boldsymbol{z}^T\boldsymbol{\lambda}(t) \leq \boldsymbol{w}_1^T \limsup_{t\to\infty} |\boldsymbol{\lambda}_1(t)| + |\boldsymbol{w}_2|^T \limsup_{t\to\infty} |\boldsymbol{\lambda}_2(t)|$, the desired result follows. □

Proposition 6.7 implies that, after a critical failure, UC cannot drive the system to a proper and safe operating point. This type of instability suggests a way to detect critical failures. Specifically, since Proposition 6.7 guarantees that at least one dual variable becomes arbitrarily large in UC operation when (6.2) is infeasible, we can set thresholds for the dual variables and raise an infeasibility warning if any of them is exceeded. By doing so, critical failures can be detected in a distributed fashion during the normal operations of UC.

Note that the dual variables for non-critical failures are usually bounded in practice unless certain degeneracy in (6.2) happens. This, however, does not impact the stability of UC. That being said, non-critical failures may also cause relatively large dual variable values in transient states. The choice of detection thresholds thus inevitably involves trade-offs. Specifically, tighter thresholds allow critical failures to be detected more promptly so that the system only experiences a short period of instability. On the other hand, tighter thresholds also lead to a larger false

alarm rate for non-critical failures. As we will show in the next section, when a failure is detected being critical, certain protection mechanisms will be involved so that the system is stabilized with potential cost of non-local response and load loss. Therefore, these thresholds should be chosen carefully by the operator in accordance to specific system parameters and application scenarios.

Constraint Lifting as a Remedy

In the event of a critical failure, it is impossible for UC to simultaneously achieve all of its control objectives and constraints. This can lead to instability and thus successive failures. We can mitigate this by progressively lifting certain constraints from UC in two different ways without compromising the basic objective of stabilizing the system:

- The zero area control error constraints (6.2e) between specific pairs of balancing areas can be lifted. This means that the controller now involves more balancing areas in failure mitigation.
- Loads can be shedded, which is reflected in (6.2) by enlarging the range $[\underline{d}_j, \overline{d}_j]$ for corresponding load buses.

By iteratively lifting these two types of constraints, we can guarantee the feasibility of (6.2) and ensure that the system converges to a stable point that is free from successive failures. This, however, comes with the cost of potential load loss, and thus must be carried out judiciously. The iterative relaxation procedure can follow predetermined rules specified by the system operator to prioritize different objectives. As an example, one can minimize load loss by relaxing possibly all area control error constraints before relaxing injection bounds on load buses. This will utilize all the contingency and regulation reserves globally across all areas to meet demand and shed load only as a last resort. In contrast, if the localization of failure impact should be prioritized, the operator can choose to first lift load injection bounds in the associated areas and then progressively lift area control error constraints to get more balancing areas involved.

In practice, these two types of constraint lifting can be combined and implemented iteratively, following the predetermined rules from the system operator. Specifically, the system operator may assess the node importance of the grid and design a hierarchical constraint lifting procedure, which specifies the order for involving balancing areas and the allowance for injection adjustment. Once the procedure is

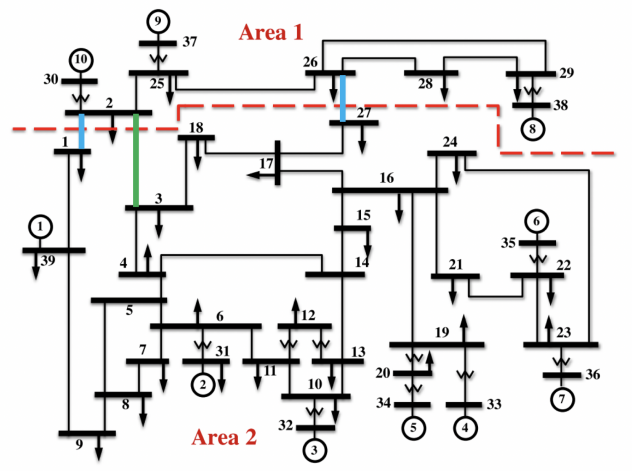

Figure 6.2: IEEE 39-bus network with two control areas from [3]. The two blue tie lines are switched off to create a tree structure with $(2, 3)$ as bridge.

specified, the real-time response of UC can be implemented accordingly by changing the dynamics of dual updates; see [43] for the detailed design of UC dynamics.

6.5 An Illustrative Example

In this section, we illustrate the dynamic response of our approach for the IEEE 39-bus network with parameters adapted from [3]. It consists of two control areas, which are connected by three tie lines, namely $(1, 2)$, $(2, 3)$ and $(26, 27)$.

We switch off the tie lines $(1, 2)$ and $(26, 27)$, chosen heuristically as those with the smallest absolute line flow. Two control areas are then connected in a tree structure as shown in Figure 6.2. We implement the unified controller on all nodes as follows. We only allow to adjust generations at first, but, if a severe failure is detected, the controller is then allowed to reduce loads. As a last resort, zero area control error can be lifted. The threshold is set to 0.5pu for dual variables.

As illustrated in Figure 6.3, in the case of the non-severe failure $(4, 14)$, the dual variables are always below the threshold and the system quickly converges to a safe equilibrium. On the other hand, the failure $(6, 7)$ leads to unstable oscillations of dual variables and a severe warning is raised at 10 sec, as depicted in Figure 6.4. The controller is then allowed to shed loads, action that quickly re-stabilizes the system. Note that the flow on line $(25, 26)$ remains unchanged at steady state for both failures, as it belongs to a non-associated control area.

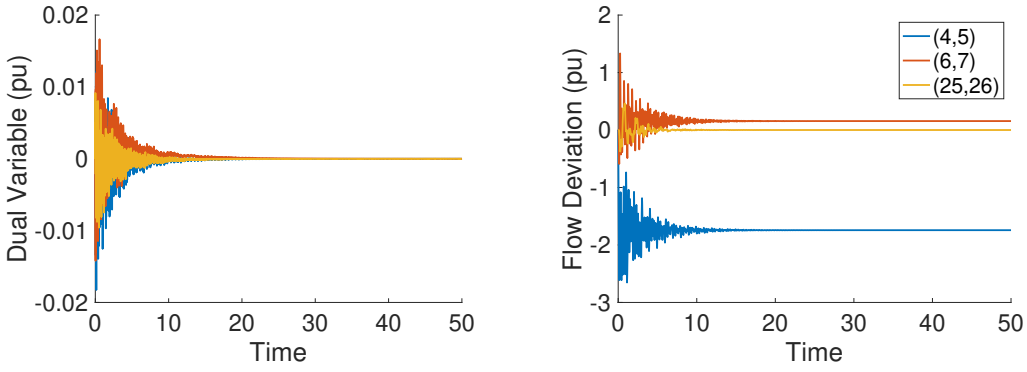

(a) Dual variable dynamics (b) Line flow dynamics

Figure 6.3: System dynamics after the non-severe failure of line $(4, 14)$. The controller is only allowed to reduce generations.

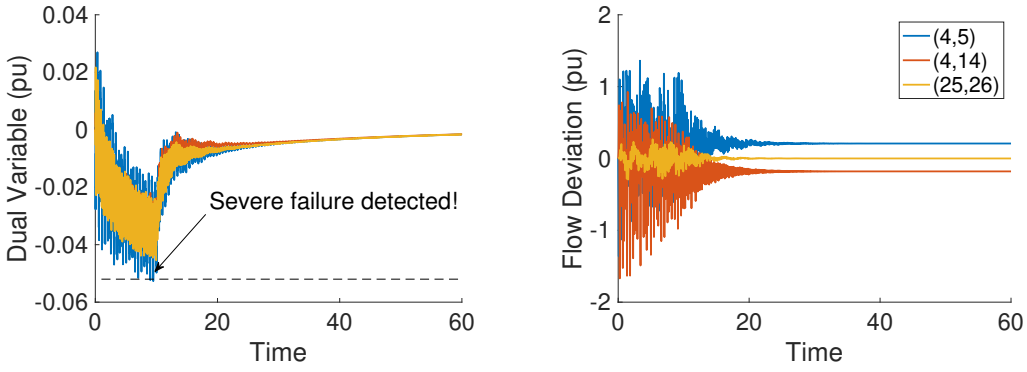

(a) Dual variable dynamics (b) Line flow dynamics

Figure 6.4: System dynamics after the severe failure of line $(6, 7)$. A warning is raised at time 10 sec, at which point the controller is allowed to shed loads.

6.6 Case Studies

In this section, we evaluate the performance of the proposed control strategy on the IEEE 118-bus and IEEE 2736-bus (the Polish network) test systems, with respect to $N - k$ security standard and localization performance under different levels of system congestion.

$N - k$ Security under Different Congestion Levels

We first focus on system robustness with respect to $N - k$ security standard on the IEEE 118-bus system. This test network has two balancing areas shown as Area 1 and Area 2 in Fig. 6.5. To form a tree-partitioned network, three lines $(15, 33)$, $(19, 34)$, and $(23, 24)$ are switched off, obtaining what we henceforth refer to as the

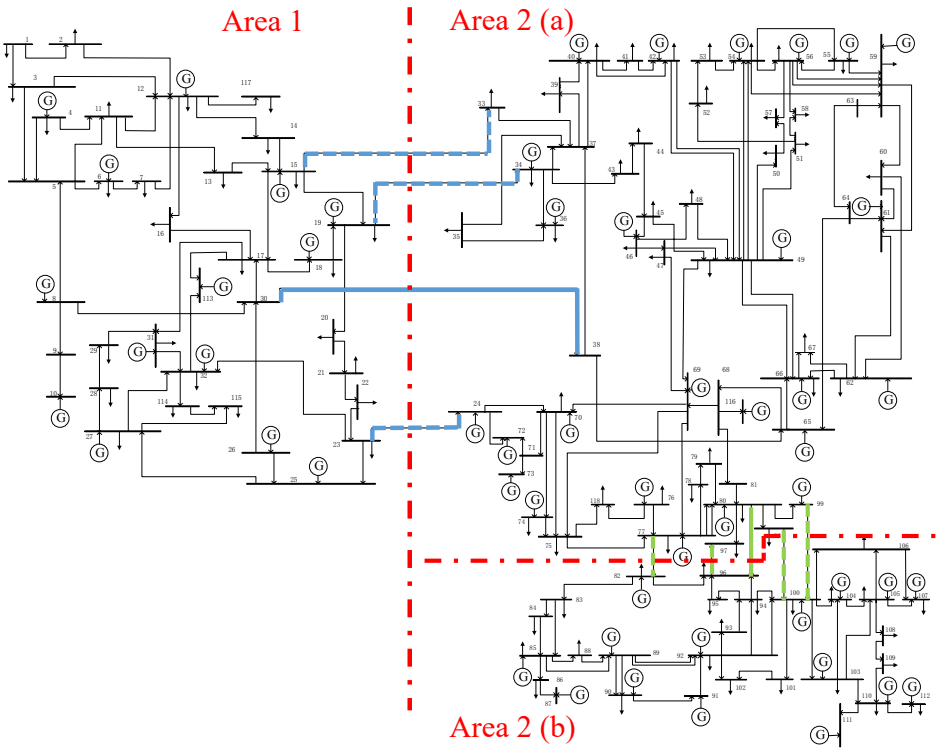

Figure 6.5: One line diagram of the IEEE 118-bus test network.

revised network.

We compare UC on the tree-partitioned revised network, as specified by our proposal, and classical AGC on the *original* network. UC is modeled by the optimization problem (6.2) and AGC is modeled by (6.2) without the line limits (6.2f). A failure scenario is said to be *vulnerable* if the initial failure leads to successive failures or loss of load. To compare the performance between our proposed approach and AGC, we collect statistics on (a) vulnerable scenarios as a percentage of the total simulated scenarios, and (b) load loss rate (LLR) which is defined as the ratio of the total load loss to the original total demand. Note that we do not perform time-domain simulations, but directly compute the equilibrium point of the closed-loop systems under UC and AGC by solving the coressponding optimization, respectively. This reduces the computational complexity and allows us to systematically evaluate our proposed control method in a wide range of simulation settings. Moreover, we assume that the detection threshold is set relatively large so that the failures can be accurately classified into critical and non-critical failures. Therefore, constraint lifting only happens for critical failures.

The failure scenarios are created as follows. First, we generate a variety of load

injections by adding random perturbations to the nominal load profile from [95] and then solve the DC OPF to obtain the corresponding generator operating points over the actual IEEE test networks. For a fair comparison, we use the same generation and load operating points over the revised network and calculate the pre-contingency flows with DC power flow equations. Second, we sample over the collection of all subsets that consist of k transmission lines of the IEEE 118-bus test network. Finally, for each sampled subset of k lines, we remove all lines in this subset as initial failure and simulate the cascading process thus triggered. Specifically, for $k = 1, 2, 3$ initial line failures, we generate 100, 15, and 15 load profiles and further compute the optimal generation dispatch by DC OPF. For each load profile, we iterate over every single transmission line failure, and sample 3,000 and 5,000 failure scenarios for $k = 2, 3$ line failures, respectively. In total, our simulations cover the cases $k = 1, 2, 3$ with roughly 138,600 failure scenarios, as summarized in Table. 6.1.

Table 6.1: Simulation setup for $N - k$ security evaluation.

Case	$k = 1$	$k = 2$	$k = 3$
# of Load Profiles	100	15	15
# of Sampled Failures	186	3000	5000
Total Scenarios	18600	45000	75000

Fig. 6.6(a) shows the average, minimum, and maximum percentage of vulnerable scenarios across all sampled failure scenarios, while Fig. 6.6(b) plots the complementary cumulative distribution (CCDF) of the load loss rates. The simulation results show that the proposed control incurs both substantially fewer vulnerable scenarios and much less loss of load in all cases compared to AGC. This difference is particularly pronounced when multiple lines are tripped simultaneously ($k = 2, 3$). We highlight that in our simulations, UC operates over the tree-partitioned network (while AGC operates over the original network) in which some of the tie-lines are switched off and hence some transfer capacity is removed from the system. Moreover, the newly created bridge $(30, 38)$ in the tree-partitioned network is never vulnerable under the proposed control in all the scenarios we have studied.

We then illustrate the improvement of the proposed approach over AGC under different congestion levels. To do so, we scale down the line capacities to $\alpha = 0.9, 0.8, 0.7$ of the base values and collect statistics for all single line initial failures ($k = 1$). Our results are summarized in Fig. 6.7, which again show that the proposed approach significantly outperforms AGC in all scenarios, especially those in which

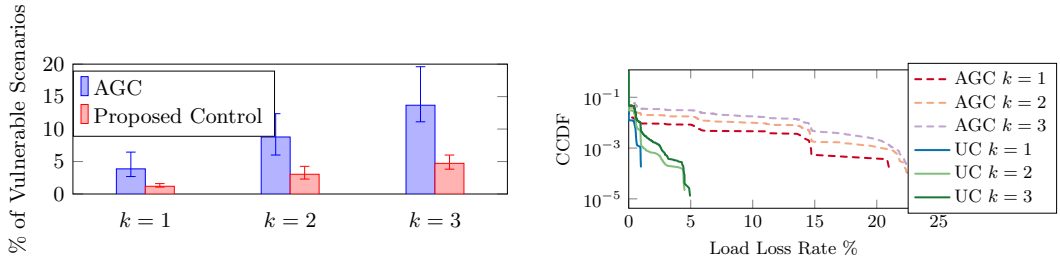

(a) Average fraction of vulnerable scenarios for $k = 1, 2, 3$.

(b) CCDF for load loss rate for $k = 1, 2, 3$.

Figure 6.6: System robustness in terms of the $N - k$ security standard.

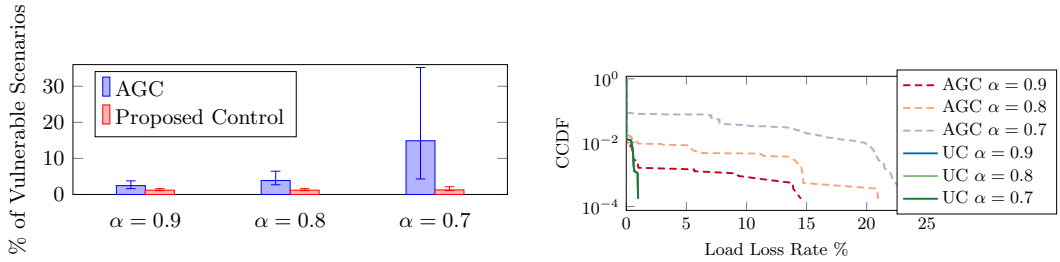

(a) Average fraction of vulnerable scenarios for different congestion levels.

(b) CCDF for load loss rate for different congestion levels.

Figure 6.7: System robustness under different levels of congestion obtained scaling line capacities by the factor α.

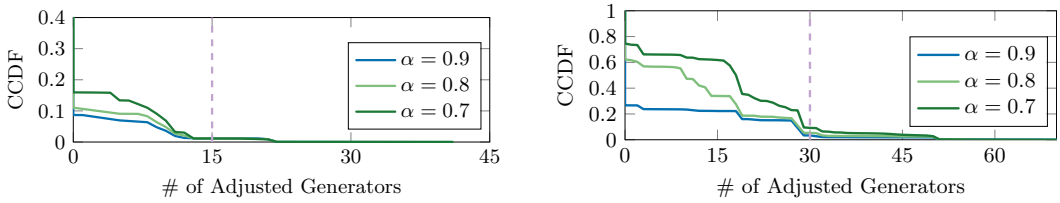

(a) CCDF for generator response on IEEE 118-bus network.

(b) CCDF for generator response on IEEE Polish network.

Figure 6.8: Generator response over IEEE 118-bus and Polish network.

the system is congested. Again in all these scenarios, the bridge is never vulnerable under the proposed control.

We remark that UC outperforms AGC even if both control methods operate over the tree-partitioned network since AGC does not enforce line limits. There are only a few failure scenarios with a lower load loss rate under AGC. However, those failures always propagate through multiple stages and require a significantly longer time to re-stabilize the system.

Table 6.2: Statistics on failure localization over the IEEE 118-bus test network.

Line Capacity	$\alpha = 0.9$	$\alpha = 0.8$	$\alpha = 0.7$
Avg. % of Vul. Sce.	3.53	3.68	3.82
Avg. (Max.) LLR(%)	0.55 (1.06)	0.56 (2.17)	0.59 (2.21)

Localized Failure Mitigation

In this subsection, we consider a specific constraint lifting rule that progressively involves other areas by relaxing area control error constraints only if local load shedding within the associated areas is not enough to make problem (6.2) feasible. This rule prioritizes localization of the initial failure. By implementing it, we show that the proposed control strategy can localize cascading failures within the associated areas with negligible load loss. The experiments are carried out over two networks: (a) a finer tree-partitioned version of the IEEE 118-bus test network, and (b) the much larger-scale Polish network, consisting of 2736 buses and 3504 lines.

For the IEEE 118-bus test network, we switch off 4 additional lines, $(77, 82)$, $(96, 97)$, $(98, 100)$, and $(99, 100)$, which refines the bridge-blocks used in the previous subsection since it further decomposes Area 2 into two balancing areas (as shown in Fig. 6.5). The generator capacities are scaled down by 60% so that the total generation reserve is roughly 20%. We create different congestion levels by scaling the line capacities according to a factor $\alpha = 0.9, 0.8, 0.7$ and iterate over all single transmission lines as initial failures. The injections are the same as that for the $N-1$ test in the previous subsection.

The statistics on the fraction of vulnerable scenarios and load loss rates (LLRs) for this experiment are summarized in Table 6.2. We observe that the proposed control strategy never incurs more than 2.21% LLR across all tested injections and congestion levels. Furthermore, for this specific network, the proposed approach localizes *all* failures to the associated areas, i.e., the tie-line constraints are never lifted. This localization phenomenon can more clearly be noticed in Fig. 6.8(a), which shows the CCDF of the number of generators whose operating points are adjusted in response to the initial failures. The majority of failures lead to operating point adjustments on less than 15 generators, which is roughly the number of generators within a single balancing area. The small portion of failures that impact more than 15 generators are bridge failures, which by definition have two associated areas and thus more associated generators.

Table 6.3: Statistics on failure localization over the Polish network.

Line Capacity	$\alpha = 0.9$	$\alpha = 0.8$	$\alpha = 0.7$
Scenarios Mitigated with one Area (%)	92.39	88.63	86.91
Scenarios Mitigated with 2-3 Areas (%)	6.44	9.48	10.40
Scenarios Mitigated with All Areas (%)	1.17	1.89	2.69
Avg. (Max.) LLR(%)	0.05 (2.93)	0.05 (2.94)	0.07 (3.24)
Avg. # of Gen. Adj.	6.52	11.66	16.37

For the Polish network, we switch off 78 transmission lines from the original network, creating a tree-partitioned network with 4 areas of 1430, 818, 359 and 129 buses, respectively. Similar to the setup for the IEEE-118 test network, the generation capacities are scaled properly so that the total generation reserve is roughly 20%, and the line capacities are scaled down to $\alpha = 0.9, 0.8, 0.7$ to create different congestion levels. We then iterate over all single line failures and the statistics from our experiments are summarized in Table 6.3. Our results show that for this test network, more than 86% of the single line failures can be mitigated locally within a single area for all congestion levels. In addition, the worst case LLR is roughly 3% across all simulated scenarios, with an average that is no higher than 0.07%. Similar to the IEEE 118-bus test network, the number of generators whose operating points are adjusted by the proposed control strategy in response to the failures is small, as shown in Fig. 6.8(b), confirming failure localization.

6.7 Conclusion

In this chapter, we have proposed a complementary approach to grid reliability by integrating the network bridge-block decomposition and the unified controller for frequency regulation to achieve fast-timescale failure control. It provides strong analytical guarantees of both the localization and mitigation of failures. Our case studies on the IEEE 118-bus and 2736-bus test systems show that the proposed control scheme can greatly improve overall reliability compared to the current practice. In particular, this novel control prevents successive failures from happening while localizing the impacts of initial failures. When load shedding is inevitable, the proposed strategy incurs significantly less load loss.

Chapter 7

FAILURE MITIGATION: LOCAL INJECTION RESPONSE

Chapter 6 proposes a distributed control algorithm that will automatically respond to failures and drive the system to a safe post-contingency operating point. While our proposed approach is promising and provides strong guarantees in both failure mitigation and localization, the fast-timescale unified controller requires real-time measurements of the system states and is challenging to implement with current power system infrustructure.

On the other hand, optimization-based load shedding algorithms [39, 40, 64, 77, 78] directly adjust injections in response to failures, with the goal to minimize the loss of power demand (possibly through multiple stages of the cascade). These approaches require a centralized controller to monitor the system states, calculate the control action for each node, and communicate the derived injection adjustments[1]. Such control algorithms thus require a longer time to take effect after failures.

In this chapter, we propose a different approach for corrective control that has strong structural properties. We directly adjust the post-contingency injections by solving an optimization problem, which we refer as the *Optimal Injection Adjustment* (OIA) problem. The OIA problem exhibits a local injection adjustment pattern so that fast and accurate control actions can be applied for large-scale networks.

Our contribution is two-fold. We first theoretically prove that the control resulting from OIA exhibits a local injection adjustment pattern: at any given node an injection adjustment is not required unless at least one of its neighboring nodes closer to the contingency already reached its adjustment limit. Secondly, we compare OIA with traditional optimization-based corrective controls that focus on optimal load shedding (OLS) [64, 77, 78] using numerical experiments. These experiments highlight that OIA achieves near-optimal control costs using localized control actions. Specifically, OIA requires 80% fewer nodes to adjust their operational set-points than traditional OLS, yet achieves similar control costs. However, to achieve local response, OIA sometimes pushes lines toward (or beyond) their capacity limit and so we additionally consider a variation, named OIA-LL, which imposes line limits

[1]Distributed control might be achieved if we restrict the set of control actions and consider special cases [39].

explicitly in order to ensure that the adjustments prescribed by OIA-LL do not overload any lines. Our experiments highlight that OIA-LL provides nearly the same benefits as OIA with respect to control costs and that the injection adjustments, though less local than OIA, are still significantly more localized than that under OLS.

The design of OIA paves the way for further study of local corrective control policies. By exposing the topological pattern of optimal corrective actions, our analytic results show that it is possible to provide near-optimal corrective control using local injection adjustments. Such a structural property is highly desirable in large-scale power networks where distributed fast control policies are preferred. Further, our numerical results highlight the trade-off between the locality and control costs, especially when it comes to enforcing line capacity limits.

7.1 Problem Formulation

DC Power Flow and Redistribution

To begin, we review the DC power flow model and characterize how the flow redistribution happens after a failure.

Consider a power transmission network $\mathcal{G} = (\mathcal{N}, \mathcal{E})$. Given the power injections and phase angles $\boldsymbol{p}, \boldsymbol{\theta} \in \mathbb{R}^n$, the branch flows $\boldsymbol{f} \in \mathbb{R}^m$ are obtained as the solution to the following DC power flow equations:

$$\boldsymbol{p} = \boldsymbol{C}\boldsymbol{f}, \tag{7.1a}$$

$$\boldsymbol{f} = \boldsymbol{B}\boldsymbol{C}^T\boldsymbol{\theta}. \tag{7.1b}$$

Define the Laplacian matrix $\boldsymbol{L} = \boldsymbol{C}\boldsymbol{B}\boldsymbol{C}^T$. It is known that there exists a unique branch flow solution $\boldsymbol{f} = \boldsymbol{B}\boldsymbol{C}^T\boldsymbol{L}^\dagger\boldsymbol{p}$ to the above power flow equations, provided that the power injections are balanced ($\sum_{j\in\mathcal{G}} p_j = 0$) for the graph $\mathcal{G}$. Using a classical result in circuit analysis, it is easy to show that the branch flow solution of (7.1) is also the unique optimal solution of the following quadratic optimization problem:

$$\min_{\boldsymbol{f}} \quad \boldsymbol{f}^T\boldsymbol{B}^{-1}\boldsymbol{f} \tag{7.2a}$$

$$\text{s.t.} \quad \boldsymbol{p} = \boldsymbol{C}\boldsymbol{f}. \tag{7.2b}$$

The quadratic form $\boldsymbol{f}^T\boldsymbol{B}^{-1}\boldsymbol{f} = \sum_{e\in\mathcal{E}} B_e^{-1} f_e^2$ that appears as the objective function has been shown in [105] to be an approximation for the power losses in the AC network. The same quantity has also been studied in [106] and [58], where it is referred to as

network tension and is proven to be monotonically increasing during any cascading failure process. In [106] it has been shown that while an arbitrary load shedding may increase the network tension, there exists a load shedding configuration that can guarantee its reduction.

Now, suppose the transmission line $\hat{e} = (s, t)$ trips. To distinguish between pre- and post-contingency quantities, we add a superscript $(\cdot)^{\text{pre}}$ to those referring to pre-contingency network. Specifically, we assume the pre-contingency network $\mathcal{G}^{\text{pre}} = (\mathcal{N}^{\text{pre}}, \mathcal{E}^{\text{pre}})$ comprises the same nodes, i.e., $\mathcal{N}^{\text{pre}} = \mathcal{N}$, and has exactly one more transmission line, namely $\mathcal{E}^{\text{pre}} = \mathcal{E} \cup \{\hat{e}\}$. We denote its pre-contingency flow as $\alpha := f_{\hat{e}}^{\text{pre}} = f_{s,t}^{\text{pre}} \in \mathbb{R}$. Denote by $\boldsymbol{f}_{-\hat{e}} := (f_e, e \in \mathcal{E}^{\text{pre}} \setminus \{\hat{e}\} \in \mathbb{R}^m)$ the vector of branch flows on the surviving lines. Let $\boldsymbol{e}_{s,t}$ be the incidence vector of line (s, t) such that its s-th element is 1, t-th element is -1, and 0 otherwise. The post-contingency deviations of $\Delta\boldsymbol{p} = \boldsymbol{p} - \boldsymbol{p}^{\text{pre}}$, $\Delta\boldsymbol{\theta} = \boldsymbol{\theta} - \boldsymbol{\theta}^{\text{pre}}$ and $\Delta\boldsymbol{f} = \boldsymbol{f}_{-\hat{e}} - \boldsymbol{f}_{-\hat{e}}^{\text{pre}}$ satisfy:

$$\alpha\boldsymbol{e}_{s,t} + \Delta\boldsymbol{p} = \boldsymbol{C}\Delta\boldsymbol{f}, \tag{7.3a}$$

$$\Delta\boldsymbol{f} = \boldsymbol{B}\boldsymbol{C}^T\Delta\boldsymbol{\theta}. \tag{7.3b}$$

Note that $\boldsymbol{B}, \boldsymbol{C}$ are matrices for the post-contingency network. Equation (7.3) suggests that the system deviations can be equivalently modeled by the DC power flow equations over the post-contingency network with injections $\alpha\boldsymbol{e}_{s,t} + \Delta\boldsymbol{p}$. The first term $\alpha\boldsymbol{e}_{s,t}$ characterizes the internal effect of redistributing the flow of the outaged line $\hat{e}$. The second term $\Delta\boldsymbol{p}$ characterizes the external effect of injection adjustments of either generations or loads after the failure. Note that the power balancing condition $\sum_j \Delta p_j = 0$ is implicitly required to satisfy (7.3a).

Optimal Injection Adjustment

We can now discuss how to respond to the initial failure. Here, we formulate an optimization problem that aims to minimize the flow deviations by adjusting the node power injections in response to line failures. The key to our approach is to focus on the post-contingency injection adjustments $\Delta\boldsymbol{p}$, which capture both generators and loads flexibility and are thus bounded by generator capacity limits or load shedding allowance. For any node $i \in \mathcal{N}$ we denote its injection adjustment and corresponding constraints as

$$\Delta\underline{p}_i \leq \Delta p_i \leq \Delta\overline{p}_i.$$

For each injection adjustment $\Delta\boldsymbol{p}$ satisfying the above constraints, the post-contingency flow deviations $\Delta\boldsymbol{f}$ can then be computed from (7.3).

We henceforth drop the notation $\Delta(\cdot)$ for compactness, but all the quantities $\boldsymbol{p}$, $\boldsymbol{f}$, and $\boldsymbol{\theta}$ will still denote *deviations* from their original values in the pre-contingency network.

We quantify the magnitude of the flow deviation on each surviving line l by means of a non-negative "cost function" $c_e(f_e)$, which we take to be strictly monotonically increasing with the absolute value of f_e. Given such a family of cost functions, we formulate the **optimal injection adjustment (OIA) problem**, whose goal is to determine the injection adjustments that minimize the cost of post-contingency flow deviations. Formally, given a pre-contingency network $\mathcal{G}^{\text{pre}}$ with a branch flow α on the line $\hat{e} = (s,t) \in \mathcal{E}^{\text{pre}}$ to be tripped, the OIA(α,s,t) problem is formulated on the post-contingency network $\mathcal{G}$ as follows:

$$\min_{\boldsymbol{f},\boldsymbol{p},\boldsymbol{\theta}} \quad \sum_{e\in\mathcal{E}} c_e(f_e) \tag{7.4a}$$

$$\text{s.t.} \quad \alpha \boldsymbol{e}_{s,t} + \boldsymbol{p} = \boldsymbol{C}\boldsymbol{f}, \tag{7.4b}$$

$$\boldsymbol{f} = \boldsymbol{B}\boldsymbol{C}^T\boldsymbol{\theta} \tag{7.4c}$$

$$\underline{\boldsymbol{p}} \le \boldsymbol{p} \le \overline{\boldsymbol{p}}. \tag{7.4d}$$

We assume that the generators and loads in our model are controllable and both components can either increase or decrease their injections. As a result, for every node $i \in \mathcal{N}$, its adjustment limit satisfies $\underline{p}_i < 0 < \overline{p}_i$.

To build intuition for the OIA problem, notice that ignoring the constraint (7.4d) yields a trivial (unique) optimal solution $\boldsymbol{p}^* = -\alpha \boldsymbol{e}_{s,t}$. This suggests that if the adjustments at the end-points of the failed transmission line are allowed to be large enough, i.e., $\max(\underline{p}_t, -\overline{p}_s) \le \alpha \le \min(\overline{p}_t, -\underline{p}_s)$, pre-contingency branch flows of the grid can be restored.

Beyond this simple case, the OIA problem can prioritize different system requirements by choosing appropriate cost functions. For instance, $c_e(f_e) = |f_e|$ characterizes the total post-contingency absolute flow deviations, which can be useful to determine the capacity reserves for transmission lines. Another possible cost function is $c_e(f_e) = B_e^{-1} f_e^2$. Note that f_e here indicates the flow deviation rather than the actual value used in network tension. This quantity has been studied in contingency analysis to quantify the severity of a line failure [57]. It is shown that the average load loss and number of outaged lines increase as this quantity increases. Thus, adjusting post-contingency injections to minimize this cost function can potentially improve grid stability against failures.

While not immediately clear, the OIA problem ensures a local response to contingencies. In particular, we show in the next section that the optimal solutions of the OIA problem exhibit a local and progressive pattern. Specifically, the optimal adjustments are localized around the failure in a way that an injection adjustment is non-zero only if at least one of its neighbors reaches the adjustment limit. This topological pattern in the adjustments ensures that it is possible to design local responses against failures while avoiding computational challenges. This is particularly important when the system requires fast timescale post-contingency corrective control policies for reliability.

A drawback of the OIA problem introduced so far is that it does not explicitly constrain post-contingency flows to satisfy the line capacity limits. As a result there may be some lines that are overloaded post-contingency. When this is a problem, it can be remedied by including the constraints explicitly via

$$\underline{\boldsymbol{f}} \leq \boldsymbol{f} \leq \overline{\boldsymbol{f}}, \tag{7.5}$$

where $\underline{\boldsymbol{f}}$ and $\overline{\boldsymbol{f}}$ are the limits for post-contingency flow deviations. We refer to the OIA with above line limits as the **optimal injection adjustment with line limits (OIA-LL) problem**. While our analytic results focus on OIA, we show via case studies in Section 7.3 that OIA-LL achieves nearly the same performance as OIA at the expense of some locality.

Finally, note that the OIA problem we consider is philosophically different than traditional corrective control policies, e.g., see [78, 107]. In these works, the focus is on the **optimal load shedding (OLS) problem** whose objective is to minimize the cost of load loss. Formally, a generalization of OLS can be formulated as:

$$\min_{\boldsymbol{f},\boldsymbol{p},\boldsymbol{\theta}} \quad \textstyle\sum_{i\in\mathcal{N}} c_i(p_i) \tag{7.6a}$$

$$\text{s.t.} \quad \alpha \boldsymbol{e}_{s,t} + \boldsymbol{p} = \boldsymbol{C}\boldsymbol{f}, \tag{7.6b}$$

$$\boldsymbol{f} = \boldsymbol{B}\boldsymbol{C}^T\boldsymbol{\theta} \tag{7.6c}$$

$$\underline{\boldsymbol{p}} \leq \boldsymbol{p} \leq \overline{\boldsymbol{p}}, \tag{7.6d}$$

$$\underline{\boldsymbol{f}} \leq \boldsymbol{f} \leq \overline{\boldsymbol{f}}, \tag{7.6e}$$

where the objective is to explicitly minimize the cost of injection adjustments $c_i(p_i)$ (e.g., the loss of load, the cost of generator ramping) while enforcing post-contingency flows under line capacity as a constraint (7.6e). This is a generalization of classical OLS because it allows loads to fluctuate both up and down around the

pre-contingency injection, instead of only down. This generalization allows for a more fair comparison between OLS and OIA.

In contrast to OLS, the OIA problem does not minimize the cost of injection adjustments directly, but encodes the adjustment limit into constraint (7.4d). Specifically, the traditional approaches tend to impose a larger adjustment limit in (7.6d) in order to make the optimization feasible. On the other hand, the OIA problem (7.4) is always feasible and one can impose a more strict limit in (7.4d) so that a lower cost for control actions is implicitly achieved. It should be noted, however, that a strict injection adjustment limit may result in unsafe post-contingency line flows. Therefore, the limit should be designed carefully based on the system parameters and application scenarios. As we will show in Section 7.3 through numerical experiments, the OIA provides a near-optimal but much more local injection adjustments in response to failures. The overloaded lines are avoided with the OIA-LL method.

7.2 Theoretical Analysis

In this section, we study the OIA and OIA-LL problems and their benefits for contingency response. We provide analytic results that characterize the topological patterns of the optimal solutions to the OIA problem. These patterns lead to possible local, distributed, and fast responses against failures.

We begin with the case where the post-contingency network is a tree. In this case, for any choice of the cost functions, the optimal solutions of the OIA problem have a distinctive feature: the injection of any node is not adjusted unless its preceding nodes toward the endpoints s and t of the outaged line reach their adjustment limits. We prove that a similar characterization holds for general post-contingency networks (possibly including loops) if the cost function $c_e(f_e) = B_e^{-1} f_e^2$ is used. Recall that this cost prioritizes grid stability.

For ease of presentation, we assume the direction of pre-contingency flow over the outage line $\hat{e} = (s, t)$ is from node s toward node t, i.e., $\alpha > 0$. All proofs in this section are deferred to Section 7.5.

Tree Post-Contingency Network

We first analyze the optimal solutions of the OIA problem (7.4) in the case in which the post-contingency network $\mathcal{G}$ is a tree. Our main result, Theorem 7.3, states that the optimal injection adjustment at each node i can be determined by checking whether the adjustment limit is reached by all the *preceding* nodes (see

Definition 7.1) along the paths connecting node i toward nodes s and t.

Definition 7.1. *Given two nodes i, j, consider a simple path (i.e., without repeated nodes) $P = [i = u_0, u_1, u_2, \ldots, u_r = j]$ connecting nodes i and j. We denote the node preceding node j in the path P toward node i as $u_i^P(j) := u_{r-1}$, and denote the set of all nodes preceding node j along the path P as $\mathcal{U}_i^P(j) := \{i = u_0, u_1, \ldots, u_{r-1}\}$. Moreover, we define $\mathcal{U}_i^P(i) = \emptyset$.*

Note that there exists a unique simple path for every pair of nodes i and j when the post-contingency network is a tree. Thus we omit the superscript $(\cdot)^P$ in this subsection for notation simplicity.

In order to build to the presentation of Theorem 7.3, we develop a construction of the post-contingency flow deviations $\boldsymbol{f} \in \mathbb{R}^m$. In general, the power flow equation (7.1b) requires $\boldsymbol{f}$ to lie in the column space of matrix $\boldsymbol{B}\boldsymbol{C}^T$; however, such an image space is essentially $\mathbb{R}^m$ as range$(\boldsymbol{B}\boldsymbol{C}^T) = m$ when the post-contingency network is a tree [108]. Therefore, constraint (7.4c) in OIA problem is actually redundant for tree networks, since for any arbitrary flow vector $\boldsymbol{f} \in \mathbb{R}^m$, we can always construct the corresponding phase angles $\boldsymbol{\theta}$ and power injections $\boldsymbol{p}$ such that the DC power flow equations (7.4c) and (7.4b) naturally hold. In particular, we have $\boldsymbol{\theta} = \boldsymbol{L}^\dagger \boldsymbol{C}\boldsymbol{f}$ and $\boldsymbol{p} = \boldsymbol{C}\boldsymbol{f} - \alpha \boldsymbol{e}_{s,t}$.

This fact plays a critical role in the proof of the following lemma, which characterizes the necessary conditions to determine the sign of optimal injection adjustment for every node i other than nodes s or t.

Lemma 7.2. *Assume that the cost function is strictly increasing in absolute flow deviations and that the post-contingency network is a tree. For node $i \neq s, t$ and its preceding node $u_s(i)$ toward node s and preceding node $u_t(i)$ toward node t, the optimal solutions $\boldsymbol{p}^*, \boldsymbol{f}^*$ of the optimization* (7.4) *satisfy:*

- *If $p_i^* > 0$, then $f_{u_t(i),i}^* < 0$, $p_{u_t(i)}^* = \overline{p}_{u_t(i)}$;*
- *If $p_i^* < 0$, then $f_{u_s(i),i}^* > 0$, $p_{u_s(i)}^* = \underline{p}_{u_s(i)}$.*

Lemma 7.2 suggests that for any given node i other than nodes s or t, if the optimal control is to increase its injection, then its preceding node $u_t(i)$ toward node t must reach the maximal adjustment limit. Moreover, the direction of corresponding optimal flow deviation is from node i toward node $u_t(i)$. Similarly, if the optimal

control at node i is to decrease its injection, then the preceding node $u_s(i)$ toward node s reaches the minimal adjustment limit with the flow deviation from node $u_s(i)$ toward node i.

Applying Lemma 7.2 repeatedly, one can show that if the optimal injection adjustment at node i is non-zero, then there must exist a path connecting node i to node s or t along which the optimal injection adjustments of all the nodes reach their limits. Moreover, the direction of optimal flow deviations are determined based on the sign of p_i^*. We formally characterize this topological pattern in the following theorem, which is the main result of this section.

Theorem 7.3. *Assume the post-contingency network is a tree and that the cost function is strictly increasing in absolute flow deviations. For any optimal solutions $\boldsymbol{p}^*$ of* (7.4)*, the optimal injection adjustment at node $i \neq s, t$ satisfies:*

(a) If there exists $j \in \mathcal{U}_t(i)$ with $p_j^* < \overline{p}_j$, then $p_i^* \leq 0$;

(b) If there exists $j \in \mathcal{U}_s(i)$ with $p_j^* > \underline{p}_j$, then $p_i^* \geq 0$.

In particular, if there exist both $j \in \mathcal{U}_t(i)$ with $p_j^* < \overline{p}_j$ and $j' \in \mathcal{U}_s(i)$ with $p_{j'}^* > \underline{p}_{j'}$, then $p_i^* = 0$.

Theorem 7.3 illustrates that the optimal solution to (7.4) is to progressively adjust the injections starting from nodes s and t, which aligns with intuition. Specifically, the contingency causes an excessive injection α at node s and a power deficit $-\alpha$ at node t for the post-contingency system. To compensate for such imbalances, the optimal response at every other node depends on its preceding nodes toward the endpoints of the failures. In particular, there is no incentive for a node to adjust its injection when there is a preceding node that does not reach its adjustment limit. Therefore, the injection adjustments follow a progressive pattern from the endpoints of the contingency. In fact, there is an (tight) upper bound for the total absolute injection adjustments of all the nodes as shown in the following lemma.

Lemma 7.4. *Assume the post-contingency network is a tree and that the cost function is strictly increasing in absolute flow deviations. Then, every optimal solutions $\boldsymbol{p}^*$ of* (7.4) *satisfies the following inequalities: (i) $p_s^* < 0$ and $p_t^* > 0$; (ii) $\sum_{i \in \mathcal{V}} \left| p_i^* \right| \leq 2\alpha$.*

The next corollary follows immediately from combining Theorem 7.3 and Lemma 7.4. It suggests that the progressive injection adjustments are guaranteed to terminate so that the adjusted nodes are localized around nodes s and t.

Corollary 7.5. *Assume the post-contingency network is a tree and that the cost function is strictly increasing in absolute flow deviations. Then, for any optimal solutions $\boldsymbol{p}^*$ of* (7.4)*, the optimal injection adjustment p_i^* at node $i \neq s, t$ satisfies the following properties:*

- *If $\sum_{j \in \mathcal{U}_s(i)} -\underline{p}_j \geq \alpha$, then $p_i^* \geq 0$;*
- *If $\sum_{j \in \mathcal{U}_t(i)} \overline{p}_j \geq \alpha$, then $p_i^* \leq 0$.*

In particular, if both $\sum_{j \in \mathcal{U}_s(i)} -\underline{p}_j \geq \alpha$ and $\sum_{j \in \mathcal{U}_t(i)} \overline{p}_j \geq \alpha$ hold, then $p_i^* = 0$.

General Post-Contingency Networks

The characterization proved in the case of tree networks does not hold in general. However, we show here that the localization properties observed in the case of tree networks extend to general networks when the cost function $c_e(f_e) = B_e^{-1} f_e^2$ is adopted. Recall that the cost function $c(\boldsymbol{f}) = \boldsymbol{f}^T \boldsymbol{B}^{-1} \boldsymbol{f}$ is popular in the contingency literature, where it is usually regarded as a metric to quantify the severity of a failure.

Loops complicate the behavior of general networks as there may be multiple simple paths connecting nodes i and j. For clarity, in this subsection we add back the superscript $(\cdot)^P$ for $u_i^P(j)$ and $\mathcal{U}_i^P(j)$ to indicate a specific simple path P connecting node j towards node i. We now present the main result of this section, which extends Theorem 7.3 to general networks and characterizes the conditions to determine post-contingency injection deviations. Moreover, if the post-contingency injections for both endpoints of a transmission line remain the same, the post-contingency flow is unchanged as well, suggesting that flow deviations are localized along the lines with adjusted injections.

Theorem 7.6. *Assuming a connected post-contingency network and taking $c_e(f_e) = B_e^{-1} f_e^2$ as cost function, the optimal injection adjustment p_i^* at node $i \neq s, t$ for the optimal solution $\boldsymbol{p}^*$ of* (7.4) *satisfies the following properties:*

(a) If for every simple path P connecting node i and t there exists $j \in \mathcal{U}_t^P(i)$ with $p_j^* < \overline{p}_j$, then $p_i^* \leq 0$;

(b) If for every simple path P connecting node i and s there exists $j \in \mathcal{U}_s^P(i)$ *with* $p_j^* > \underline{p}_j$*, then* $p_i^* \geq 0$*.*

In addition, for line $(i, j) \in \mathcal{E}$*, if* $\underline{p}_i < p_i^* < \overline{p}_i$ *and* $\underline{p}_j < p_j^* < \overline{p}_j$*, then we have* $f_{i,j}^* = 0$*.*

Similarly to Corollary 7.5 in the case of a tree post-contingency network, the optimal injection adjustments are localized around the endpoints of the failure for general networks as well. We formalize this in the following result.

Corollary 7.7. *Assuming a connected post-contingency network and taking* $c_e(f_e) = B_e^{-1} f_e^2$ *as cost function, the optimal injection adjustment at any node* $i \neq s, t$ *for the optimal solution* $\boldsymbol{p}^*$ *of* (7.4) *satisfies the following properties:*

- *If* $\sum_{j \in \mathcal{U}_s^P(i)} -\underline{p}_j \geq \alpha$ *for all simple paths P connecting node i toward node s, then* $p_i^* \geq 0$*;*
- *If* $\sum_{j \in \mathcal{U}_t^P(i)} \overline{p}_j \geq \alpha$ *for all simple paths P connecting node i toward node t, then* $p_i^* \leq 0$*.*

An implicit, but important, component of the above results is that the optimal injection adjustments are localized around the line failure, which provides computational gains. Specifically, define the following quantities for every node $i \neq s, t$:

$$d_s(i) = \min_P \sum_{j \in \mathcal{U}_s^P(i)} -\underline{p}_j \quad \text{and} \quad d_t(i) = \min_P \sum_{j \in \mathcal{U}_t^P(i)} \overline{p}_j.$$

These two quantities can be computed for every node in the network using a variant of Dijkstra's algorithm with complexity $O(n^2)$. Corollary 7.7 suggests that for a single line failure (s, t), the optimal injection adjustments will be localized within a subset of nodes around node s and t of α, i.e., for node $i \in \mathcal{N}_{st}(\alpha) := \{v \in \mathcal{N} : d_s(v) \geq \alpha, d_t(v) \geq \alpha\}$, $p_i^* = 0$. Moreover, for a line (i, j) with $i, j \in \mathcal{N}_{st}(\alpha)$, $f_{i,j}^* = 0$. This localized pattern helps accelerate the computation of (7.4). For instance, the size of set $\mathcal{N} \setminus \mathcal{N}_{st}(\alpha)$ is usually much smaller than the actual network size. Many variables in (7.4) can thus be set as 0 and redundant constraints can be removed, allowing for a faster and more local response against failures.

7.3 Case Study

In this section, we use numerical simulations to evaluate the performance of OIA and OIA-LL in response to failures in the IEEE 118-bus test network and compare it with a classical corrective control approach, OLS.

Setup

We simulate failure scenarios for the IEEE 118-bus test network, using the system parameters and the pre-contingency operating conditions described in [95]. We associate each transmission line with a capacity that is 1.2 times the amount of pre-contingency flow on that line. Considering individually every transmission line whose removal does not disconnect the network as the initial failure, we simulate the post-contingency system state under three control policies (OIA, OIA-LL, and OLS) and additionally contrast these with what happens when no control is applied.

For OIA, we select $c_e(f_e) = B_e^{-1} f_e^2$ as the cost function since the post-contingency network is not a tree in general. For every node i we set the adjustment limits proportionally to its pre-contingency injection, namely

$$-\beta \left|p_i^{\text{pre}}\right| \leq p_i \leq \beta \left|p_i^{\text{pre}}\right|,$$

with $\beta > 0$. In our simulations, we choose $\beta = 0.1, 0.3, 1.0$ to represent various levels of the injection adjustment limit, where a larger β captures a more lenient allowance. For its variation OIA-LL that enforces line limits as well, we choose $\beta = 1.0$ to guarantee its feasibility.

For the traditional corrective control OLS, recall that we allow generations and loads to fluctuate around the pre-contingency values for a fair comparison with OIA. We thus use $c_i(p_i) = |p_i|$ as the cost function to penalize the total post-contingency injection adjustments. Similarly to OIA-LL, we choose $\beta = 1.0$ so that OLS is guaranteed to be feasible.

The performance of OIA

To illustrate the performance of OIA, we study the trade-off between locality and injection adjustment as a function of the post-contingency injection adjustment flexibility, captured by the parameter β.

Figure 7.1 illustrates the failure mitigation performance of OIA for different β's. Specifically, we investigate the fraction of transmission lines whose post-contingency flows exceed line capacity and the relative injection adjustment to the pre-contingency

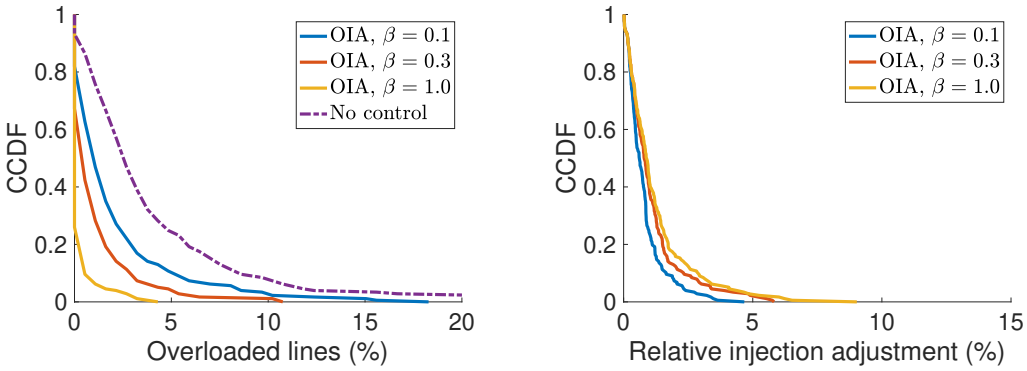

Figure 7.1: CCDF of the fraction of overloaded transmission lines (left) and the relative injection adjustment (right).

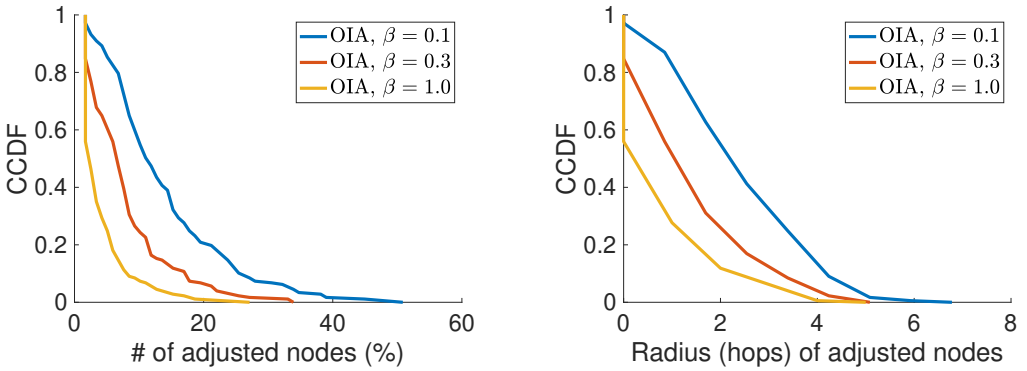

Figure 7.2: CCDF of the fraction of nodes with injection adjustment and the radius (in hops) of the adjusted nodes to the endpoints of an initial failure.

injections for every single-line failure. Figure 7.1 demonstrates the complementary cumulative distribution function (CCDF) for these two metrics. It is shown that, even under a strict adjustment limit (small β), OIA outperforms the baseline where no control is implemented in terms of preventing overloaded lines. Moreover, transmission lines become less likely to be overloaded as β increases. However, a more lenient limit potentially leads to larger injection adjustments.

Figure 7.2 compares the localization performance for OIA with various β's. To quantify the locality, we compute the fraction of nodes with adjusted injections and the radius (in hops) for the subset of adjusted nodes to the endpoints of initial failure. Clearly, a larger β achieves better localization performance: fewer nodes that are closer to the contingency are adjusted for failure mitigation.

To summarize, a larger β prevents lines being overloaded and uses a more local response, at a possible cost of larger amount of injection adjustments. It is thus crucial to carefully tune the parameter β to prioritize different control objectives.

Comparing OIA and OLS

We now compare the performance of OIA and OIA-LL with the more traditional approach OLS. For a fair comparison, we fix $\beta = 1.0$ for OIA, to minimize the chance of overloaded lines. This results in fewer than 0.3% of lines being overloaded with OIA on average. We also compare OIA with its augmented version, OIA-LL, that directly enforces post-contingency line flows and hence has no overloaded lines.

Figure 7.3 illustrates the comparison between OIA, OIA-LL and OLS. Both OIA and OIA-LL achieve similar results in terms of the relative injection adjustments and the fraction of nodes with injection adjustment, while OIA-LL requires nodes from a broader region to participate in the mitigation process. Furthermore, OIA-LL leads to a larger portion of lines with flow deviations than OIA. On the other hand, OLS achieves smallest injection adjustments, but leads to largest amount of nodes and transmission lines affected after failures.

Figure 7.4 shows the Pareto curve for OIA, demonstrating the trade-off between the adjustment cost and the locality of control actions. The curve is generated by simulating with $\beta > 0.3$ for OIA so that the average number of overloaded lines remains below 1%. For comparison, we demonstrate the performance of OIA-LL and OLS as well. The key point here is that OLS is far from the Pareto frontier of OIA, thus highlighting that OIA achieves a better trade-off between localizing responses and the size of injection adjustments. Enforcing line limits in OIA-LL means that it is also outside the Pareto frontier of OIA, but control still remains local, at the expense of a slightly larger control cost (note the scale of the y-axis); which means that it is closer to the Pareto frontier of OIA than OLS. We summarize the numerical results in Table 7.1.

Table 7.1: Summary of OIA, OIA-LL, and OLS

Properties	**OIA**	**OIA-LL**	**OLS**
Injection adjustment	slightly larger	slightly larger	lowest
# of nodes adjusted	sparse	sparse	dense
localization performance	high	medium	low
guarantee on line limits	no	yes	yes

7.4 Conclusion

In this chapter, we have formulated a novel corrective control policy that achieves near-optimal control costs using localized control actions in response to failures.

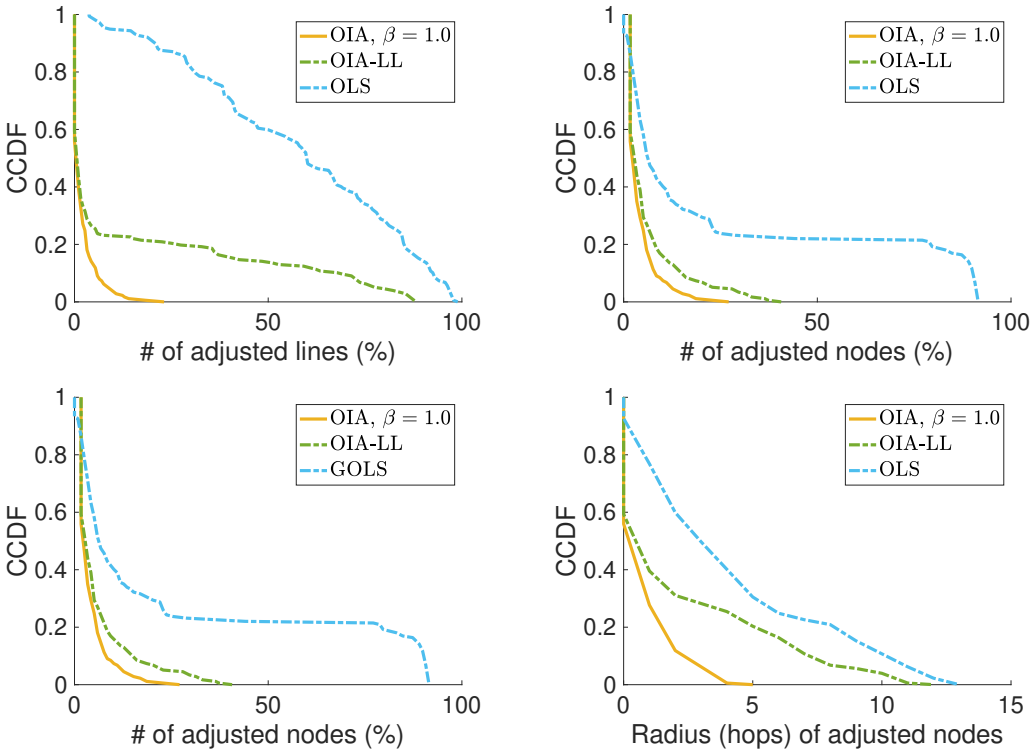

Figure 7.3: Comparison of OIA, OIA-LL, and OLS.

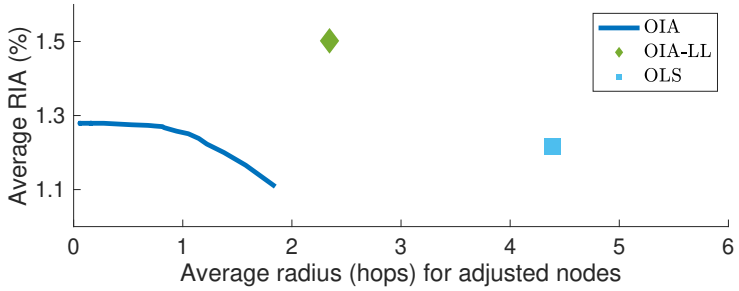

Figure 7.4: Pareto curve of OIA, OIA-LL, and OLS trading off relative injection adjustment (y-axis) and radius of adjusted nodes.

Both theoretical analysis and case studies validate the properties and capabilities of the proposed approach. This shows the feasibility of local corrective control, and there are a number of important directions for future exploration of this topic, e.g., (i) theoretical analysis for the trade-off between the locality and control costs, (ii) localized, distributed, and fast control policy design for large-scale power networks, (iii) analytical comparisons between the optimal injection adjustment and other corrective control policies, and (iv) generalization and validation with the non-linear AC power flow model.

7.5 Proofs

Proof of Lemma 7.2

We prove only the first claim as the proof of the second is analogous. Define $\hat{\boldsymbol{p}} := \boldsymbol{p}^* + \alpha \boldsymbol{e}_{s,t}$ which satisfies the flow conservation rule $\hat{\boldsymbol{p}} = \boldsymbol{C}\boldsymbol{f}^*$. For sake of contradiction, assume $f^*_{u_t(i),i} \geq 0$. Since $\hat{p}_i = p^*_i > 0$ and $f^*_{u_t(i),i} \geq 0$, there must exist a node $v_1 \neq t$ with $f^*_{i,v_1} > 0$ due to the flow conservation rule. If $\hat{p}_{v_1} \geq 0$, we can further find another node $v_2 \neq t$ with flow directing from v_1 to v_2. Such a construction can be repeated until $\hat{p}_{v_k} < 0$ at node v_k. We remark that node v_k always exists, otherwise the flow conservation rule cannot be satisfied. In addition, $p^*_{v_k} < 0$ since $v_k \neq t$ and $\hat{p}_{v_k} < 0$. Therefore, if $f^*_{v_t(i),i} \geq 0$, we can always find a simple path $P = [i = v_0, v_1, v_2, \ldots, v_k]$ with all flows directed from i towards v_k. Now, define $\gamma := \min(p^*_i, \min_{0 \leq l \leq k-1} f^*_{v_l,v_{l+1}}, -p^*_{v_k}) > 0$. Construct a new flow $\tilde{\boldsymbol{f}}$ by uniformly decreasing by γ the flows only along the path P, i.e., $\tilde{f}_e = f^*_e - \gamma$ for $e \in P$, and $\tilde{f}_e = f^*_e$ otherwise. Define $\tilde{\boldsymbol{p}} = \boldsymbol{p}^* - \gamma \boldsymbol{e}_{i,v_k}$. The tree structure guarantees that they satisfy constraints (7.4c) and (7.4b). In addition, one can check that $\tilde{\boldsymbol{p}}$ also satisfy constraint (7.4d). However, the constructed flow $\tilde{\boldsymbol{f}}$ yields a strictly lower cost, contradicting the assumption that $\boldsymbol{p}^*$ is optimal. If $p^*_{u_t(i)} < \overline{p}_{u_t(i)}$, we can similarly define $\gamma := \min(p^*_i, -f^*_{u_t(i),i}, \overline{p}_{u_t(i)} - p^*_{u_t(i)}) > 0$, and let $\tilde{\boldsymbol{p}} = \boldsymbol{p}^* - \gamma \boldsymbol{e}_{i,u_t(i)}$. It can be checked that $\tilde{\boldsymbol{p}}$ is feasible and that the corresponding flow $\tilde{\boldsymbol{f}}$ achieves lower cost, contradicting the assumption that $\boldsymbol{p}^*$ is optimal. □

Proof of Lemma 7.4

(i) For the sake of contradiction, suppose $p^*_s \geq 0$. For every other node $i \neq s$, we have $s \in \mathcal{U}_s(i)$ and $p^*_s > \underline{p}_s$. Theorem 7.3 then implies that $p^*_i \geq 0$. Thus, we have $\sum_{i \in \mathcal{V}} p^*_i \geq p^*_s > 0$, which contradicts the power balancing condition. Therefore, $p^*_s \leq 0$. Similarly, we can show $p^*_t \geq 0$.

(ii) Define $\mathcal{N}_+ = \{i \in \mathcal{N} : p^*_i > 0\}$ as the set of nodes with positive injection deviations at optimum. The claim that $\sum_{i \in \mathcal{N}} \left|p^*_i\right| \leq 2\alpha$ is equivalent to $\sum_{i \in \mathcal{N}_+} p^*_i \leq \alpha$ since $\boldsymbol{p}^*$ is balanced. For the sake of contradiction, assume $\sum_{i \in \mathcal{N}_+} p^*_i > \alpha$. It is easy to check that $t \in \mathcal{N}_+$ and $s \notin \mathcal{N}_+$. Let $\hat{\boldsymbol{p}} = \boldsymbol{p}^* + \alpha \boldsymbol{e}_{s,t}$. Considering the set $\mathcal{N}_+$ as a group, the flow conservation rule implies that there exists a line $(i, j_1) \in \mathcal{E}$ with $i \in \mathcal{N}_+$, $j_1 \in \mathcal{N} \setminus \mathcal{N}_+$ and $f^*_{i,j_1} > 0$. If $p^*_{j_1} = 0$, one can further find another $j_2 \in \mathcal{N} \setminus \mathcal{N}_+$ with $(j_1, j_2) \in \mathcal{E}$ and $f^*_{j_1 j_2} > 0$. We can repeat this process and the flow conservation rule guarantees that there must exist a path $P := [i, j_1, j_2, \ldots, j_k]$ such that $p^*_i > 0$, $p^*_{j_1}, \ldots, p^*_{j_{k-1}} = 0$, and $p^*_{j_k} < 0$ with non-zero flows from node i towards node k. Similarly to the proof of Lemma 7.2, we can uniformly reduce the flow by

$\gamma := \min(p_i^*, \min_{e \in P} f_e^*, -p_{j_k}^*)$ with feasible injections $\tilde{\boldsymbol{p}} = \boldsymbol{p}^* - \gamma \boldsymbol{e}_{i,j_k}$. This leads to a strictly smaller objective, which contradicts the optimality of $\boldsymbol{p}^*$. □

Proof of Theorem 7.6

Along the lines of Lemma 7.2, we can show that if $p_i^* > 0$ and $i \neq t$, then there exists a path P connecting node t and i such that $f^*_{u_t^P(i),i} < 0$ and $p^*_{u_t^P(i)} = \overline{p}_{u_t^P(i)}$. Applying this claim repeatedly yields Theorem 7.6(a) and (b).

To prove such a claim, we follow a strategy similar to that of Lemma 7.2. Define $\hat{\boldsymbol{p}} := \boldsymbol{p}^* + \alpha \boldsymbol{e}_{s,t}$. For the sake of contradiction, assume that $f^*_{u_t^P(i),i} \geq 0$ for every path connecting t and i. Then, there must exist a simple path $P' = [i = v_0, v_1, v_2, \ldots, v_k]$ such that $t \notin P'$, $f^*_{v_l,v_{l+1}} > 0$ for $0 \leq l \leq k-1$, and $\hat{p}_{v_1} = \cdots = \hat{p}_{v_{k-1}} = 0, \hat{p}_{v_k} < 0$. Define $\gamma := \min(p_i^*, \min_{0 \leq l \leq k-1} f_{v_l,v_{l+1}^*}, -p_{v_k}^*) > 0$. Construct a new power injection vector $\tilde{\boldsymbol{p}} = \boldsymbol{p}^* - \gamma \boldsymbol{e}_{i,v_k}$, which can be checked to satisfy the $\underline{\boldsymbol{p}} \leq \tilde{\boldsymbol{p}} \leq \overline{\boldsymbol{p}}$. We further have $\tilde{\boldsymbol{p}} + \alpha \boldsymbol{e}_{s,t} = C\tilde{\boldsymbol{f}}$, where $\tilde{f}_e := f_e^* - \gamma$ for $e \in P'$ and $\tilde{f}_e := f_e^*$ otherwise. Given that the corresponding flow $\boldsymbol{f}' := \boldsymbol{B}\boldsymbol{C}^T\boldsymbol{L}^\dagger(\tilde{\boldsymbol{p}} + \alpha \boldsymbol{e}_{s,t})$ minimizes (7.2), we have $\boldsymbol{f}'^T\boldsymbol{B}^{-1}\boldsymbol{f}' \leq \tilde{\boldsymbol{f}}^T\boldsymbol{B}^{-1}\tilde{\boldsymbol{f}} < \boldsymbol{f}^{*T}\boldsymbol{B}^{-1}\boldsymbol{f}^*$. Thus we have constructed a feasible $\tilde{\boldsymbol{p}}$ with a strictly lower objective, which contradicts the assumption that $\boldsymbol{p}^*$ is optimal. One can similarly prove that $p^*_{u_t^P(i)} = \overline{p}_{u_t^P(i)}$.

Finally, the last part of the theorem, which states that $f^*_{i,j} = 0$ if $\underline{p}_i < p_i^* < \overline{p}_i$ and $\underline{p}_j < p_j^* < \overline{p}_j$, can be proved from the KKT conditions of problem (7.4). □

Bibliography

[1] NERC, "1996 system disturbances: Review of selected 1996 electric system disturbances in North America," report, The Disturbance Analysis Working Group, North American Electric Reliability Council, Princeton Forrestal Village, Princeton, NJ, 2002.

[2] P. D. Hines, I. Dobson, and P. Rezaei, "Cascading power outages propagate locally in an influence graph that is not the actual grid topology," *IEEE TPS*, vol. 32, no. 2, pp. 958–967, 2017.

[3] C. Zhao, E. Mallada, S. Low, and J. Bialek, "A unified framework for frequency control and congestion management," in *2016 Power Systems Computation Conference (PSCC)*, 2016.

[4] E. C. R. Council, "The economic impacts of the August 2003 blackout," *Washington, DC*, 2004.

[5] L. L. Lai, H. T. Zhang, S. Mishra, D. Ramasubramanian, C. S. Lai, and F. Y. Xu, "Lessons learned from July 2012 Indian blackout," in *9th IET International Conference on Advances in Power System Control, Operation and Management (APSCOM 2012)*, pp. 1–6, IET, 2012.

[6] B. A. Carreras, V. E. Lynch, I. Dobson, and D. E. Newman, "Critical points and transitions in an electric power transmission model for cascading failure blackouts," *Chaos: An Interdisciplinary Journal of Nonlinear Science*, vol. 12, no. 4, pp. 985–994, 2002.

[7] M. Anghel, K. A. Werley, and A. E. Motter, "Stochastic model for power grid dynamics," in *2007 40th Annual Hawaii International Conference on System Sciences*, pp. 113–113, IEEE, 2007.

[8] J. Yan, Y. Tang, H. He, and Y. Sun, "Cascading failure analysis with DC power flow model and transient stability analysis," *IEEE Transactions on Power Systems*, vol. 30, no. 1, pp. 285–297, 2014.

[9] A. Bernstein, D. Bienstock, D. Hay, M. Uzunoglu, and G. Zussman, "Power grid vulnerability to geographically correlated failures—analysis and control implications," in *2014 IEEE International Conference on Computer Communications (INFOCOM)*, pp. 2634–2642, IEEE, 2014.

[10] D. P. Nedic, I. Dobson, D. S. Kirschen, B. A. Carreras, and V. E. Lynch, "Criticality in a cascading failure blackout model," *International Journal of Electrical Power & Energy Systems*, vol. 28, no. 9, pp. 627–633, 2006.

[11] M. A. Rios, D. S. Kirschen, D. Jayaweera, D. P. Nedic, and R. N. Allan, "Value of security: Modeling time-dependent phenomena and weather conditions," *IEEE Transactions on Power Systems*, vol. 17, no. 3, pp. 543–548, 2002.

[12] J. Song, E. Cotilla-Sanchez, G. Ghanavati, and P. D. Hines, "Dynamic modeling of cascading failure in power systems," *IEEE Transactions on Power Systems*, vol. 31, no. 3, pp. 2085–2095, 2015.

[13] C. D. Brummitt, R. M. D'Souza, and E. A. Leicht, "Suppressing cascades of load in interdependent networks," *Proceedings of the National Academy of Sciences*, vol. 109, no. 12, pp. E680–E689, 2012.

[14] Z. Kong and E. M. Yeh, "Resilience to degree-dependent and cascading node failures in random geometric networks," *IEEE Transactions on Information Theory*, vol. 56, no. 11, pp. 5533–5546, 2010.

[15] P. Crucitti, V. Latora, and M. Marchiori, "A topological analysis of the Italian electric power grid," *Physica A: Statistical Mechanics and Its Applications*, vol. 338, no. 1-2, pp. 92–97, 2004.

[16] I. Dobson, B. A. Carreras, and D. E. Newman, "A loading-dependent model of probabilistic cascading failure," *Probability in the Engineering and Informational Sciences*, vol. 19, no. 1, pp. 15–32, 2005.

[17] Z. Wang, A. Scaglione, and R. J. Thomas, "A Markov-transition model for cascading failures in power grids," in *2012 45th Hawaii International Conference on System Sciences*, pp. 2115–2124, IEEE, 2012.

[18] M. Rahnamay-Naeini, Z. Wang, N. Ghani, A. Mammoli, and M. M. Hayat, "Stochastic analysis of cascading-failure dynamics in power grids," *IEEE Transactions on Power Systems*, vol. 29, no. 4, pp. 1767–1779, 2014.

[19] H. Guo, C. Zheng, H. H.-C. Iu, and T. Fernando, "A critical review of cascading failure analysis and modeling of power system," *Renewable and Sustainable Energy Reviews*, vol. 80, pp. 9–22, 2017.

[20] R. Baldick, B. Chowdhury, I. Dobson, Z. Dong, B. Gou, D. Hawkins, H. Huang, M. Joung, D. Kirschen, F. Li, *et al.*, "Initial review of methods for cascading failure analysis in electric power transmission systems IEEE PES CAMS task force on understanding, prediction, mitigation and restoration of cascading failures," in *2008 IEEE Power and Energy Society General Meeting-Conversion and Delivery of Electrical Energy in the 21st Century*, pp. 1–8, IEEE, 2008.

[21] P. Hines, S. Talukdar, *et al.*, "Controlling cascading failures with cooperative autonomous agents," *International Journal of Critical Infrastructures*, vol. 3, no. 1, p. 192, 2007.

[22] I. Dobson, B. A. Carreras, and D. E. Newman, "A branching process approximation to cascading load-dependent system failure," in *37th Annual Hawaii International Conference on System Sciences, 2004. Proceedings of the*, pp. 10–pp, IEEE, 2004.

[23] I. Dobson, "Estimating the propagation and extent of cascading line outages from utility data with a branching process," *IEEE Transactions on Power Systems*, vol. 27, no. 4, pp. 2146–2155, 2012.

[24] J. Qi, I. Dobson, and S. Mei, "Towards estimating the statistics of simulated cascades of outages with branching processes," *IEEE Transactions on Power Systems*, vol. 28, no. 3, pp. 3410–3419, 2013.

[25] I. Dobson and D. E. Newman, "Cascading blackout overall structure and some implications for sampling and mitigation," *International Journal of Electrical Power & Energy Systems*, vol. 86, pp. 29–32, 2017.

[26] K. Zhou, I. Dobson, Z. Wang, A. Roitershtein, and A. P. Ghosh, "A Markovian influence graph formed from utility line outage data to mitigate large cascades," *IEEE Transactions on Power Systems*, vol. 35, no. 4, pp. 3224–3235, 2020.

[27] K. Zhou, J. R. Cruise, C. J. Dent, I. Dobson, L. Wehenkel, Z. Wang, and A. L. Wilson, "Bayesian estimates of transmission line outage rates that consider line dependencies," *IEEE Transactions on Power Systems*, vol. 36, no. 2, pp. 1095–1106, 2020.

[28] P. Hines, E. Cotilla-Sanchez, and S. Blumsack, "Do topological models provide good information about electricity infrastructure vulnerability," *Chaos: An Interdisciplinary Journal of Nonlinear Science*, vol. 20, no. 3, p. 033122, 2010.

[29] S. Arianos, E. Bompard, A. Carbone, and F. Xue, "Power grid vulnerability: A complex network approach," *Chaos: An Interdisciplinary Journal of Nonlinear Science*, vol. 19, no. 1, p. 013119, 2009.

[30] P. Dey, R. Mehra, F. Kazi, S. Wagh, and N. M. Singh, "Impact of topology on the propagation of cascading failure in power grid," *IEEE Transactions on Smart Grid*, vol. 7, no. 4, pp. 1970–1978, 2016.

[31] L. Cuadra, S. Salcedo-Sanz, J. Del Ser, S. Jiménez-Fernández, and Z. W. Geem, "A critical review of robustness in power grids using complex networks concepts," *Energies*, vol. 8, no. 9, pp. 9211–9265, 2015.

[32] S. Mei, F. He, X. Zhang, S. Wu, and G. Wang, "An improved OPA model and blackout risk assessment," *IEEE Transactions on Power Systems*, vol. 24, no. 2, pp. 814–823, 2009.

[33] B. A. Carreras, D. E. Newman, I. Dobson, and N. S. Degala, "Validating OPA with WECC data," in *2013 46th Hawaii International Conference on System Sciences*, pp. 2197–2204, IEEE, 2013.

[34] P. Henneaux, P.-E. Labeau, and J.-C. Maun, "A level-1 probabilistic risk assessment to blackout hazard in transmission power systems," *Reliability Engineering & System Safety*, vol. 102, pp. 41–52, 2012.

[35] P. Henneaux, P.-E. Labeau, J.-C. Maun, and L. Haarla, "A two-level probabilistic risk assessment of cascading outages," *IEEE Transactions on Power Systems*, vol. 31, no. 3, pp. 2393–2403, 2015.

[36] B. A. Carreras, V. E. Lynch, M. Sachtjen, I. Dobson, and D. E. Newman, "Modeling blackout dynamics in power transmission networks with simple structure," in *Proceedings of the 34th Annual Hawaii International Conference on System Sciences*, pp. 719–727, IEEE, 2001.

[37] B. A. Carreras, V. E. Lynch, I. Dobson, and D. E. Newman, "Complex dynamics of blackouts in power transmission systems," *Chaos: An Interdisciplinary Journal of Nonlinear Science*, vol. 14, no. 3, pp. 643–652, 2004.

[38] S. Soltan, D. Mazauric, and G. Zussman, "Analysis of failures in power grids," *IEEE Transactions on Control of Network Systems*, vol. 4, no. 2, pp. 288–300, 2015.

[39] D. Bienstock, "Optimal control of cascading power grid failures," in *2011 50th IEEE Conference on Decision and Control and European Control Conference*, pp. 2166–2173, IEEE, 2011.

[40] Q. Ba and K. Savla, "A dynamic programming approach to optimal load shedding control of cascading failure in dc power networks," in *2016 IEEE 55th Conference on Decision and Control (CDC)*, pp. 3648–3653, IEEE, 2016.

[41] C. Zhao, U. Topcu, N. Li, and S. Low, "Design and stability of load-side primary frequency control in power systems," *IEEE Transactions on Automatic Control*, vol. 59, no. 5, pp. 1177–1189, 2014.

[42] N. Li, C. Zhao, and L. Chen, "Connecting automatic generation control and economic dispatch from an optimization view," *IEEE Transactions on Control of Network Systems*, vol. 3, no. 3, pp. 254–264, 2016.

[43] E. Mallada, C. Zhao, and S. H. Low, "Optimal load-side control for frequency regulation in smart grids," *IEEE Transactions on Automatic Control*, vol. 62, no. 12, pp. 6294–6309, 2017.

[44] D. Bienstock, *Electrical transmission system cascades and vulnerability: An operations research viewpoint*. Society for Industrial and Applied Mathematics (SIAM), 2015.

[45] D. Mazauric, S. Soltan, and G. Zussman, "Computational analysis of cascading failures in power networks," *ACM SIGMETRICS Performance Evaluation Review*, vol. 41, no. 1, pp. 337–338, 2013.

[46] O. Alsac, B. Stott, and W. Tinney, "Sparsity-oriented compensation methods for modified network solutions," *IEEE Transactions on Power Apparatus and Systems*, no. 5, pp. 1050–1060, 1983.

[47] B. Stott, O. Alsac, and F. Alvarado, "Analytical and computational improvements in performance-index ranking algorithms for networks," *International Journal of Electrical Power & Energy Systems*, vol. 7, no. 3, pp. 154–160, 1985.

[48] T. Guler, G. Gross, and M. Liu, "Generalized line outage distribution factors," *IEEE Transactions on Power Systems*, vol. 22, no. 2, pp. 879–881, 2007.

[49] T. Guler and G. Gross, "Detection of island formation and identification of causal factors under multiple line outages," *IEEE Transactions on Power Systems*, vol. 22, no. 2, pp. 505–513, 2007.

[50] M. K. Enns, J. J. Quada, and B. Sackett, "Fast linear contingency analysis," *IEEE Transactions on Power Apparatus and Systems*, no. 4, pp. 783–791, 1982.

[51] J. Guo, Y. Fu, Z. Li, and M. Shahidehpour, "Direct calculation of line outage distribution factors," *IEEE Transactions on Power Systems*, vol. 24, no. 3, pp. 1633–1634, 2009.

[52] P. R. Gribik, D. Shirmohammadi, S. Hao, and C. L. Thomas, "Optimal power flow sensitivity analysis," *IEEE Transactions on Power Systems*, vol. 5, no. 3, pp. 969–976, 1990.

[53] A. Hauswirth, S. Bolognani, G. Hug, and F. Dörfler, "Generic existence of unique lagrange multipliers in ac optimal power flow," *IEEE Control Systems Letters*, vol. 2, no. 4, pp. 791–796, 2018.

[54] J. Strake, F. Kaiser, F. Basiri, H. Ronellenfitsch, and D. Witthaut, "Non-local impact of link failures in linear flow networks," *New Journal of Physics*, vol. 21, no. 5, p. 053009, 2019.

[55] K. S. Turitsyn and P. Kaplunovich, "Fast algorithm for N-2 contingency problem," in *2013 46th Hawaii International Conference on System Sciences*, pp. 2161–2166, IEEE, 2013.

[56] P. Kaplunovich and K. Turitsyn, "Fast and reliable screening of N-2 contingencies," *IEEE Transactions on Power Systems*, vol. 31, no. 6, pp. 4243–4252, 2016.

[57] S. Soltan, A. Loh, and G. Zussman, "Analyzing and quantifying the effect of k-line failures in power grids," *IEEE Transactions on Control of Network Systems*, vol. 5, no. 3, pp. 1424–1433, 2017.

[58] L. Guo, C. Liang, and S. H. Low, "Monotonicity properties and spectral characterization of power redistribution in cascading failures," *55th Annual Allerton Conference*, 2017.

[59] A. Ghosh, S. Boyd, and A. Saberi, "Minimizing effective resistance of a graph," *SIAM Review*, vol. 50, no. 1, pp. 37–66, 2008.

[60] F. Dorfler and F. Bullo, "Kron reduction of graphs with applications to electrical networks," *IEEE Transactions on Circuits and Systems I: Regular Papers*, vol. 60, no. 1, pp. 150–163, 2012.

[61] L. Guo and S. H. Low, "Spectral characterization of controllability and observability for frequency regulation dynamics," in *2017 IEEE 56th Annual Conference on Decision and Control (CDC)*, pp. 6313–6320, IEEE, 2017.

[62] O. Alsac and B. Stott, "Optimal load flow with steady-state security," *IEEE Transactions on Power Apparatus and Systems*, no. 3, pp. 745–751, 1974.

[63] A. Monticelli, M. Pereira, and S. Granville, "Security-constrained optimal power flow with post-contingency corrective rescheduling," *IEEE Transactions on Power Systems*, vol. 2, no. 1, pp. 175–180, 1987.

[64] L. Roald, S. Misra, T. Krause, and G. Andersson, "Corrective control to handle forecast uncertainty: A chance constrained optimal power flow," *IEEE Transactions on Power Systems*, vol. 32, no. 2, pp. 1626–1637, 2016.

[65] X. Wang, W. Shao, and V. Vittal, "Adaptive corrective control strategies for preventing power system blackouts," *2005 Power Systems Computation Conference (PSCC)*, 2005.

[66] W. Shao and V. Vittal, "Corrective switching algorithm for relieving overloads and voltage violations," *IEEE Transactions on Power Systems*, vol. 20, no. 4, pp. 1877–1885, 2005.

[67] J. W. Bialek and V. Vahidinasab, "Tree-partitioning as an emergency measure to contain cascading line failures," *IEEE Transactions on Power Systems*, vol. 37, no. 1, pp. 467–475, 2021.

[68] S. Liu, Z. Lin, Y. Zhao, Y. Liu, Y. Ding, B. Zhang, L. Yang, Q. Wang, and S. E. White, "Robust system separation strategy considering online wide-area coherency identification and uncertainties of renewable energy sources," *IEEE Transactions on Power Systems*, vol. 35, no. 5, pp. 3574–3587, 2020.

[69] K. Sun, D.-Z. Zheng, and Q. Lu, "Splitting strategies for islanding operation of large-scale power systems using obdd-based methods," *IEEE Transactions on Power Systems*, vol. 18, no. 2, pp. 912–923, 2003.

[70] C. Wang, B. Zhang, Z. Hao, J. Shu, P. Li, and Z. Bo, "A novel real-time searching method for power system splitting boundary," *IEEE Transactions on Power Systems*, vol. 25, no. 4, pp. 1902–1909, 2010.

[71] H. Li, G. W. Rosenwald, J. Jung, and C.-C. Liu, "Strategic power infrastructure defense," *Proceedings of the IEEE*, vol. 93, no. 5, pp. 918–933, 2005.

[72] A. Peiravi and R. Ildarabadi, "A fast algorithm for intentional islanding of power systems using the multilevel kernel k-means approach," *Journal of Applied Sciences*, vol. 9, no. 12, pp. 2247–2255, 2009.

[73] B. Yang, V. Vittal, G. T. Heydt, and A. Sen, "A novel slow coherency based graph theoretic islanding strategy," in *2007 IEEE Power Engineering Society General Meeting*, pp. 1–7, IEEE, 2007.

[74] L. Ding, F. M. Gonzalez-Longatt, P. Wall, and V. Terzija, "Two-step spectral clustering controlled islanding algorithm," *IEEE Transactions on Power Systems*, vol. 28, no. 1, pp. 75–84, 2012.

[75] A. Esmaeilian and M. Kezunovic, "Prevention of power grid blackouts using intentional islanding scheme," *IEEE Transactions on Industry Applications*, vol. 53, no. 1, pp. 622–629, 2016.

[76] T. Medicherla, R. Billinton, and M. Sachdev, "Generation rescheduling and load shedding to alleviate line overloads-analysis," *IEEE Transactions on Power Apparatus and Systems*, no. 6, pp. 1876–1884, 1979.

[77] S. Koch, S. Chatzivasileiadis, M. Vrakopoulou, and G. Andersson, "Mitigation of cascading failures by real-time controlled islanding and graceful load shedding," in *2010 IREP Symposium Bulk Power System Dynamics and Control-VIII (IREP)*, pp. 1–19, IEEE, 2010.

[78] M. Parandehgheibi, E. Modiano, and D. Hay, "Mitigating cascading failures in interdependent power grids and communication networks," in *2014 IEEE International Conference on Smart Grid Communications (SmartGridComm)*, pp. 242–247, IEEE, 2014.

[79] F. R. Chung and F. C. Graham, *Spectral graph theory*. No. 92, American Mathematical Society, 1997.

[80] S. Chaiken, "A combinatorial proof of the all minors matrix tree theorem," *SIAM Journal on Algebraic Discrete Methods*, vol. 3, no. 3, pp. 319–329, 1982.

[81] C. Zhao, E. Mallada, S. H. Low, and J. Bialek, "Distributed plug-and-play optimal generator and load control for power system frequency regulation," *International Journal of Electrical Power & Energy Systems*, vol. 101, pp. 1–12, 2018.

[82] A. R. Bergen, *Power systems analysis*. Pearson Education India, 2009.

[83] A. E. Motter and Y.-C. Lai, "Cascade-based attacks on complex networks," *Physical Review E*, vol. 66, no. 6, p. 065102, 2002.

[84] C. D. Brummitt, R. M. D'Souza, and E. A. Leicht, "Suppressing cascades of load in interdependent networks," *Proceedings of the National Academy of Sciences*, vol. 109, no. 12, pp. E680–E689, 2012.

[85] R. E. Tarjan and U. Vishkin, "An efficient parallel biconnectivity algorithm," *SIAM Journal on Computing*, vol. 14, no. 4, pp. 862–874, 1985.

[86] A. Wood and B. Wollenberg, *Power Generation, Operation, and Control*. Wiley-Interscience, 1996.

[87] W. Rudin, *Real and Complex Analysis, 3rd Ed.* USA: McGraw-Hill, Inc., 1987.

[88] V. Vittal, W. Kliemann, Y.-X. Ni, D. Chapman, A. Silk, and D. Sobajic, "Determination of generator groupings for an islanding scheme in the manitoba hydro system using the method of normal forms," *IEEE Transactions on Power Systems*, vol. 13, no. 4, pp. 1345–1351, 1998.

[89] H. You, V. Vittal, and Z. Yang, "Self-healing in power systems: An approach using islanding and rate of frequency decline-based load shedding," *IEEE Transactions on Power Systems*, vol. 18, no. 1, pp. 174–181, 2003.

[90] J. Li, C.-C. Liu, and K. P. Schneider, "Controlled partitioning of a power network considering real and reactive power balance," *IEEE Transactions on Smart Grid*, vol. 1, no. 3, pp. 261–269, 2010.

[91] R. J. Sánchez-García, M. Fennelly, S. Norris, N. Wright, G. Niblo, J. Brodzki, and J. W. Bialek, "Hierarchical spectral clustering of power grids," *IEEE Transactions on Power Systems*, vol. 29, no. 5, pp. 2229–2237, 2014.

[92] Z. Liu, A. Clark, L. Bushnell, D. S. Kirschen, and R. Poovendran, "Controlled islanding via weak submodularity," *IEEE Transactions on Power Systems*, vol. 34, no. 3, pp. 1858–1868, 2018.

[93] A. J. Wood, B. F. Wollenberg, and G. B. Sheblé, *Power generation, operation, and control*. John Wiley & Sons, 2013.

[94] D. Bienstock and A. Verma, "The $N-k$ problem in power grids: New models, formulations, and numerical experiments," *SIAM Journal on Optimization*, vol. 20, no. 5, pp. 2352–2380, 2010.

[95] R. D. Zimmerman, C. E. Murillo-Sánchez, and R. J. Thomas, "MATPOWER: Steady-state operations, planning, and analysis tools for power systems research and education," *IEEE Transactions on Power Systems*, vol. 26, no. 1, pp. 12–19, 2010.

[96] P. D. Hines, I. Dobson, E. Cotilla-Sanchez, and M. Eppstein, "Dual graph and random chemistry methods for cascading failure analysis," in *2013 46th Hawaii International Conference on System Sciences*, pp. 2141–2150, IEEE, 2013.

[97] D. L. H. Aik and G. Andersson, "Analysis of voltage and power interactions in multi-infeed HVDC systems," *IEEE Transactions on Power Delivery*, vol. 28, no. 2, pp. 816–824, 2013.

[98] F. Kaiser, V. Latora, and D. Witthaut, "Network isolators inhibit failure spreading in complex networks," *Nature Communications*, vol. 12, no. 1, pp. 1–9, 2021.

[99] F. Kaiser and D. Witthaut, "Topological theory of resilience and failure spreading in flow networks," *Physical Review Research*, vol. 3, no. 2, p. 023161, 2021.

[100] S. Babaeinejadsarookolaee, A. Birchfield, R. D. Christie, C. Coffrin, C. DeMarco, R. Diao, M. Ferris, S. Fliscounakis, S. Greene, R. Huang, *et al.*, "The power grid library for benchmarking AC optimal power flow algorithms," *arXiv preprint arXiv:1908.02788*, 2019.

[101] D. Bienstock and S. Mattia, "Using mixed-integer programming to solve power grid blackout problems," *Discrete Optimization*, vol. 4, no. 1, pp. 115 – 141, 2007.

[102] L. Guo, C. Liang, A. Zocca, S. H. Low, and A. Wierman, "Line failure localization of power networks part i: Non-cut outages," *IEEE Transactions on Power Systems*, vol. 36, no. 5, pp. 4140–4151, 2021.

[103] L. Guo, C. Liang, A. Zocca, S. H. Low, and A. Wierman, "Line failure localization of power networks part ii: Cut set outages," *IEEE Transactions on Power Systems*, vol. 36, no. 5, pp. 4152–4160, 2021.

[104] A. Zocca, C. Liang, L. Guo, S. H. Low, and A. Wierman, "A spectral representation of power systems with applications to adaptive grid partitioning and cascading failure localization," *arXiv preprint arXiv:2105.05234*, 2021.

[105] J. K. Johnson and M. Chertkov, "A majorization-minimization approach to design of power transmission networks," in *49th IEEE Conference on Decision and Control (CDC)*, pp. 3996–4003, IEEE, 2010.

[106] C. Lai and S. H. Low, "The redistribution of power flow in cascading failures," in *2013 51st Annual Allerton Conference on Communication, Control, and Computing (Allerton)*, pp. 1037–1044, Oct 2013.

[107] S. Pahwa, C. Scoglio, S. Das, and N. Schulz, "Load-shedding strategies for preventing cascading failures in power grid," *Electric Power Components and Systems*, vol. 41, no. 9, pp. 879–895, 2013.

[108] N. Biggs, *Algebraic Graph Theory*. Cambridge University Press, 2nd ed., 1993.